# Dynamics and Control of SEDSAT
# Tethered Multi-Probe for Thermospheric Research
# Flight Data Analysis of SEDS-II Satellite

Grant NAG8-1046

***Tethered Systems Dynamics and Flight Data Analysis***

**Final Report**

First Year Research Activity for the period 22 February 1994 through 21 February 1995

Principal Investigators
Enrico C. Lorenzini
Gordon E. Gullahorn
Mario L. Cosmo

Co-Investigator
Mario D. Grossi

May 1995

Prepared for
National Aeronautics and Space Administration
Marshall Space Flight Center, Alabama 35812

Smithsonian Institution
Astrophysical Observatory
Cambridge, Massachusetts 02138

## TABLE OF CONTENTS

## SUMMARY

This report covers the three topics summarized in the following:

*1) Dynamics and Control of SEDSAT*

The orbital mechanics underlying the sling-shot technique, utilized by SEDSAT for its orbital transfer is analyzed. Then, simplified expressions for the satellite lifetime are provided in order to compute the minimum injection velocity to reach the required orbit. A control law is, then, developed for the deployment of SEDSAT on a 20-km-long tether by using the Small Expendable Deployment System. Finally, the robustness of the control law with respect to the variability of the deployer's model parameters is investigated in order to estimate the errors affecting the injection velocity at satellite release.

*2) Tethered Multi-Probe for Thermospheric Research*

Three papers, presented at the Fourth International Conference on Tethers in Space, are included in this report: (1) the first paper focuses on the chemical processes responsible for the cooling of the lower thermosphere as an effect of an increased concentration of "greenhouse gases" in the troposphere; (2) the second paper deals with the instrumentation required for measuring these cooling processes; and (3) the third paper focuses primarily on the dynamics and thermal requirements of a dual-probe tethered system deployed into the Earth's lower thermosphere for carrying out those measurements in order to prove the feasibility of such mission with present day tether technology.

*3) Analysis of SEDS-II Flight Data*

A paper, presented at the Fourth International Conference on Tethers in Space, is included in this report to illustrate the results of the analysis of the acceleration levels and dynamic noise on the SEDS-II end-mass.

## 1.0 DYNAMICS AND CONTROL OF SEDSAT

### 1.1 INTRODUCTION

The satellite SEDSAT, built by a team of students of the University of Alabama at Huntsvlle, will be injected into a higher orbit from the Space Shuttle in July 1997 by using a 20-km-long librating tether acting as a sling shot. Since the satellite is expected to have a lifetime of about 3 years, without reboosting, the height and eccentricity of the final orbit are a primary concern. The injection velocity ($\Delta V$) at the satellite release must be maximized in order to maximize the apogee height of the final orbit and consequently the satellite lifetime. Moreover, the final orbit must be as insensitive as possible to variations of the deployer's friction parameters in order to provide an accurate orbital transfer of the payload. Consequently, the magnitude, direction, and timing of the $\Delta V$ at satellite release (i.e., when the tether crosses the local vertical and the tether is cut from the Shuttle) must be accurate and as insensitive as possible to variations of the model parameters. A non-linear control law (feedforward-feedback) for driving the satellite to the desired position with the right velocity at the end of deployment was successfully tested during the flight of SEDS-II in March 1994. However, differently from SEDS-II, the deployment of SEDSAT occurs mostly at libration angles greater than 45° and, consequently, the stability of the deployment maneuver must be taken into account. As explained better in the following sections the control strategy of SEDSAT is substantially different from the control strategy of SEDS-II.

### 1.2 Orbital Injection

The $\Delta V$ imparted by a librating tether can be simply computed by utilizing the well-known Hill's equations describing the motion of a mass with respect to an orbiting reference frame on a circular orbit where the z-axis is the ascending local vertical (LV) and the x-axis is along the local horizontal (LH) towards the flight direction. We restrict our analysis to the two-dimensional case only for the sake of simplicity (the extension to a three-dimensional case is readily done but it is not necessary for our discussion):

$$\begin{aligned} \ddot{x} + 2\Omega\dot{z} &= F_x/m \\ \ddot{z} - 2\Omega\dot{x} - 3\Omega^2 z &= F_z/m \end{aligned} \tag{1}$$

For null external perturbation, i.e., $F_X = F_Z = 0$, the solution of eqns. (1) is as follows [1]:

$$x(t) = (2\dot{z}_0/\Omega)\cos(\Omega t) + (4\dot{x}_0/\Omega + 6z_0)\sin(\Omega t) + (x_0 - 2\dot{z}_0/\Omega) - (3\dot{x}_0 + 6\Omega z_0)t \tag{2.1}$$

$$z(t) = (\dot{z}_0/\Omega)\sin(\Omega t) - (2\dot{x}_0/\Omega + 3z_0)\cos(\Omega t) + (2\dot{x}_0/\Omega + 4z_0) \tag{2.2}$$

For a payload released at LV from a librating tether, whereby $\dot{z}_0 = x_0 = 0$, eqns. (2.2) yields:

$$z = -(2\dot{x}_0/\Omega + 3z_0)\cos(\Omega t) + 2\dot{x}_0/\Omega + 4z_0 \tag{3}$$

which for $\Omega t = \pi$ (i.e., half an orbit later) becomes

$$z_{\Omega t=\pi} = 7z_0 + 4\dot{x}_0/\Omega \tag{4}$$

The first term on the right hand side of eqn. (4) depends on the separation between the released satellite and the mother platform located at the origin of the coordinate frame while the second term depends upon the relative velocity at release as seen from the rotating observer. Equation (4) can be readily converted to polar coordinates $L$ and $\theta$ where $L$ is the tether length and $\theta$ the in-plane libration angle with respect to LV to yield (see Fig. 1)

$$\Delta H_{CM} = \left[7 \pm 4\sqrt{3}\sin(\bar{\theta})\right] L_{CM} \tag{5.1}$$

where we used the analytical expression for the maximum angular rate (at LV) of a freely-librating gravity-gradient pendulum with large amplitudes $\bar{\theta}$, i.e., $\dot{\theta}_{LV} = \sin(\bar{\theta})\sqrt{3}\Omega$. In eqn. (5.1) $z_{\Omega t=\pi}$ has been replaced by $\Delta H_{CM}$ which is more reminiscent of its physical meaning, that is, the height difference between the orbit of the mother platform (circular for the time being) and the apogee height of the center of mass (CM) of the released body. The reference to the center of mass will become particularly useful when dealing with an extended body like a satellite with an attached *massive* tether. The plus and minus signs, in eqn. (5), are for prograde and retrograde librations, respectively.

Equation (5.1) can be rewritten as follows

$$\Delta H_{CM} = \left(7\Omega L_{CM} \pm 4\Delta V_{swing}\right)/\Omega \tag{5.2}$$

where $L_{CM}\Omega$ is the contribution (sometimes called the *hanging* component for tether satellites) associated with the rotational motion of the orbiting frame and

$\Delta V_{swing} = \sqrt{3}\Omega \sin(\bar{\theta}) L_{CM}$ (sometimes called the *swinging* component) is the contribution associated with the libratory motion of the system with respect to the same reference frame.

If conservation of energy and angular momentum are utilized instead of the simplified Hill's equations, then, eqns. (5) are replaced by the more accurate formula:

$$\Delta H_{CM} = \frac{v_p^2 \cdot r_p - \mu}{\mu / r_p - v_p^2 / 2} + L_{CM} \tag{6.1}$$

where the perigee velocity of the CM of the released body is

$$v_p = \sqrt{\mu / R_0} + \Delta V \tag{6.2}$$

In eqns. (6), $\mu$ is the Earth's gravitational constant, $R_0$ the semi-major axis of the orbit of the mother platform (here assumed circular but readily extendible to the elliptical case), and $r_p$ the perigee radius of the released object CM.

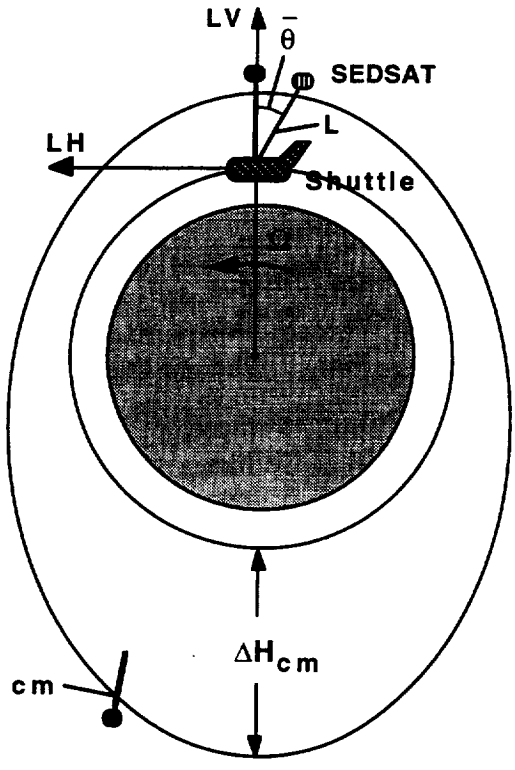


**Fig. 1.** SEDSAT system and reference frames

Equation (5.1) can be generalized (the derivation is not shown here for the sake of brevity) to the release from apoaxis of an initial orbit with small eccentricity $e$ as follows

$$\Delta H_{CM} = \left[7 \pm 4\sqrt{3}\sin(\bar{\theta}) \pm 8e\right] L_{CM} \tag{7}$$

where, in this case, $\Delta H_{CM}$ is the height difference between the apoaxis of the initial orbit and the opposite apoaxis (i.e., with a $\pi$-rad phase difference) of the orbit after release. The plus and minus signs in front of the eccentricity-related term are for a release at periaxis and apoaxis respectively. Let us analyze, for example, the case of a release at apoaxis and compare a circular and eccentric initial orbits with equal energy (i.e., $R = a$ or radius of circular orbit = semi-major axis of eccentric orbit). Clearly, the eccentricity has two opposite effects: (1) on the one hand the apogee height of the eccentric orbit is higher than the equal-energy circular orbit by the quantity $h = eR$ ; (2) on the other hand the height difference after release $\Delta H_{CM}$ for an eccentric orbit is reduced by the quantity $8eL_{CM}$ with respect to the $\Delta H_{CM}$ for a release from a circular orbit. Since $8L_{CM} << R$, for almost any conceivable tethered system, there is a net gain in the altitude of the final orbit for a release from the apogee of an eccentric initial orbit when compared to the release from an equal-energy circular orbit.

Let us now go back to eqn. (5.1) with the plus sign which, in the current orbit scenario, applies to the release of SEDSAT from the Shuttle on a circular orbit. The height accuracy of the final orbit depends on $L_{CM}$ and $\bar{\theta}$ but, while it is straight forward to provide a relatively accurate value for the tether length at the end of deployment, it is rather challenging to achieve an accurate maximum libration angle at release $\bar{\theta}$ with a passive deployer like SEDS [2-3] (i.e., a deployer that cannot reel in the tether and, more importantly, control the tether speed directly). From eqn. (5.1), the sensitivity of $\Delta H_{CM}$ with respect to variations of $\bar{\theta}$ and $L_{CM}$ is as follows:

$$\partial \Delta H_{CM} = \pm 4\sqrt{3} L_{CM} \cos(\bar{\theta}) \partial \bar{\theta} + \left[7 \pm 4\sqrt{3}\cos(\bar{\theta})\right] \partial L_{CM} \tag{8}$$

Clearly, the sensitivity is smaller for large values of $\bar{\theta}$ which is desirable because large values of $\bar{\theta}$ are required for achieving high final orbits.

### 1.3 SEDSAT Orbital Lifetime

The SEDSAT satellite has a requirement of a 3-year lifetime without reboosting once it is detached from its tether. As explained later on, the tether will be cut twice: the first

time at the Shuttle end in order to raise the apogee of its orbit after release and the second time at the satellite end, close to apogee, in order to raise the perigee of its final orbit.

Estimating lifetime a few years ahead of a long-duration space mission is always subject to large errors because of the variability of the atmospheric density, which is particularly strong at the orbital altitudes of SEDSAT. Moreover, SEDSAT is not a 3-axis-stabilized satellite and, consequently, its frontal area with respect to the wind velocity changes continually. A rough estimate of the lifetime can be obtained from relatively simple formulas obtained under simplifying assumptions as follows: spherical and corotating atmosphere, exponential atmospheric density, and average frontal area of satellite.

In accordance with the previous assumption analytical formulas can be obtained for the decay of the orbit semi-major axis per revolution $\Delta a_{rev}$ [4]. The orbital decay from an elliptical orbit due to atmospheric drag can be subdivided into two phases: (a) a circularization phase during which the apogee decays while the perigee altitude remains the same; and (b) a spiraling phase from a circular orbit to final reentry.

From the conservation of angular momentum, the velocity along the orbit can be readily obtained as follows:

$$v^2 = \left(\frac{\mu}{Q}\right)^2 (1 + e\cos\theta)^2 \approx \left(\frac{\mu}{Q}\right)^2 (1 + 2e\cos\theta) \tag{9.1}$$

where Q is the angular momentum for unit mass and the approximation on the right hand side is valid for eccentricity $e << 1$.

If an atmosphere corotating at the Earth angular speed $\Omega_E$ is considered, then

$$v^2 \approx \left(\frac{\mu}{Q}\right)^2 (1 + 2e\cos\theta)\left(1 - 2\frac{\Omega_E}{\Omega}\cos i\ (1 - e\cos\theta)\right) \tag{9.2}$$

where $i$ is the orbital inclination and $\Omega$ the instantaneous orbital rate.

By utilizing eqn. (9), the drag force on the system can be written as:

$$F = \frac{1}{2} C_D A \rho_0 \exp(h_0/H) \exp(-h/H) v^2 \tag{10}$$

An exponential atmospheric density profile has been assumed in eqn. (10) with reference density and reference height $\rho_0$ and $h_0$, and scale height H.

From the orbital energy loss per unit mass due to atmospheric drag

$$\frac{da}{dt} = \frac{2F}{\Omega m} \tag{11}$$

the semi-major axis decay per revolution is readily obtained as follows:

$$\Delta a_{rev} = \int_0^P \frac{2F}{\Omega m} dt \tag{12}$$

where P is the orbital period. It is more convenient to integrate eqn. (12) with respect to the orbital anomaly $d\theta$. Since,

$$dt = \frac{1}{\Omega_0 (1 + 2e\cos\theta)} d\theta \tag{13}$$

with $\Omega_0$ the mean orbital rate, eqn. (12) yields

$$\Delta a_{rev} = \frac{C_D A}{m} K a^2 \int_0^{2\pi} e^{\psi \cos\theta} (1 + 2e\cos\theta) d\theta \tag{14}$$

where

$$K = \rho_0 \exp[(h_0 + R_E - a)/H](1 - 2\Omega_E \sin i / \sqrt{\mu / a^3}) \tag{15.1}$$

$$\psi = ea/H \tag{15.2}$$

$R_E$ is the Earth's equatorial radius and *a* the semi-major axis of the orbit.

The integral in eqn. (14) can be decomposed into two elliptical integrals giving rise to two *modified Bessel functions* of order zero and one, respectively. In conclusion, after some algebraic manipulations:

$$\Delta a_{rev} = -2\pi (C_D A / m) a^2 K [I_0(\psi) + 2eI_1(\psi)] \qquad \text{for e} << 1 \tag{16.1}$$

$$\Delta a_{rev} = -2\pi (C_D A / m) a^2 K \qquad \text{for e} \approx 0 \tag{16.2}$$

Equation (16.2) applies to the spiraling phase in which $e \approx 0$ and, consequently, $I_0(0) = 1$ and $I_1(0) = 0$.

In eqns. (16), $C_D A/m = 1/\beta$ where $\beta$ is the satellite ballistic coefficient. Different values of $h_0$ should be adopted in eqns. (16.1) and (16.2) for the circularization and spiraling phases in order to provide good local fits of the density in the two regions of interest ($h_0 = h_p$, with $h_p$ the perigee height, does not necessarily produce the best results for orbits with small eccentricities). If $h_0 = h_p$ and $\Omega_E = 0$ (i.e., without the rotating atmosphere), then $K = \rho_p \exp(-\psi)$ and eqns. (9) reduce to more familiar formulas [5].

The decay time can be computed as follows [4]:

$$\Delta t = \int_{a_f}^{a_i} \frac{\pi}{\Delta a_{rev} \sqrt{\mu / a^3}} da \tag{17}$$

where $a_i$ and $a_f$ are the semi-major axis associated with the initial and final altitudes of the two decay phases under consideration. The integral of eqn. (17) must be computed twice for the two expressions of $\Delta a_{rev}$ of eqns. (16.1) and (16.2) and, moreover, $a_f$(circularization phase) = $a_i$ (spiraling phase) = $a_p$ (semi-major axis at perigee of circularization phase). The orbital lifetime is the sum of the decay times of the circularization and spiraling phases.

Figure 2 shows the total lifetime for the SEDSAT satellite, computed from eqns. (16) and (17), with the following numerical values: $\beta = 118$, $a_p = 330$ km, and $T_{exo} = 750$ K. This value of the exospheric temperature is the current best estimate for a SEDSAT launch date in July 1997.

The lifetime estimate, shown in Fig. 2, was compared to the lifetime estimated at NASA Marshall Space Flight Center (NASA/MSFC) by means of a computer code with a more accurate atmospheric model in which the lifetime is also a function of the argument of perigee. The lifetime of Fig. 2 is an average value of the more general values estimated at NASA/MSFC. It is evident from Fig. 2 that in order to have a lifetime $\geq 3$ years, the initial altitude of apogee must be $\geq 530$ km (with respect to a spherical Earth). Both estimates of lifetime (SAO and MSFC), however, are affected by the large uncertainties associated with the prediction of the actual Solar activity and, hence, atmospheric conditions a few years in advance.

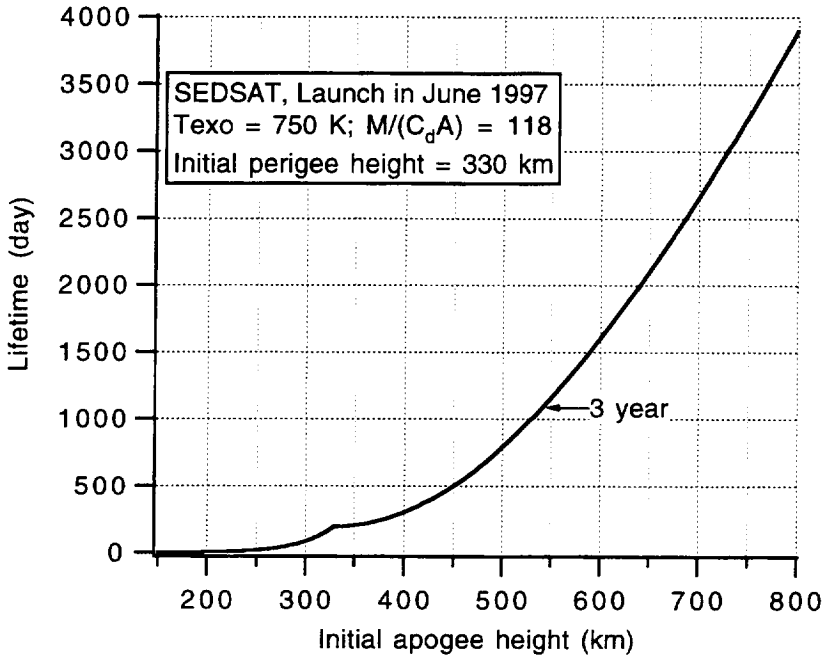


**Fig. 2.** SEDSAT lifetime vs apogee height.

### 1.4 Control of SEDSAT Deployment

SEDS Deployer's Tension Model

Before attacking the problem of controlling SEDSAT deployment and release, a few words must be said about the deployer' s tension model. The reader should consult Ref. [6] for a more detailed treatment of the subject. The tension model for the SEDS deployer is as follows:

$$T = \left[T_0 + I\rho \dot{L}^2 A_{rel}^{-E}\right] \cdot e^{B} \cdot e^{f \cdot |\theta_0 - \theta|} \tag{18}$$

where $A_{rel}$ = 1 - A $L/L_{end}$, $L_{end}$ = final tether length = 20 km, A = tether annulus solidity = 0.942, E = area exponent = 0.6, $B$ = brake parameter = $2\pi f n$ , $n$ = number of brake turns, $f$ = friction coefficient = 0.18 (best estimate), $T_0$ = static (or minimum) tension, $I$ = inertia multiplier = 4.1, $\rho$ = linear density of tether = 3.3 kg/km, $\theta_0$ = null exit angle, and $\theta$ = tether's exit angle (for a deployer aligned along the Nadir, $\theta$ coincides with the in-plane libration angle). In summary, this approximate tension model consists of a static tension term $T_0$, an hydraulic tension term proportional to $\dot{L}^2$, an exponential brake multiplier, and an exponential exit-angle multiplier. Parameters of the tension model are uncertain as they depend on environmental conditions and many other uncontrollable, or

poorly controllable, factors. The most influential, from the deployment dynamics standpoint, and also less certain parameter of the tension model is $T_0$. A likely estimate of the value of $T_0$ from the flights of SEDS-I and II is about 20 mN with an expected variability of ±10 mN.

SEDS-II-Type Deployment Control Law Attempts

A non-linear control law that made use of the feedback linearization technique was successfully tested during the flight of SEDS-II in March 1994. This control law utilized predetermined tether length, tether rate, and brake reference profiles in order to eliminate the non-linearities in the model of the plant (deployer) and the actuator (brake). A locally linear feedback, based on error signals of the actual length and rate with respect to the reference values, was used to correct the reference brake profile in order to track the reference trajectory in the state space under off-reference conditions. This control law was active throughout the SEDS-II deployment with the only exception of the first kilometer of deployed tether. The reference profiles for SEDS-II were designed to provide a null libration at the end of deployment. If the same technique were applied to SEDSAT, the reference profiles should be designed to provide a large libration at the end of deployment or equivalently a large angular rate at the crossing of LV.

The first attempts for controlling SEDSAT deployment were carried out by simply utilizing the same technique adopted successfully for deploying SEDS-II. The ejection velocity was 1.47 m/s (i.e., the ejection velocity of SEDS-II scaled by $\sqrt{m_1/m_2}$ where $m_1$ = 34 kg and $m_2$ = 26 kg are the masses of SEDSAT and SEDS-II, respectively). The final state vector was specified as to obtain the desired horizontal velocity at the crossing of the local vertical (LV) with a tether length of 20 km. The horizontal velocity of the released-system CM $\Delta V_{CM,H}$ at LV crossing (with respect to an LH-LV rotating reference frame) is simply the swinging component of the ΔV as follows

$$\Delta V_{CM,H} = \Delta V_{swing} = \sqrt{3}\Omega \sin(\bar{\theta}) L_{CM} \tag{19}$$

and, consequently, it depends upon the maximum libation amplitude at the fully deployed tether length.

In the following, we describe some sample reference profiles and the associated feedback control that were derived in order to attempt a control of SEDSAT deployment along the same line of the SEDS-II deployment.

In SEDSAT_Ref12 (the numbering is sequential from the beginning of the SEDSAT control law analysis), the final state vector is as follows:

$L = 20$ km, $\dot{L}$ =0.1 m/s, $\theta = 0$, $\dot{\theta}$ = 0.077 deg/s (i.e., $\Delta V_{CM,H} = 24$ m/s).

The initial conditions at satellite ejection are $V_0 = 1.47$ m/s and $\theta_0 = 0°$ (ejection along LV upwards). The value quoted above for the horizontal component $\Delta V_{CM,H}$ corresponds to a final libration amplitude of 42°. The brake is activated at t = 750 s (i.e., L = 1060 m) and the reference value of the minimum tension is 20 mN. The position and velocity gains of the feedback portion of the control law are $K_1 = 0.004$ and $K_2 = 0.4$, respectively. These values of the gains are larger than those adopted in SEDS-II in order to make the control law more effective in tracking the tether length and velocity profiles. Figure 3(a) shows the deployment dynamics for the reference value $T_0 = 20$ mN while Figs. 3(b)-3(f) show the dynamics for values of $T_0$ ranging from 10 mN to 30 mN. It is clear that the control law is sufficiently insensitive to variations of the minimum tension but, because of the insufficient final libration amplitude, it is unable to provide the required $\Delta V$ at LV crossing.

In reference profile SEDSAT_Ref19, the final state vector is as follows:

$L = 20$ km, $\dot{L}$ = 0.1 m/s, $\theta = 0$, $\dot{\theta}$ = 0.09 deg/s (i.e., $\Delta V_{CM,H} = 27$ m/s).

The ejection angle this time is $\theta_0 = -20°$ (upward and forward).

The value quoted above for the horizontal component $\Delta V_{CM,H}$ corresponds to a final libration amplitude of about 47°. The brake is activated at t = 500 s (L = 700 m) and the reference value of the minimum tension is 20 mN. Figures 4(a)-4(f) show that the final $\Delta V$ at LV crossing (or equivalently the final libration amplitude) is not large enough to provide the desired apogee altitude after satellite release. In fact, with a 297-km circular orbit for the Shuttle and a tether length of 20 km, a final libration amplitude $\geq 60°$ is required for attaining an apogee altitude $\geq 530$ km. Moreover, the insensitivity of the $\Delta V$ magnitude at LV crossing with respect to variations of the tension model parameters is not satisfactory.

In reference profile SEDSAT_Ref24, the final state vector is as follows:

$L = 20$ km, $\dot{L}$ = 0.1 m/s, $\theta = 0$, $\dot{\theta}$ = 0.096 deg/s (i.e., $\Delta V_{CM,H} = 31$ m/s).

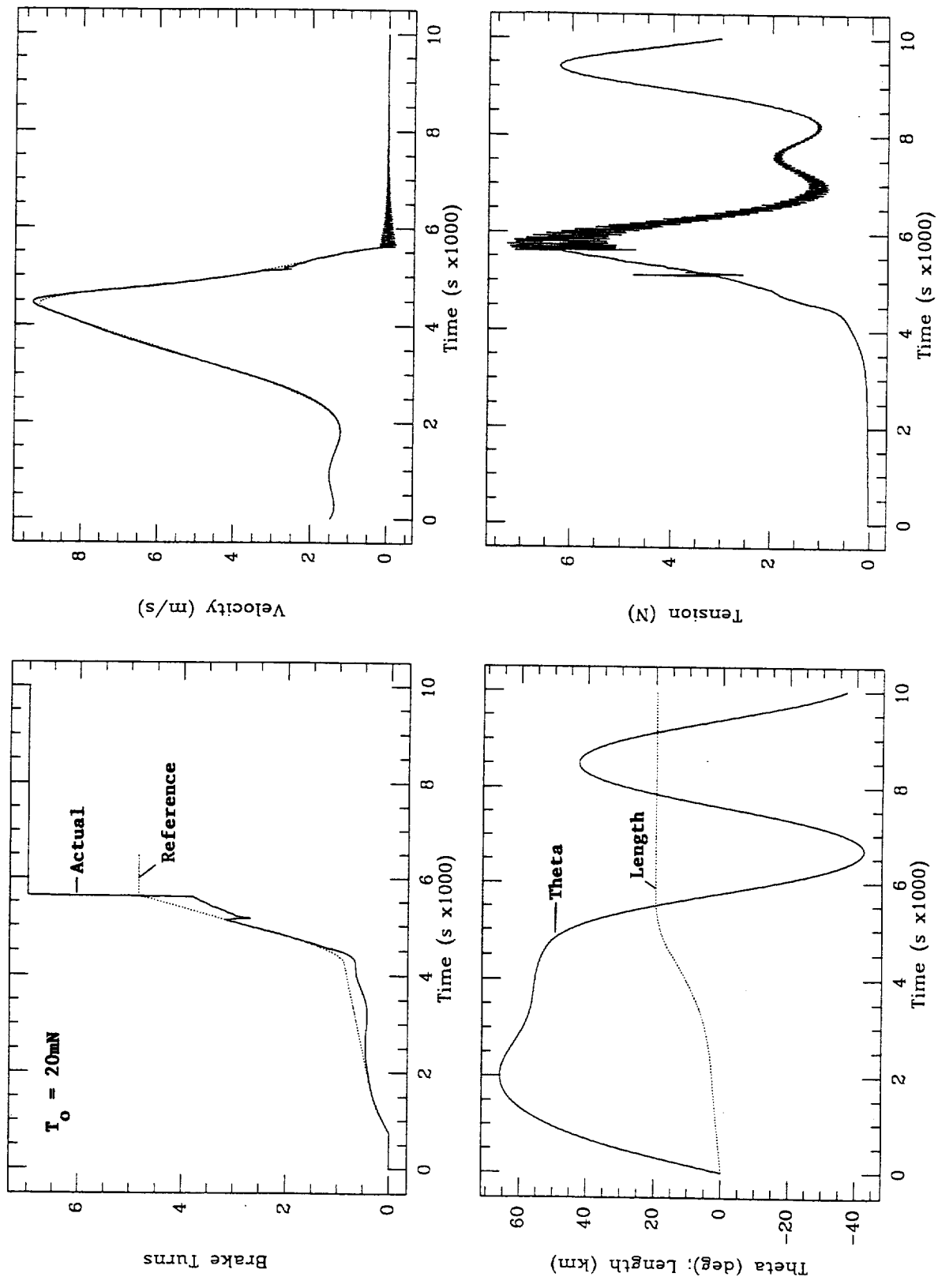


**Fig. 3(a).** Deployment dynamics for SEDS-II-type reference profile 12 (see text).

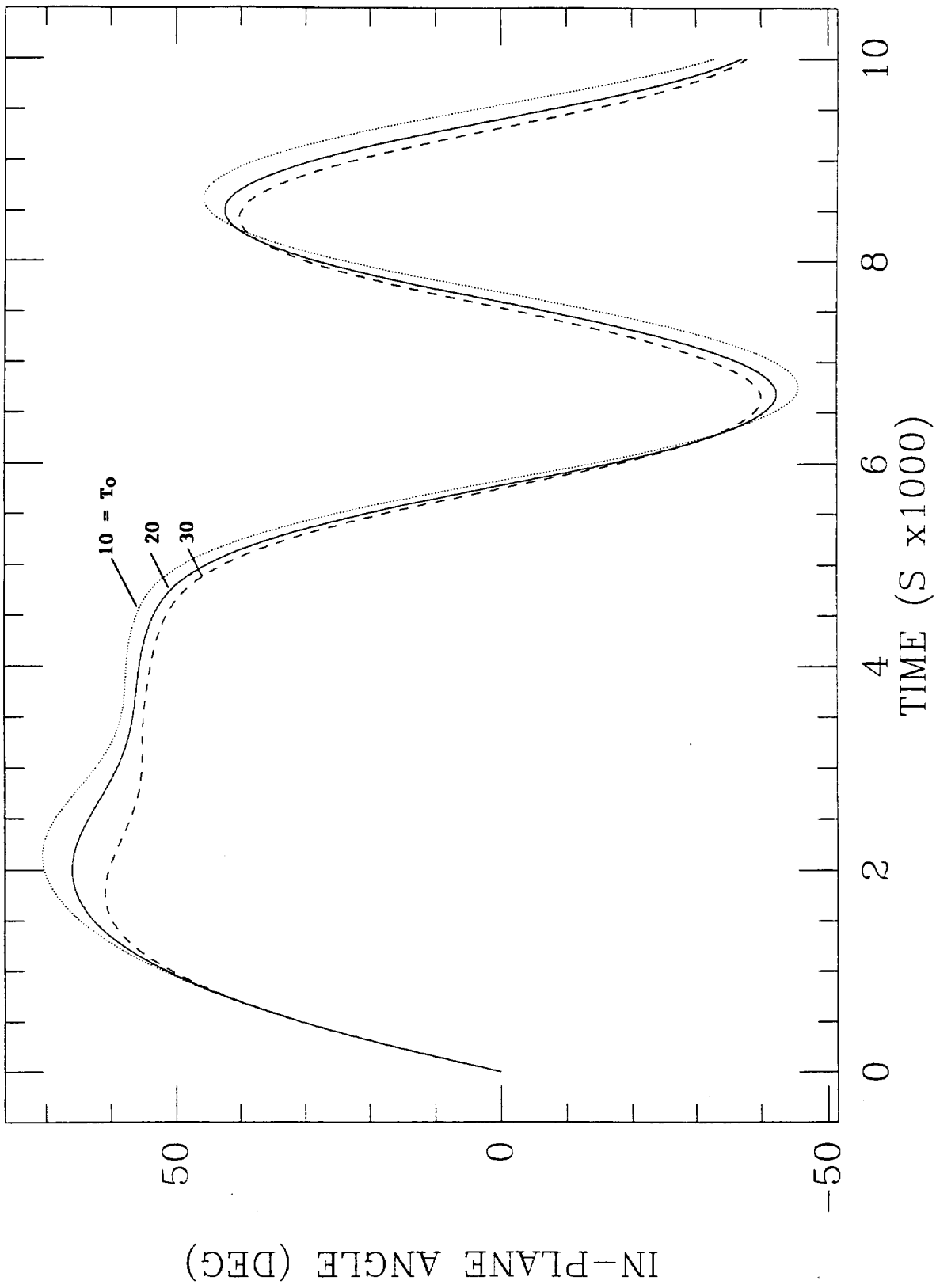


**Fig. 3(b).** Deployment dynamics for SEDS-II-type reference profile 12 (see text).

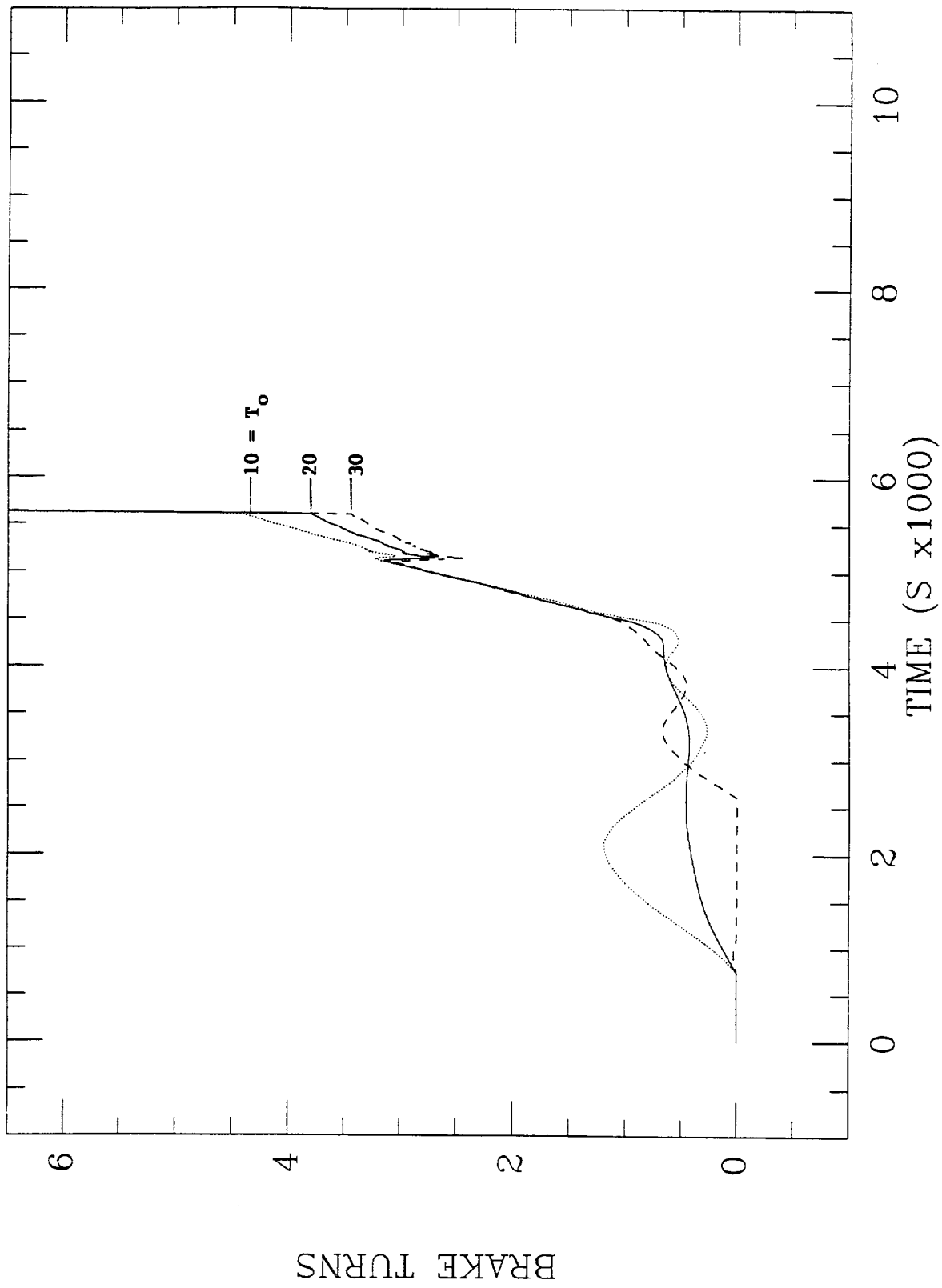


**Fig. 3(c).** Deployment dynamics for SEDS-II-type reference profile 12 (see text).

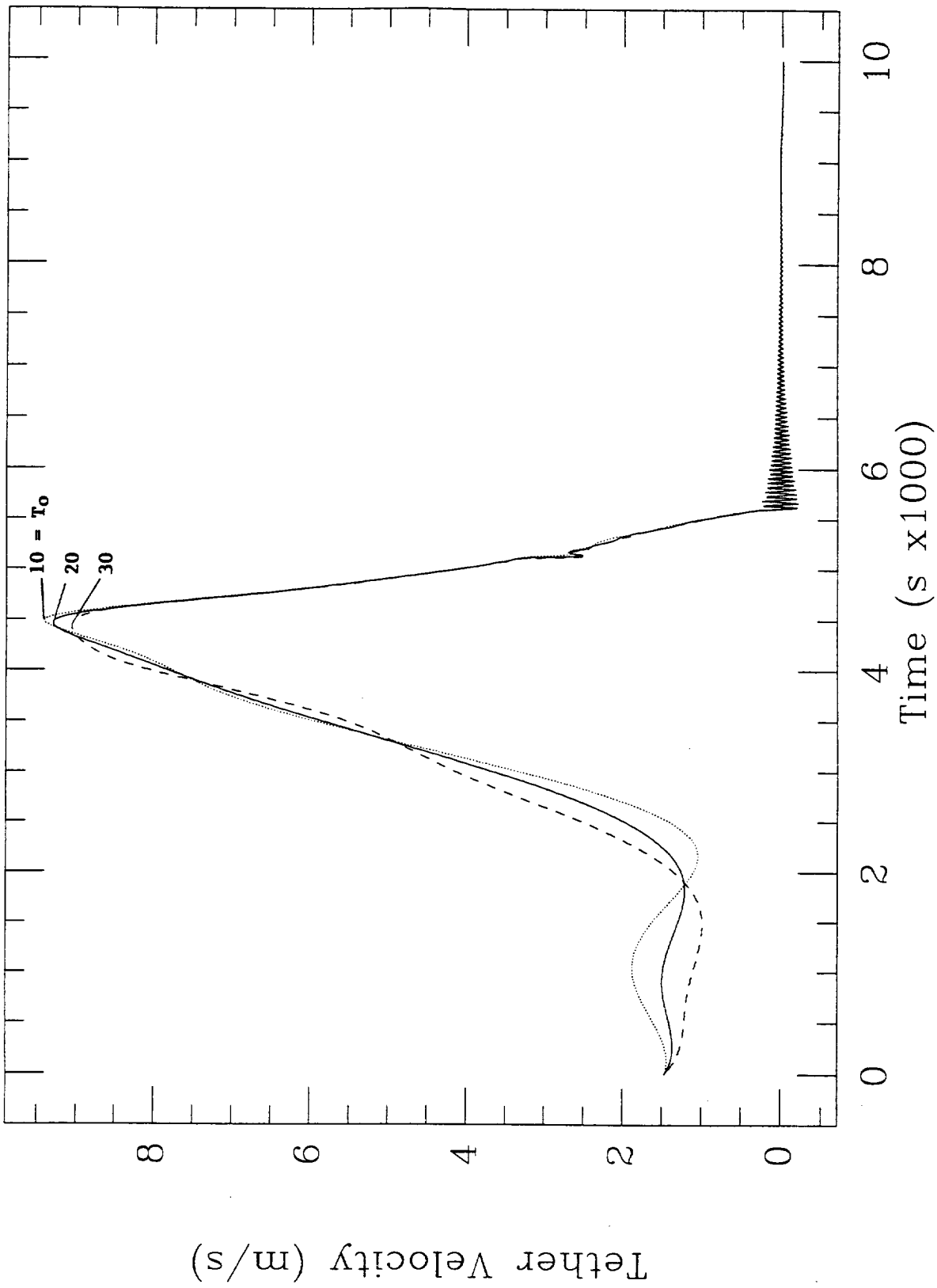


**Fig. 3(d).** Deployment dynamics for SEDS-II-type reference profile 12 (see text).

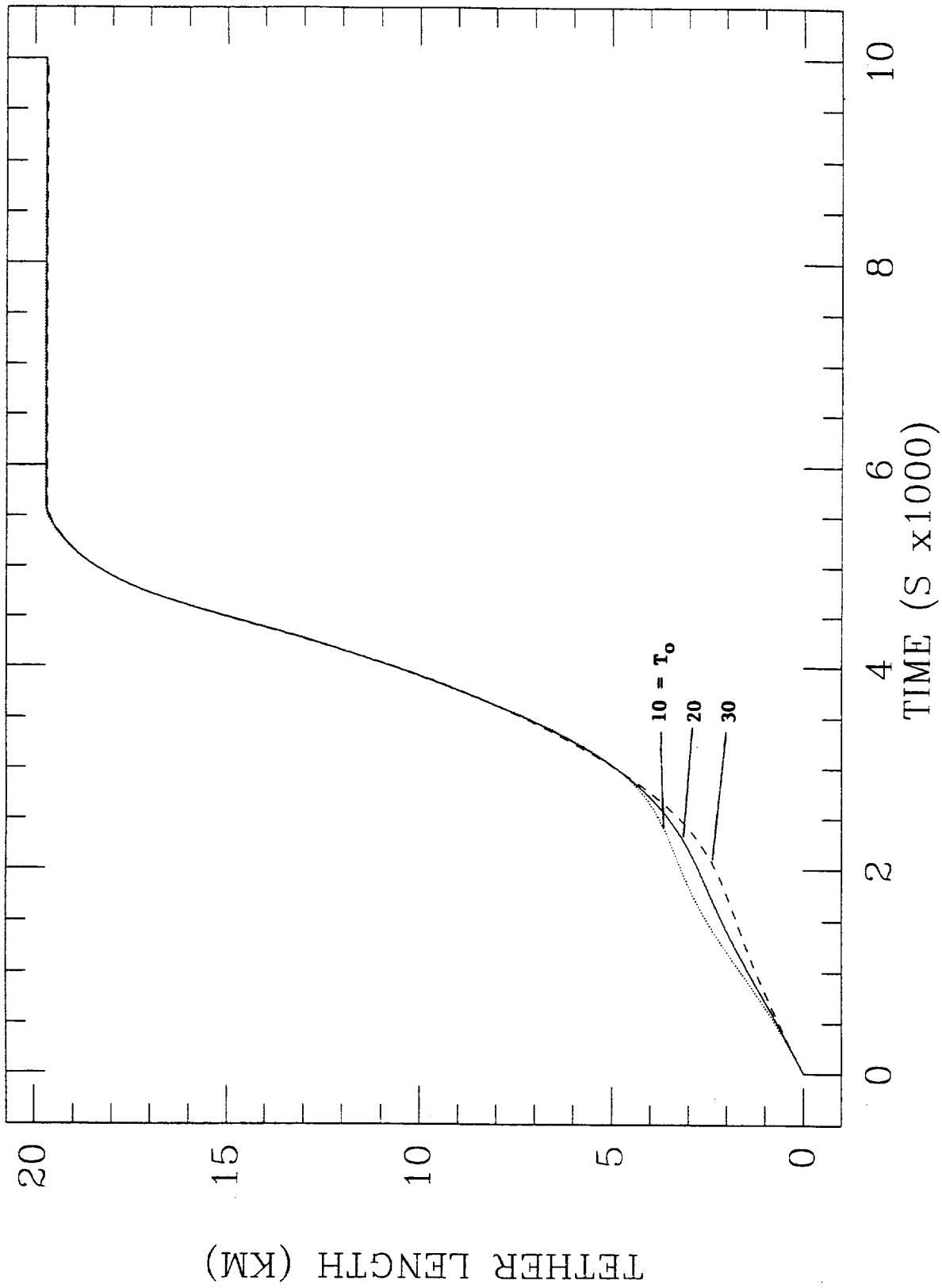


**Fig. 3(e).** Deployment dynamics for SEDS-II-type reference profile 12 (see text).

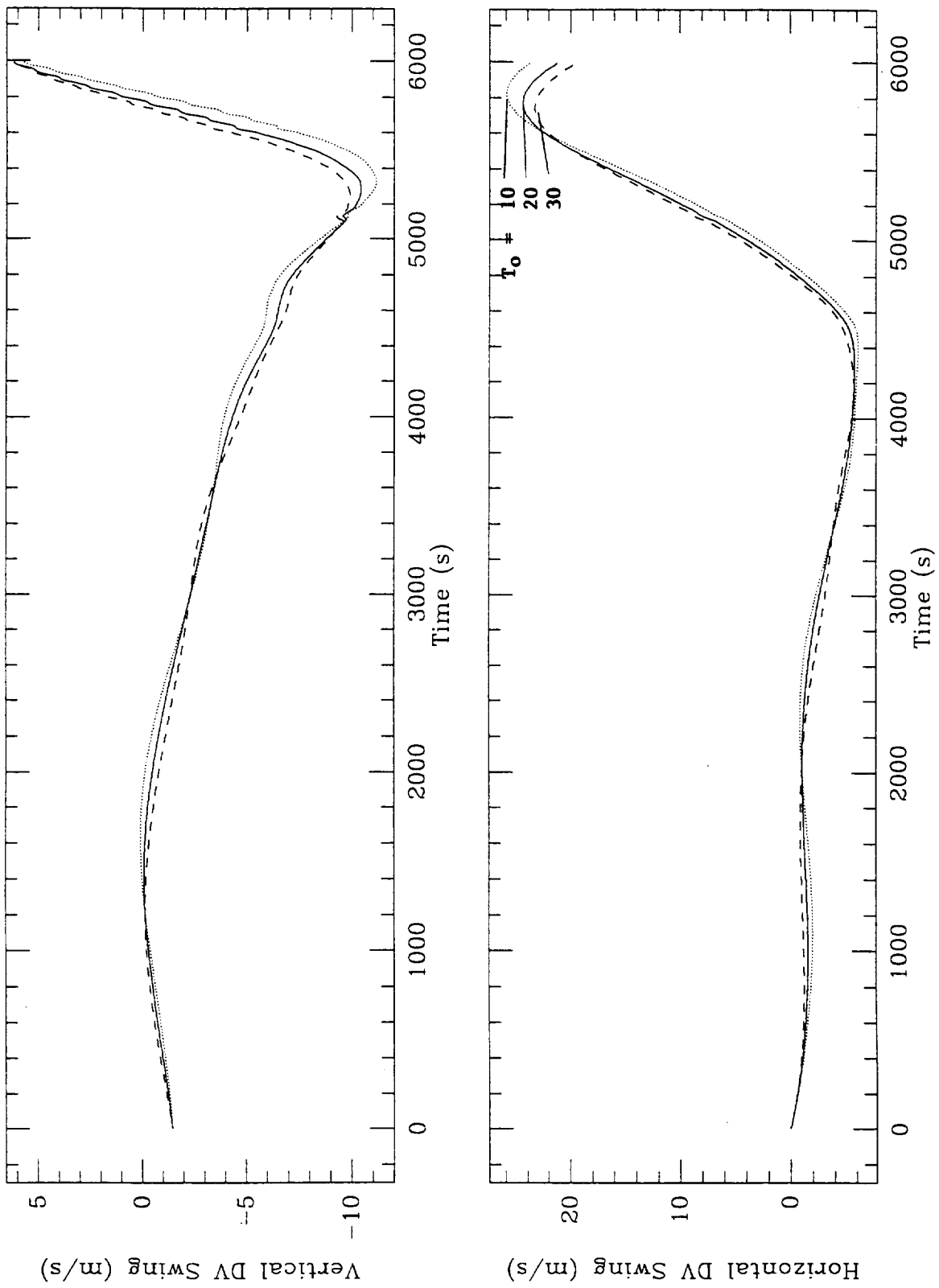


**Fig. 3(f).** Deployment dynamics for SEDS-II-type reference profile 12 (see text).

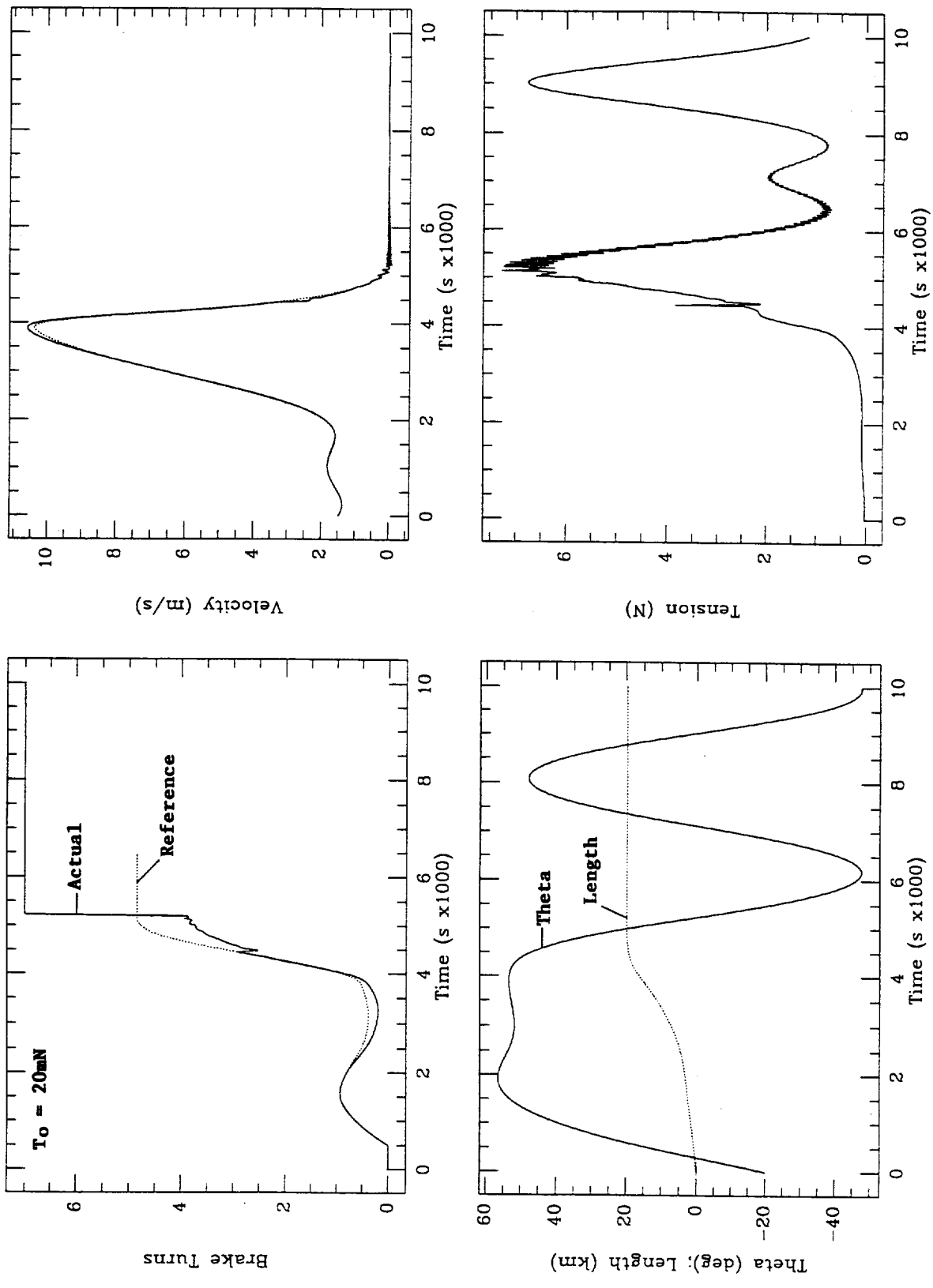


**Fig. 4(a).** Deployment dynamics for SEDS-II-type reference profile 19 (see text).

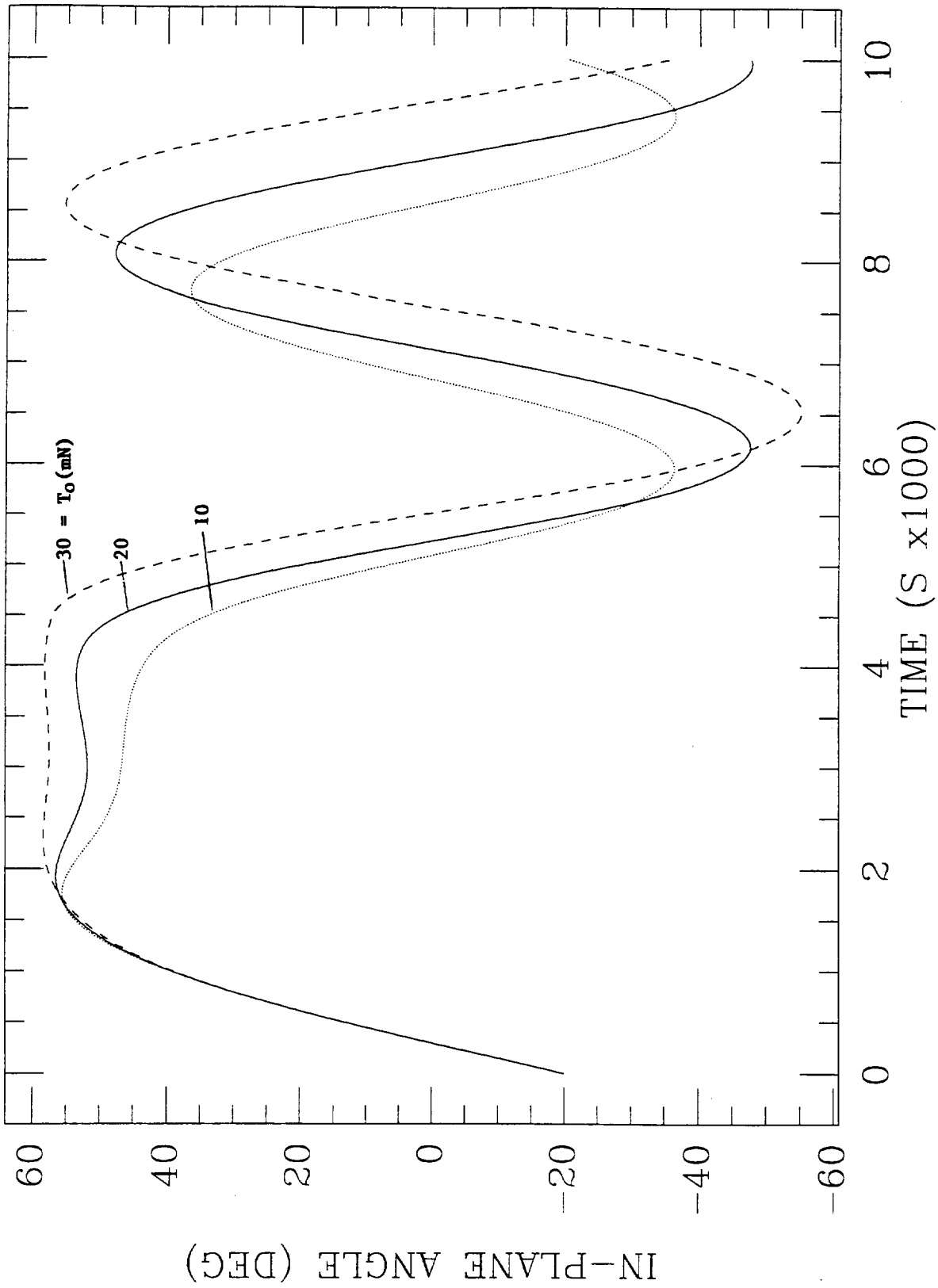


**Fig. 4(b).** Deployment dynamics for SEDS-II-type reference profile 19 (see text).

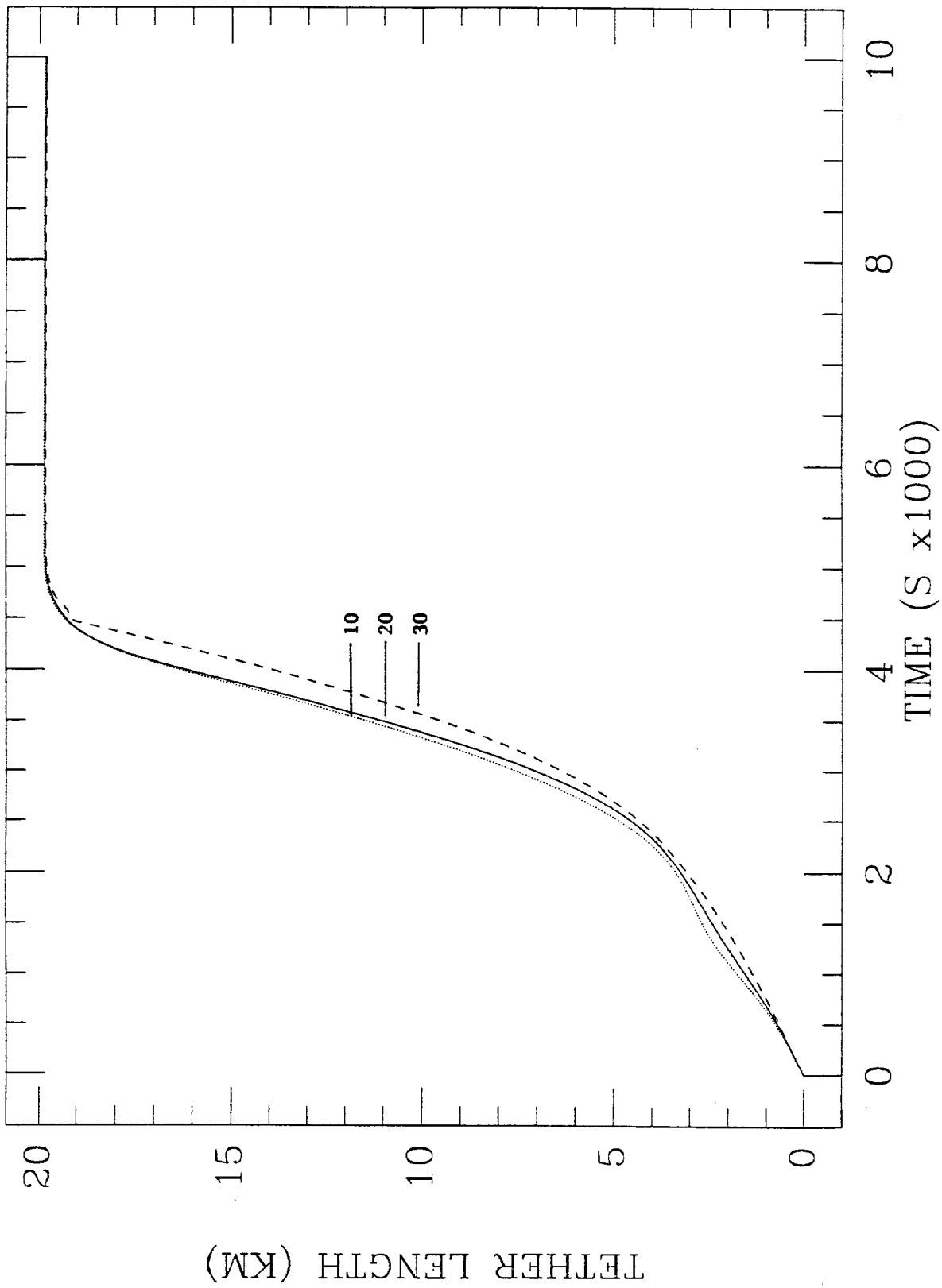


**Fig. 4(c).** Deployment dynamics for SEDS-II-type reference profile 19 (see text).

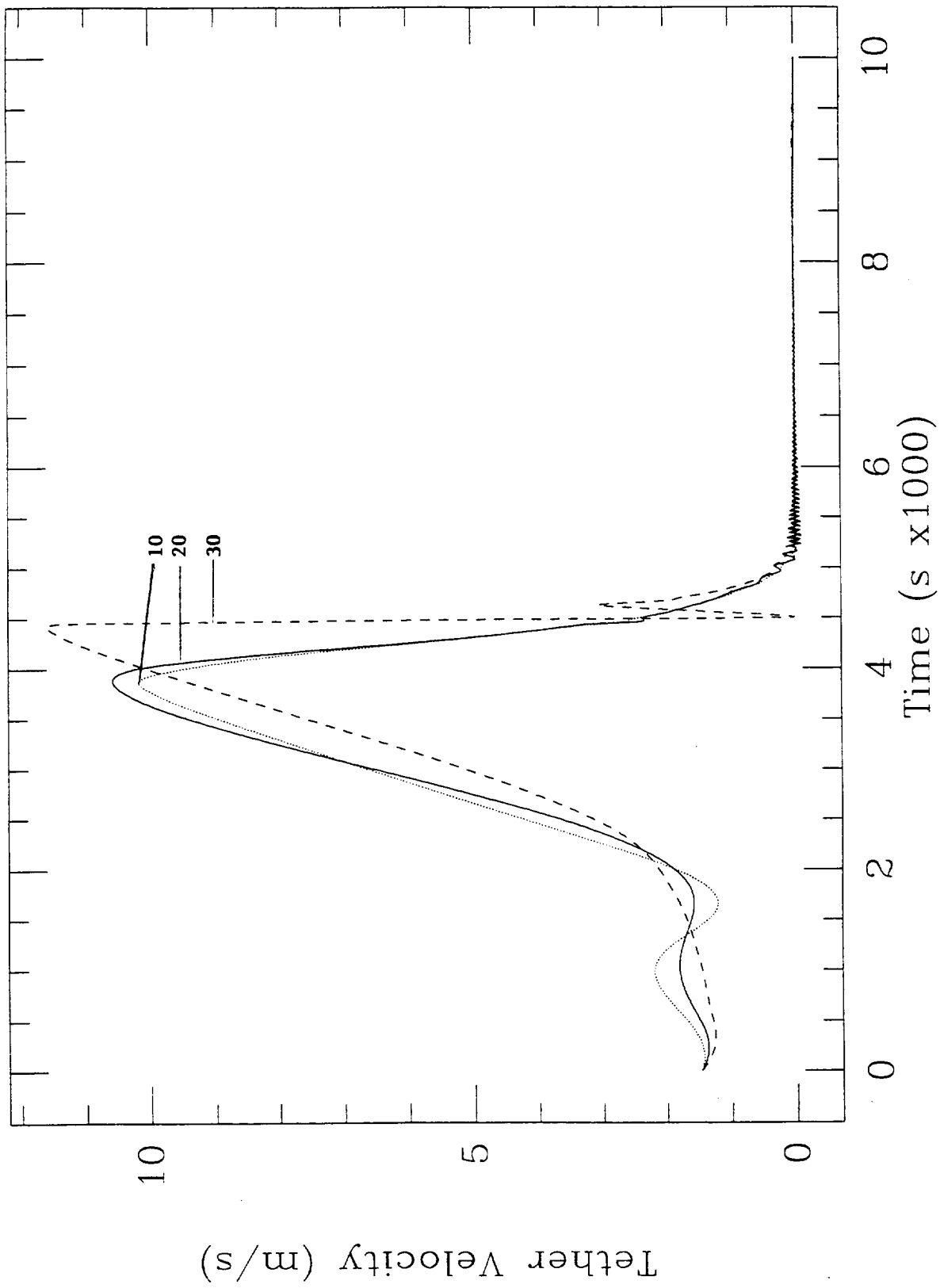


**Fig. 4(d)**. Deployment dynamics for SEDS-II-type reference profile 19 (see text).

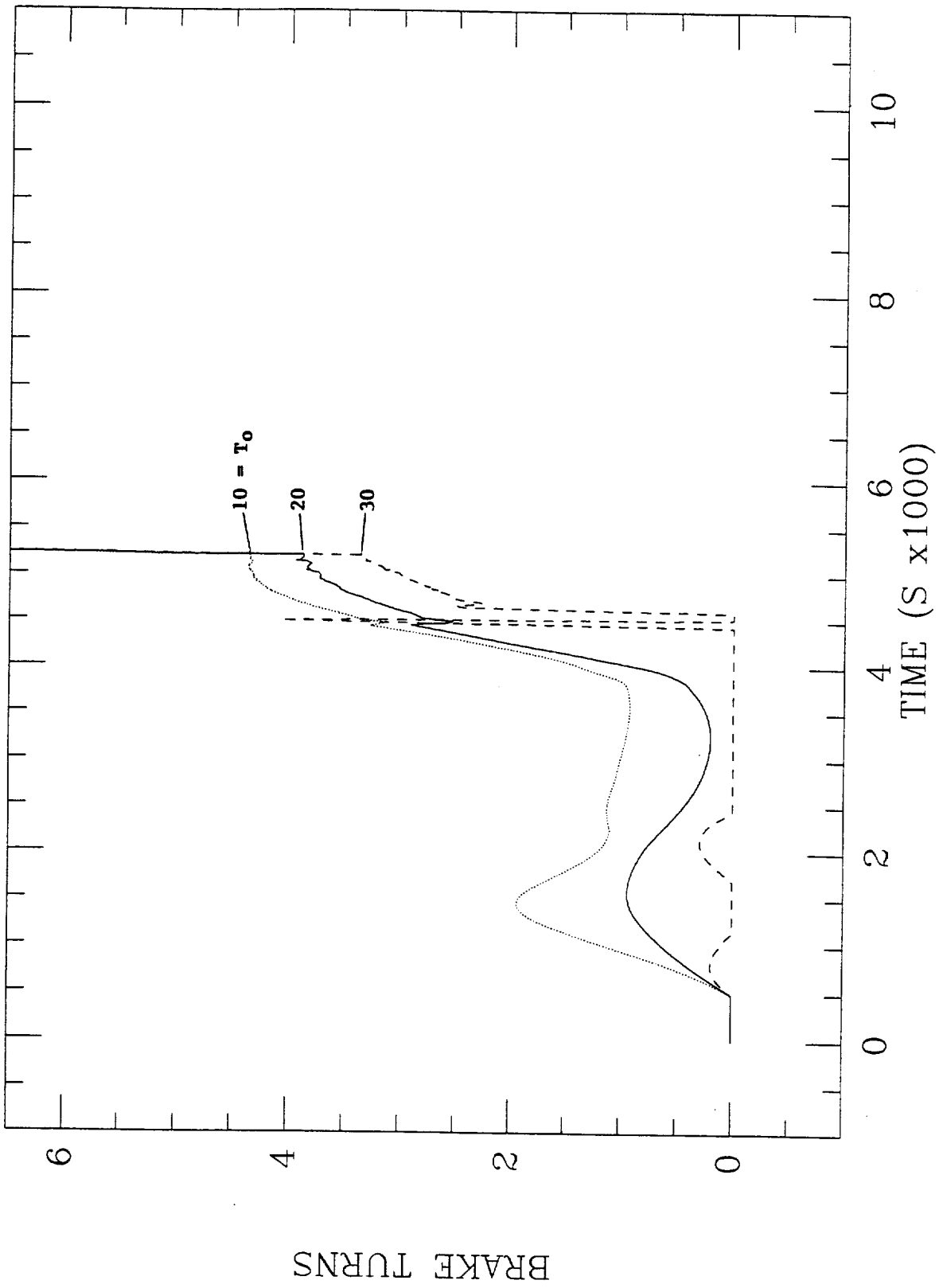


**Fig. 4(e).** Deployment dynamics for SEDS-II-type reference profile 19 (see text).

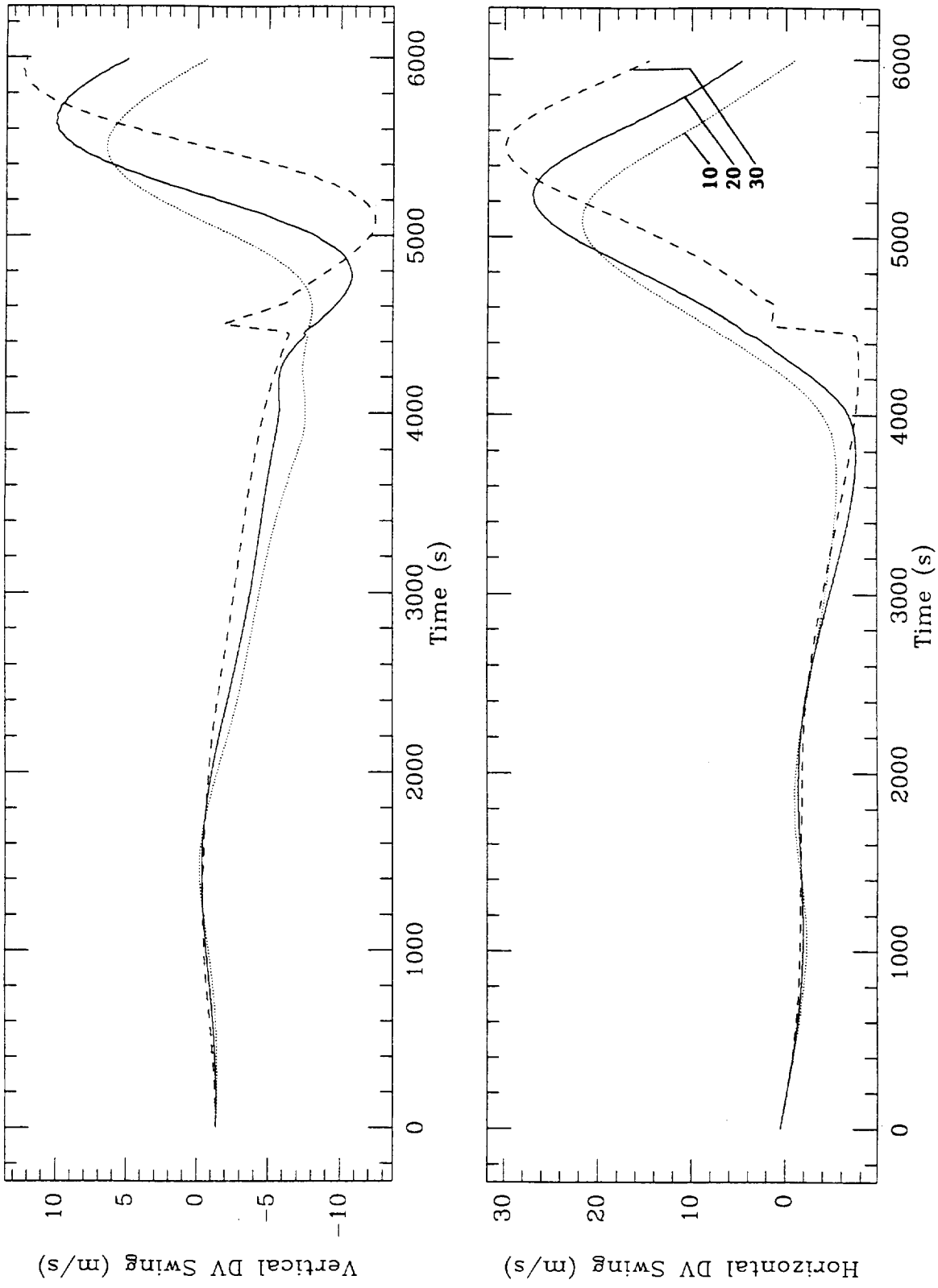


**Fig. 4(f).** Deployment dynamics for SEDS-II-type reference profile 19 (see text).

The ejection angle is $\theta_0$ = -20°, the brake is activated at t = 3840 s (L ≈ 16 km) and the reference value of the minimum tension is 20 mN. The value quoted above for $\Delta V_{CM,H}$ corresponds to a final libration amplitude of about 57°. The deployment dynamics for this case (see Figs. 5(a)-5(f)) shows that the ΔV and the timing at LV crossing are sensitive to variations of the model parameters. The magnitude of the ΔVat LV crossing, however is close to the value required for reaching the desired apogee height.

At this point we must address briefly the stability of the deployment maneuver as SEDS-II and SEDSAT operate in different regions of the phase-space $\theta - \dot{\theta}$: in SEDS-II the in-plane angle was < 45° for most of deployment while in SEDSAT, because of the required ΔV, it must be > 60° for most of the deployment.

The equation of in-plane libration of a two-mass tethered system with respect to an LH-(ascending) LV reference frame, reported here below,

$$\ddot{\vartheta} + 2\frac{\dot{L}}{L}\left(\dot{\vartheta} + \Omega\right) + \frac{3}{2}\Omega^2 sin(2\vartheta) = 0 \tag{20}$$

becomes autonomous for $\dot{L} / L$ = constant, i.e., for exponential (as function of time) maneuvers. Consequently, the stability of solutions can be analyzed in the time-invariant state space $\theta - \dot{\theta}$. Trajectories in the state space with $\theta > 45°$ or $\theta < -45°$ are unstable as they fall into the spheres of influence of two saddle points in the state space [7-8]. Figure 6 shows the phase-space diagram for an exponential deployment (i.e., $L = \alpha \dot{L}$ with α the rate parameter and to every α corresponds an in-plane angle $\bar{\theta}$ with respect to LV which is constant throughout the exponential deployment) with $\bar{\theta}$ = 15°. When the rate parameter and, consequently, $\bar{\theta}$ are increased to 45°, the two saddle points of Fig. 6 move to the + 45° and -45° points, respectively. In this situation, the stability margin is lost because the deployment trajectories are necessarily around the saddle points. The analysis in Refs. [7-8] applies, strictly speaking, to exponential maneuvers. Reference profiles for the SEDS-II-type control law are for a large portion exponential. The stability analysis above, therefore, provides indications about the stability of close-to-exponential reference profiles to be confirmed with dynamics simulations.

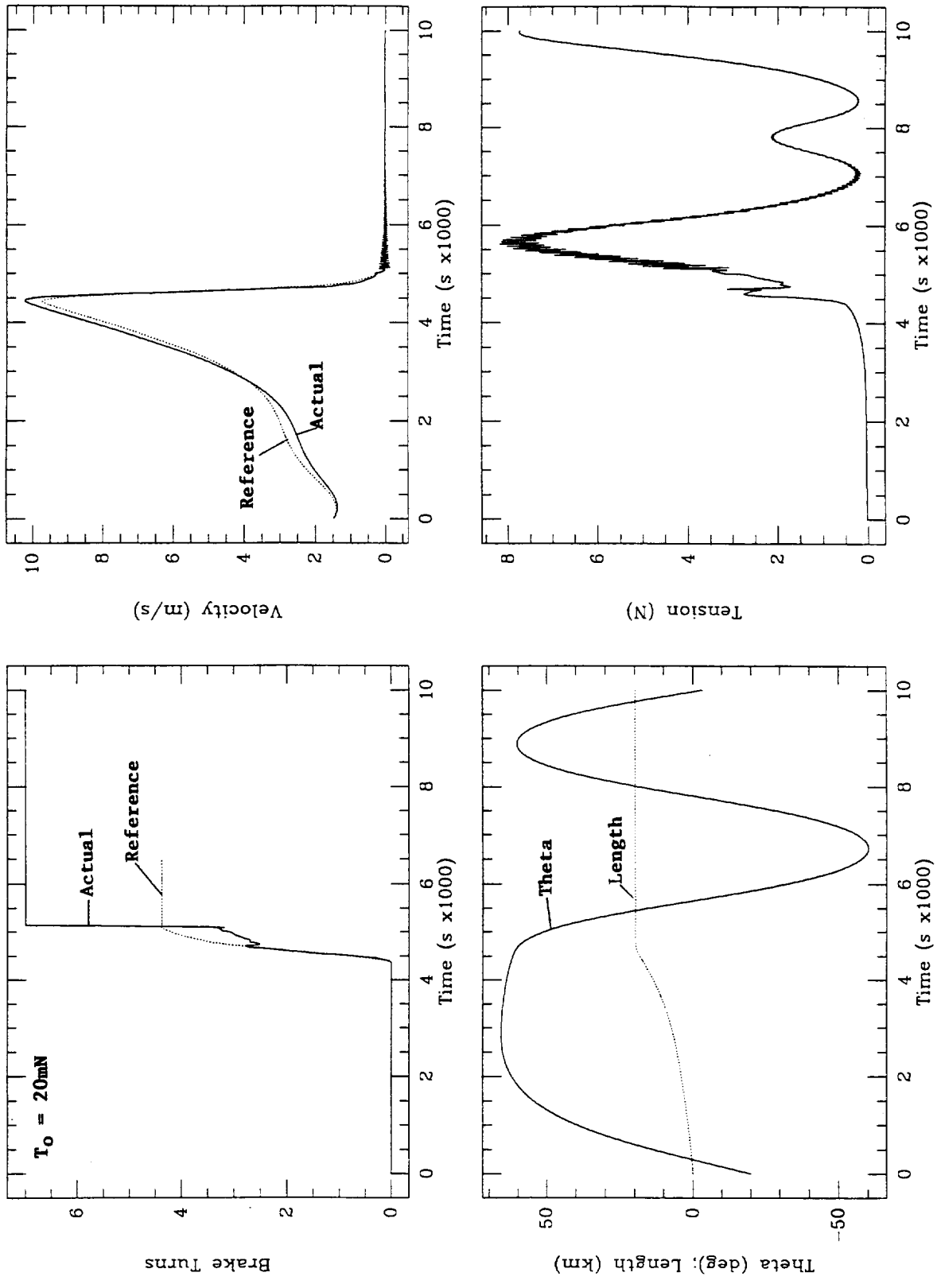


**Fig. 5(a)**. Deployment dynamics for SEDS-II-type reference profile 24 (see text).

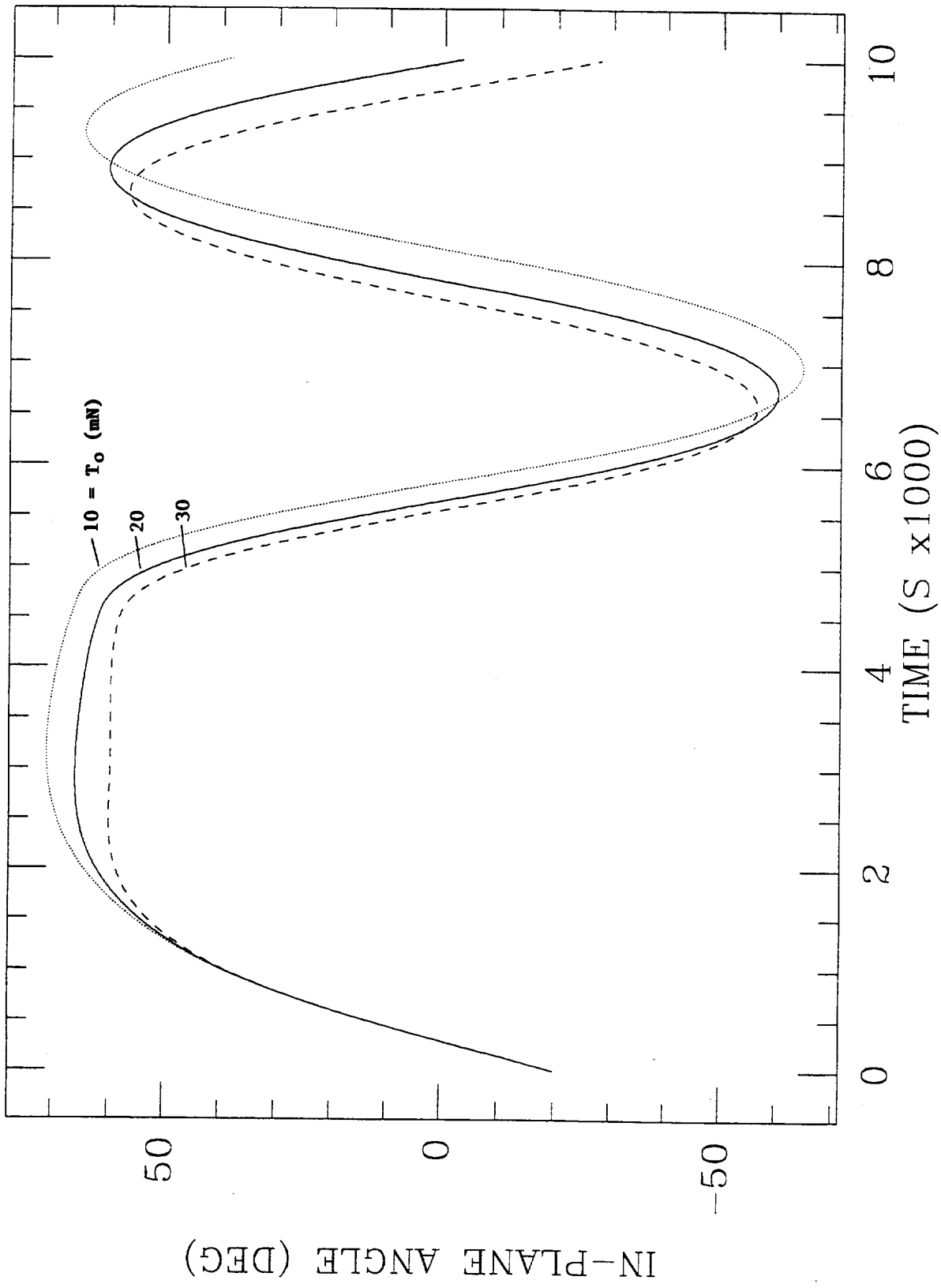


**Fig. 5(b).** Deployment dynamics for SEDS-II-type reference profile 24 (see text).

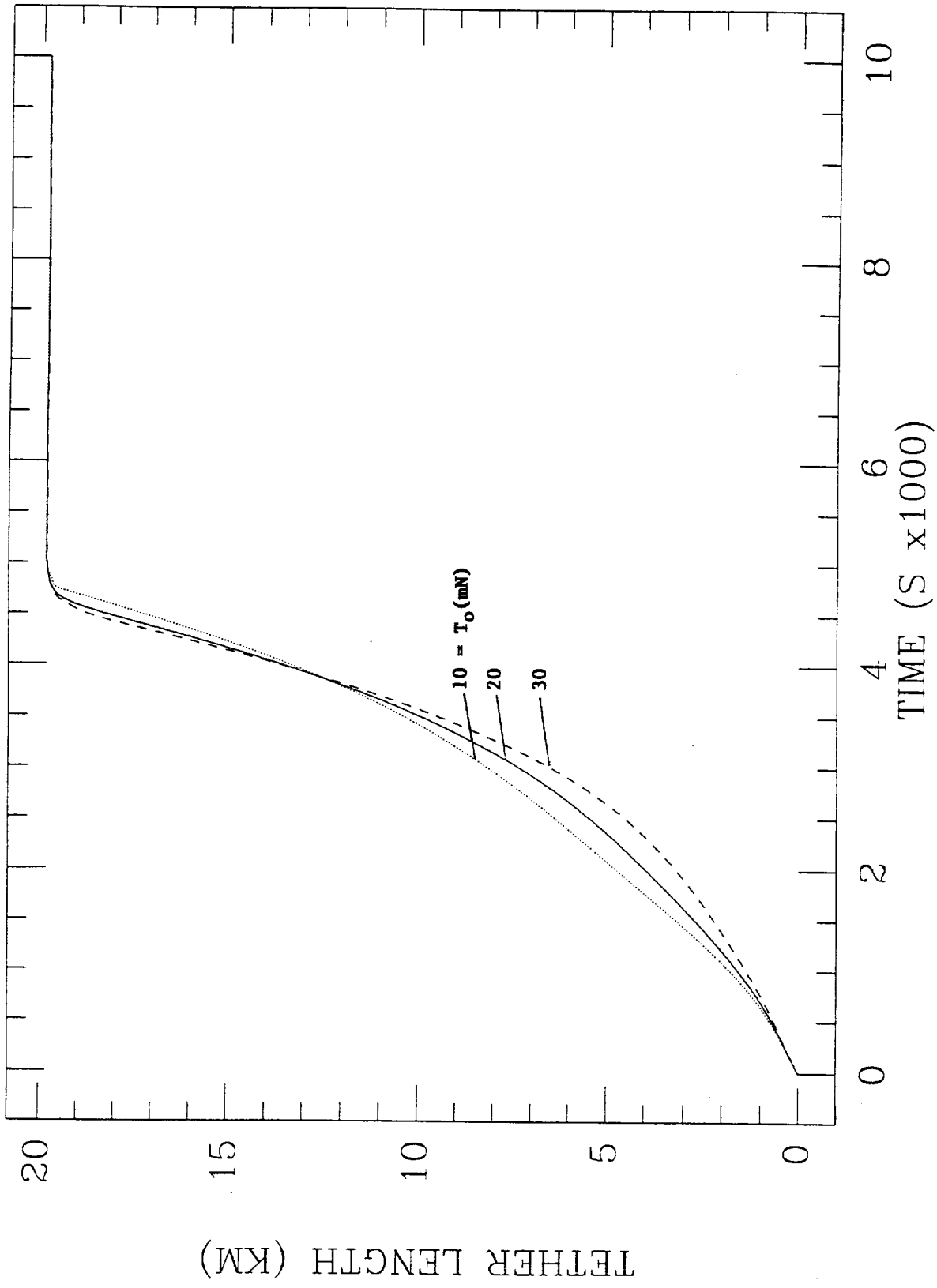


**Fig. 5(c).** Deployment dynamics for SEDS-II-type reference profile 24 (see text).

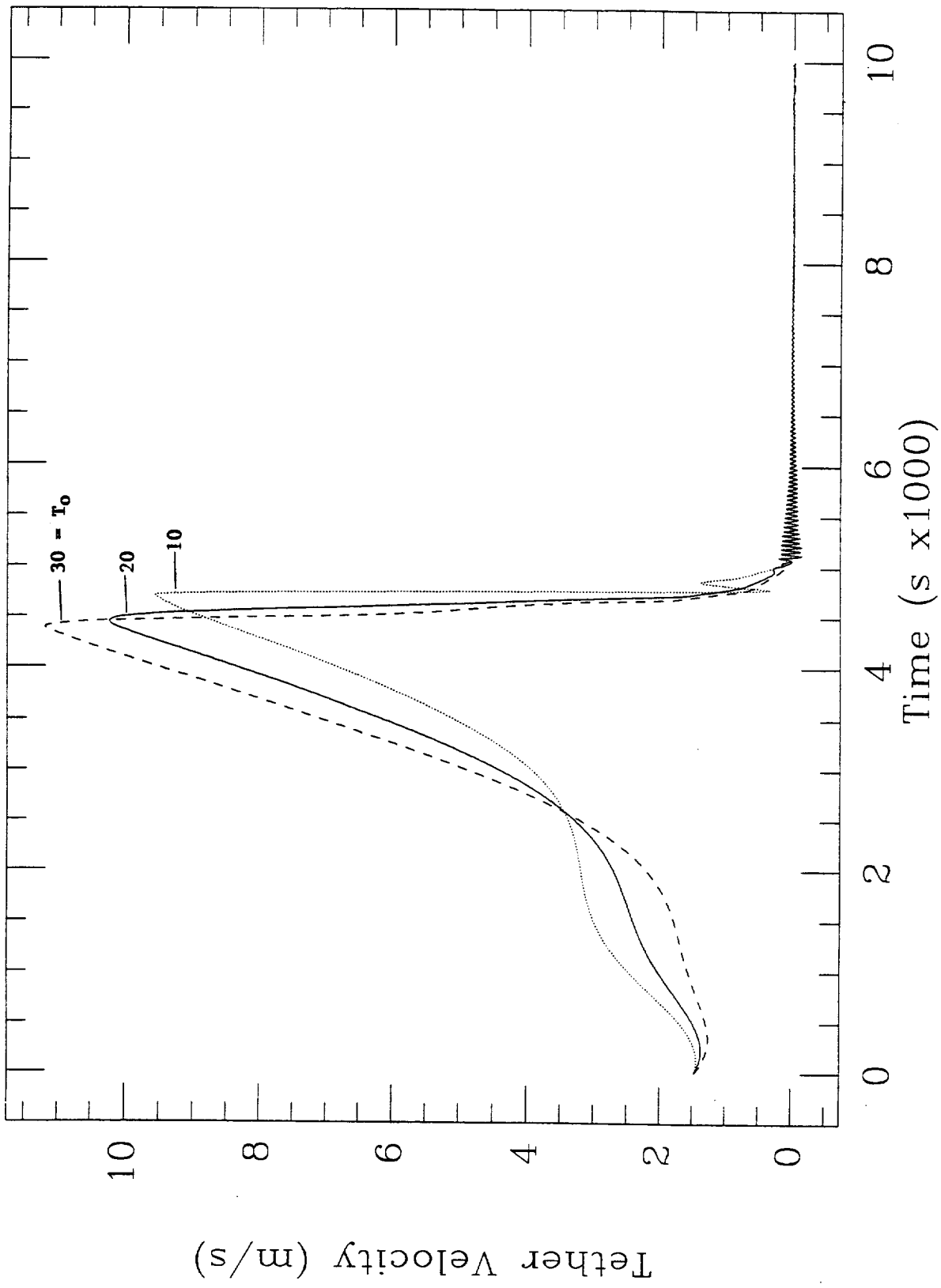


**Fig. 5(d).** Deployment dynamics for SEDS-II-type reference profile 24 (see text).

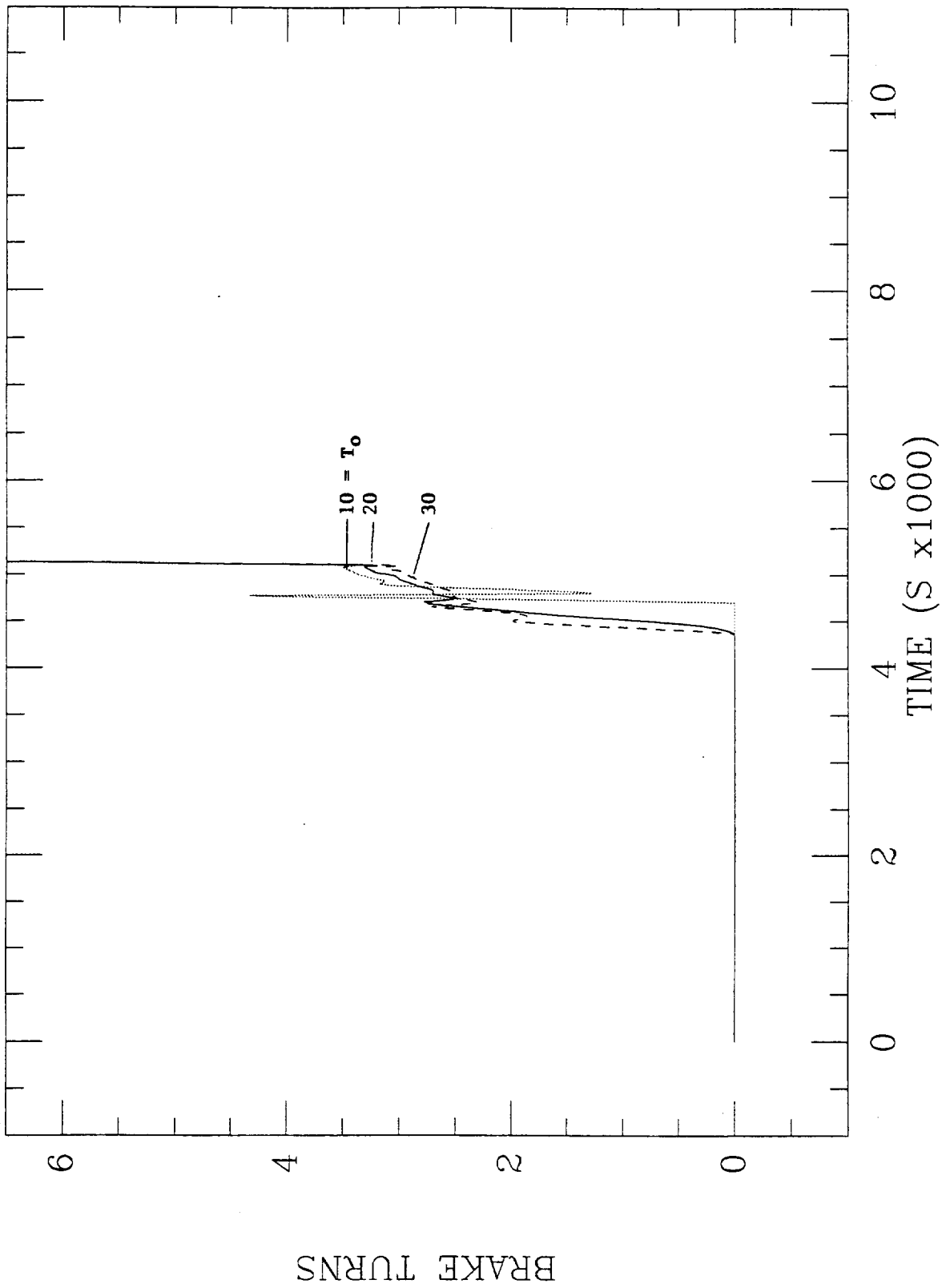


**Fig. 5(e).** Deployment dynamics for SEDS-II-type reference profile 24 (see text).

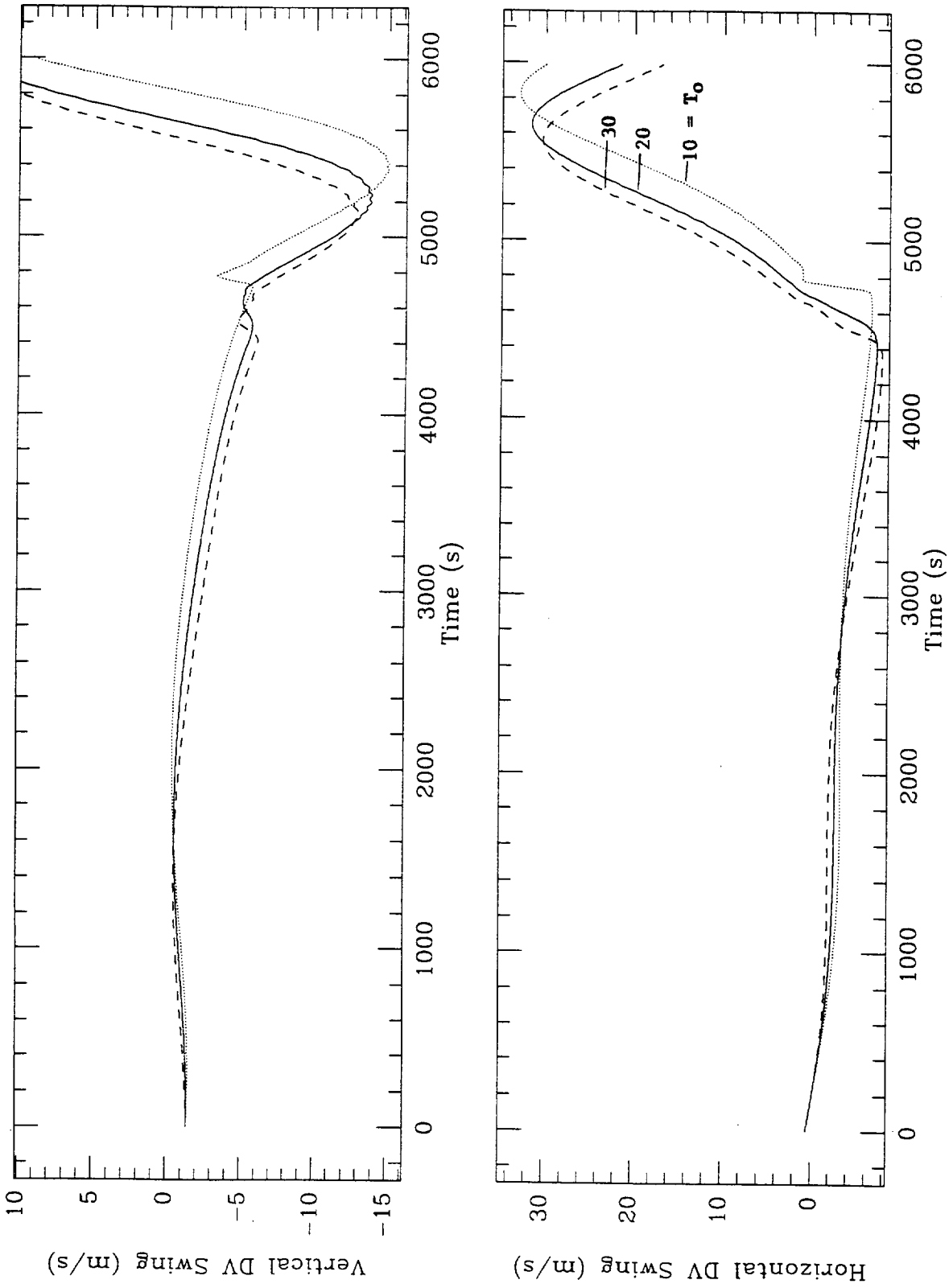


**Fig. 5(f)**. Deployment dynamics for SEDS-II-type reference profile 24 (see text).

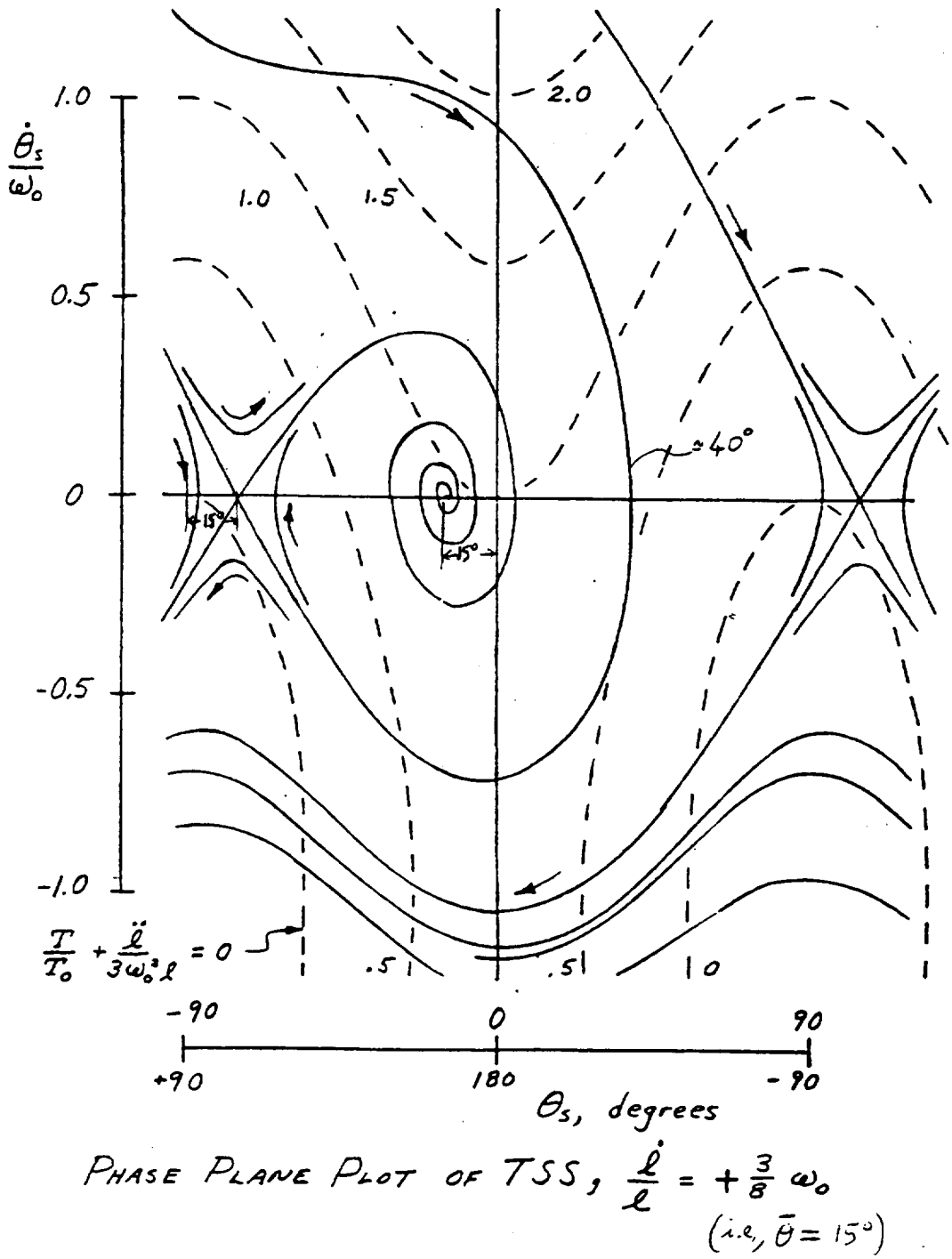


**Fig. 6**. Phase-space $\theta - \dot{\theta}$ for exponential deployment maneuvers (from Ref. 7).

New Deployment Control Law

All attempts at controlling SEDSAT with the strategy adopted for SEDS-II resulted in an unstable response of the in-plane angle and, consequently, in an unsatisfactory robustness of the control law with respect to variations of the deployer model's parameters. Satisfactory results, as shown earlier, could be obtained only for final libration angles < 45°(which are too small for providing the required $\Delta V$ at release) confirming the conclusions of the time-invariant stability analysis of Refs. [7-8].

A different control strategy was followed for SEDSAT aimed at obtaining a high $\Delta V$ (and hence a high final libration angle) and, at the same time, satisfactory insensitivity to variations of the model parameters.

The sensitivity of the $\Delta V$ at release vs the initial conditions at satellite ejection for different values of the deployer model's parameters was analyzed numerically by using two different simulators for tethered systems dynamics [8-10]. The analysis of the sensitivity of the final libration angle (which is related to $\Delta V_H$) to the initial conditions at satellite ejection from the Shuttle was carried out by J. Pelaez, visiting the Smithsonian Astrophysical Observatory from the Politechnical University of Madrid. The results are plotted in Fig. 7 vs the non-dimensional tension parameter

$$\Lambda = \frac{m\, L_{End}\Omega^2}{T_0} \tag{21}$$

It is interesting to notice that for values of the ejection velocity $V_0 > 3.88$ m/s, there are suitable values of the ejection angle for which the desired final libration amplitude is independent of variations of the minimum tension. However, these value of the ejection velocity are too high for Shuttle deployment operations in which the possibility of a tether and satellite rebound at short range is a paramount safety concern.

Since the ejection velocity must be lower than 1.5 m/s for Shuttle safety considerations, a second analysis was done by setting the ejection velocity at the nominal 1.47 m/s (provided by the current SEDS ejection system) and by analyzing the sensitivity of the time from satellite ejection to the crossing of LV vs the ejection angle.

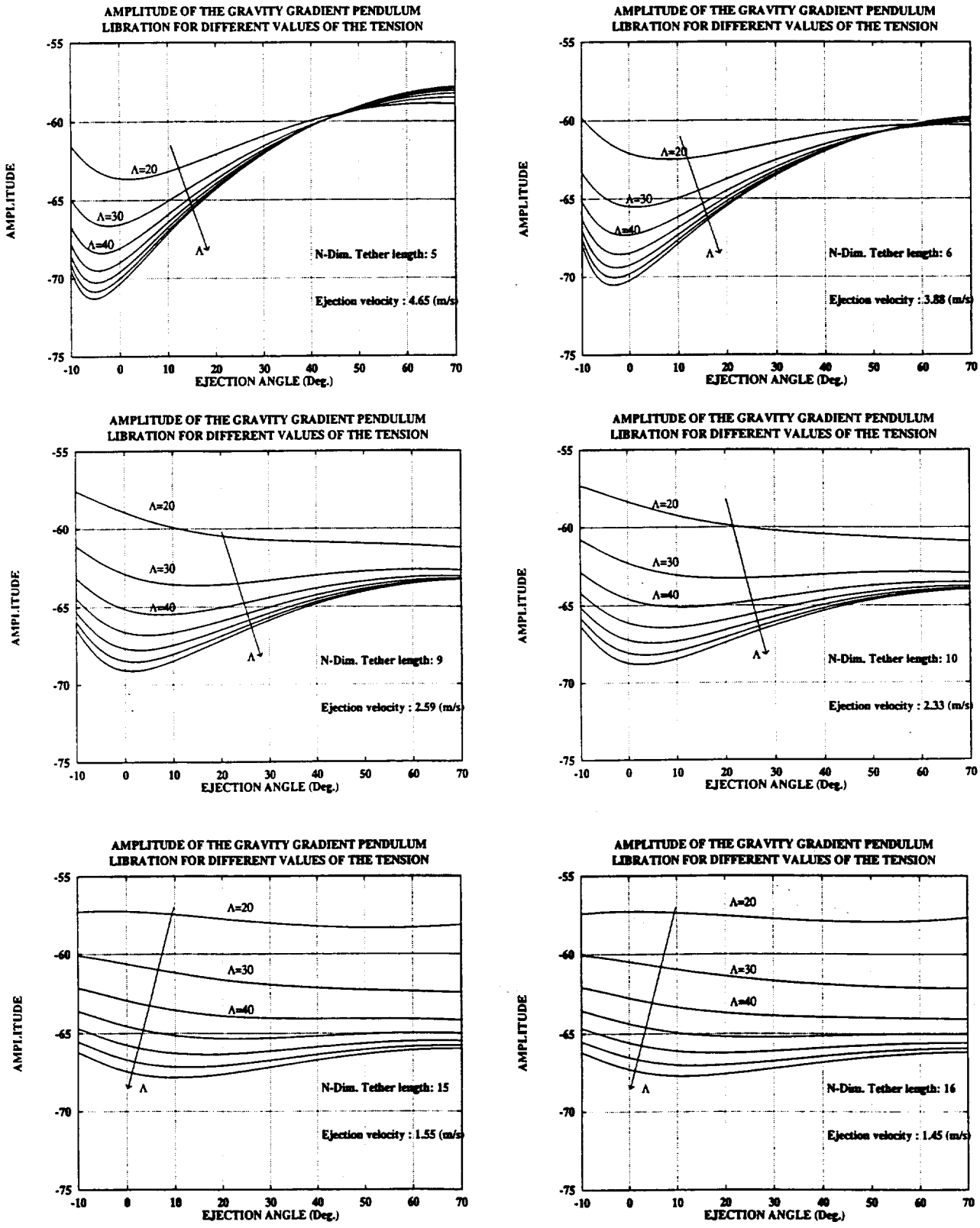


**Fig. 7.** Final libration amplitude vs ejection angle for different values of the non-dimensional minimum tether tensions and ejection velocities.

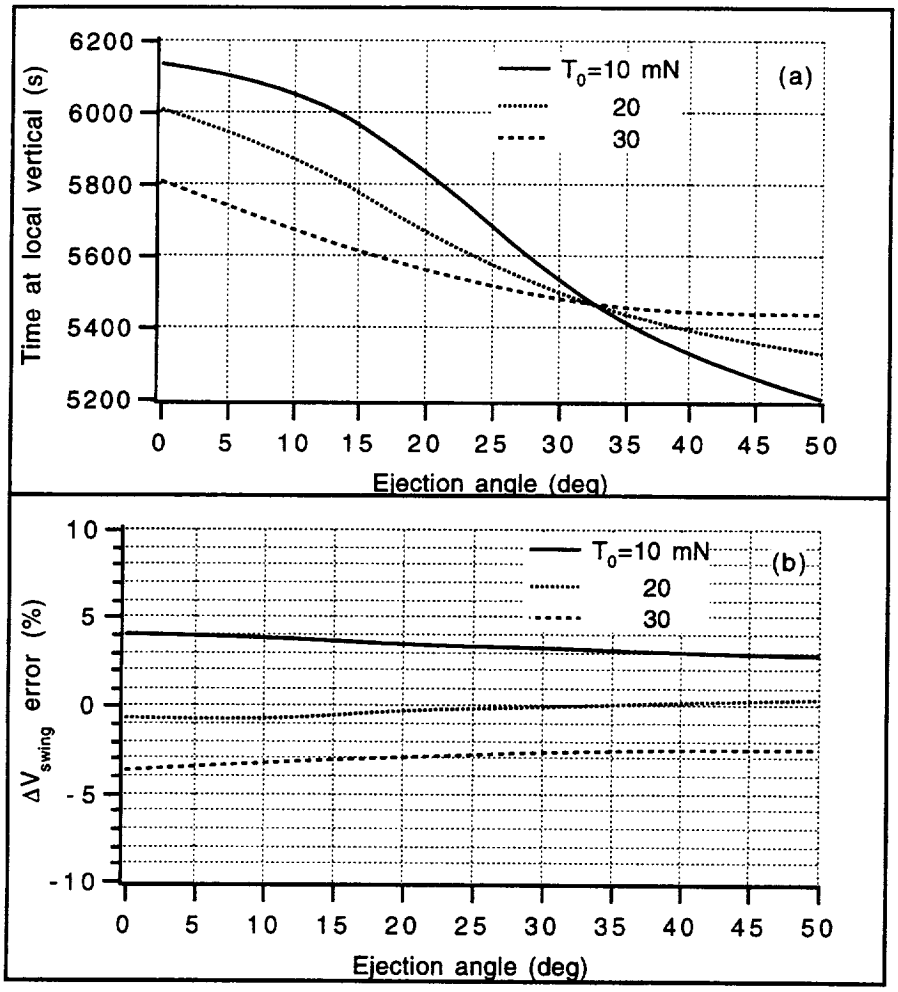


**Figs. 8**. Sensitivity of deployment maneuver to the ejection angle $\theta_0$ of the satellite for $V_0$ = 1.47 m/s: (a) time of tether crossing LV and (b) percent error of $\Delta V_{swing}$ (see text) at LV crossing.

The results of this second analysis are summarized in Figs. 8 which show: (a) the time of the tether crossing LV vs the in-plane ejection angle $\theta_0$ at the start of deployment for different values of $T_0$ and (b) the percent error of the $\Delta V_{swing}$ (the *swinging* component) at satellite release vs $\theta_0$. The error affecting the *hanging* component $L_{CM}\Omega$ in eqn. (8), which is not shown here, is usually negligible with respect to the error affecting the swinging component.

It is clear from Fig. 8(a) that the time of LV crossing is independent of the minimum deployer's tension $T_0$ for an ejection angle $\theta_0 \approx 32°$ (differently from the convention used previously, the plus sign means in the forward direction). Moreover, the tether length is also independent of the static deployer's tension for $\theta_0 \approx 32°$ (see Fig. 9). Consequently, preserving the timing to reach LV requires smaller ejection velocities than preserving the final libration amplitude (and $\Delta V$ at LV crossing). If the former solution is implemented the $\Delta V$ at LV will vary with a change of the minimum tension but the error affecting the $\Delta V$ is within the desired bounds for the expected range of minimum tensions. In conclusion, the braking phase should start as late as possible during deployment in order to preserve the stable timing of the overall deployment maneuver obtained through the previous selection of the initial conditions. It is readily seen from Fig. 9 that any braking action taking place after $t \geq 4000$ s would have a small impact on the time sensitivity of the maneuver.

The slowing down of the deployment velocity is accomplished by means of the non-linear control law developed for SEDS-II [11]. However, contrary to SEDS-II, this (late) braking phase has a very small effect on the libration angle, as it primarily affects the tether speed profile close to the end of deployment. The addition of the braking phase to the free deployment shifts slightly the value of $\theta_0$ insensitive to $T_0$ from 32° to 31° which will be the value adopted from now on. Consequently, most of the deployment of SEDSAT is carried out without any active control and the brake is activated only in the last 16-20 km of deployed tether length solely for reducing the tether exit velocity to zero. The braking phase is accomplished with a feedforward-feedback control law which is robust with respect to variations of the deployer's friction parameters. The tether libration is minimally affected by this late braking phase whereas the insensitivity of the velocity vector and timing at release is provided by a suitable set of initial conditions at the start of deployment.

The reference profiles for the SEDSAT deployment control law were derived by imposing that the brake is activated for $t \geq 4000$ s (i.e., $L \geq 16$ km) with the following final state vector:

$$L = 20 \text{ km}, \ \dot{L} = 0.1 \text{ m/s}, \ \theta = 0, \ \dot{\theta} = 0.09 \text{ deg/s}.$$

The final libration speed was weighted very lightly in the cost function of the optimization procedure [9] because, as previously mentioned, it is no longer dependent on the braking action but rather on the initial conditions at satellite ejection.

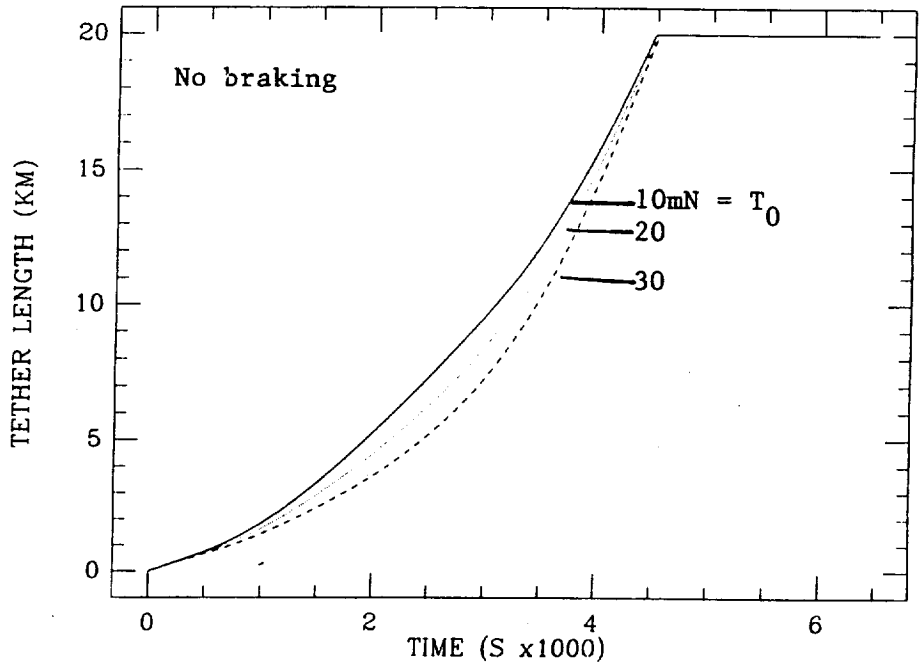


**Fig. 9**. Tether length vs time for different static tension values (no braking).

The initial conditions at ejection are as follows:

$\theta_0 = -31°$ (upward and forward) and $V_0 = 1.47$ m/s.

Because of a slight increase of the SEDSAT satellite, a mass = 34 kg is adopted in deriving reference profile 39. Also the feedback gains are $k_1 = 0.002$ and $k_2 = 0.2$ (like in SEDS-II) in order to limit the reaction of the control law to the sling/scrub transition. The brake is activated at t = 4000 s ($L \approx 16$ km) and the reference value of the minimum tension is 20 mN. The value of $\Delta V_{CM,H}$ at LV crossing is 32 m/s which corresponds to a final libration amplitude of about 63°. By adding the hanging component $\Omega L_{CM}$, the total $\Delta V$ at release is 53 m/s. The deployment dynamics is shown in Figs. 10(a)-10(f). The $\Delta V$ and the timing at LV crossing are now insensitive to variations of the minimum deployer's tension. The magnitude of the $\Delta V$ at release is sufficient for reaching the desired apogee height.

Reference profile 39 and the parameters of the associated control law are summarized in Appendix A of this report.

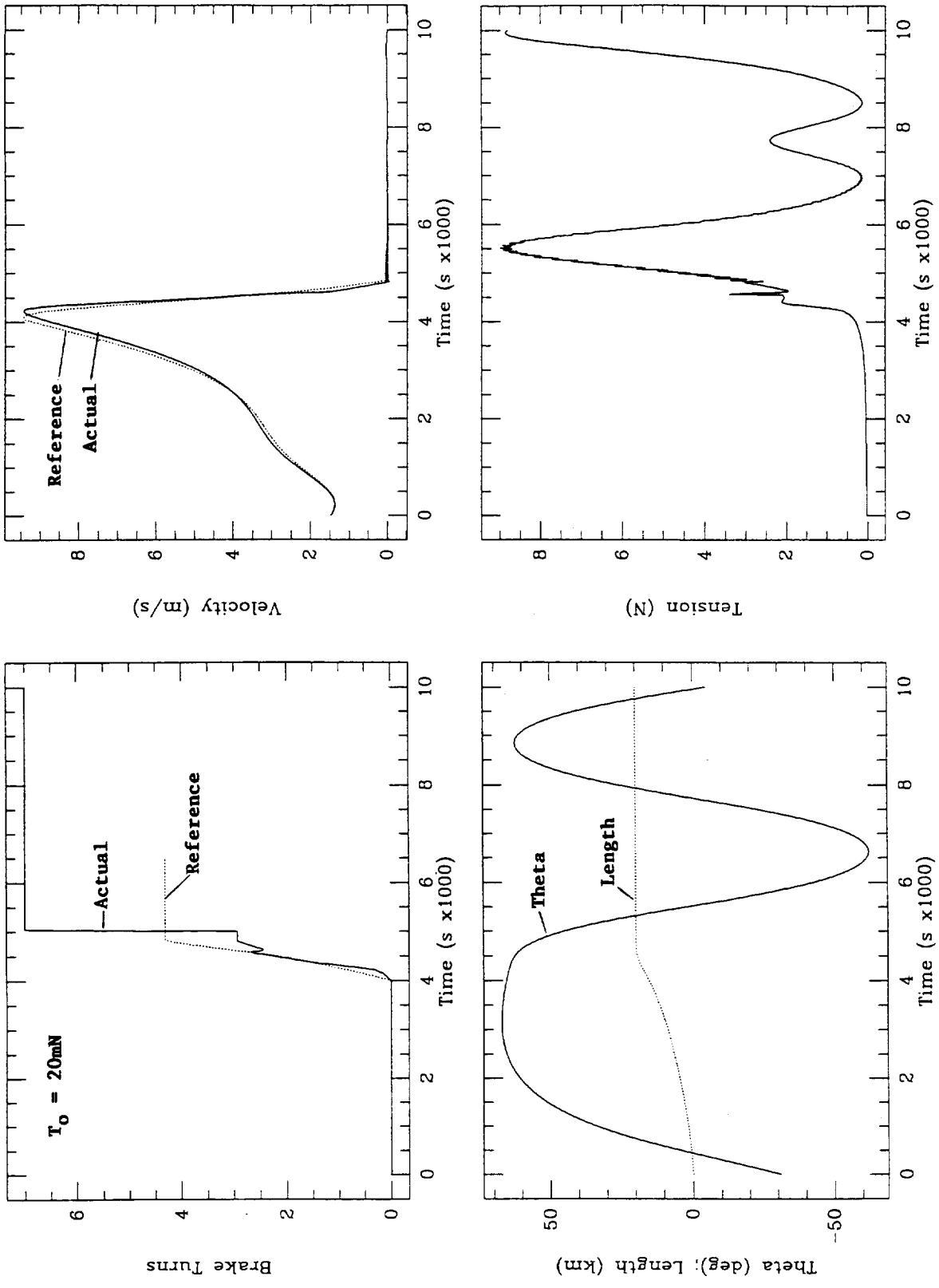


**Fig. 10(a)**. Dynamic response of SEDSAT during deployment for reference 39 (see text).

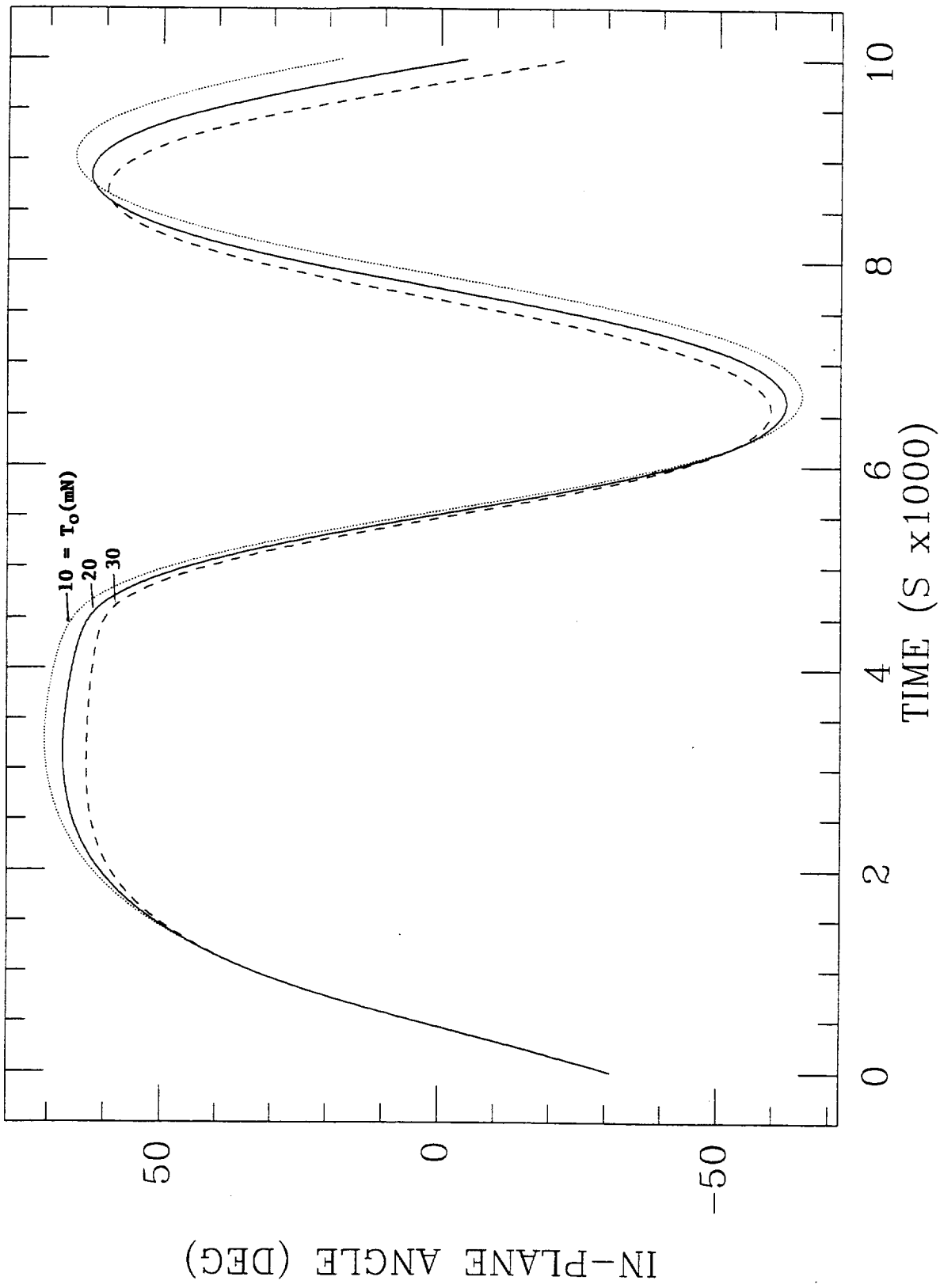


**Fig. 10(b).** Dynamic response of SEDSAT during deployment for reference 39 (see text).

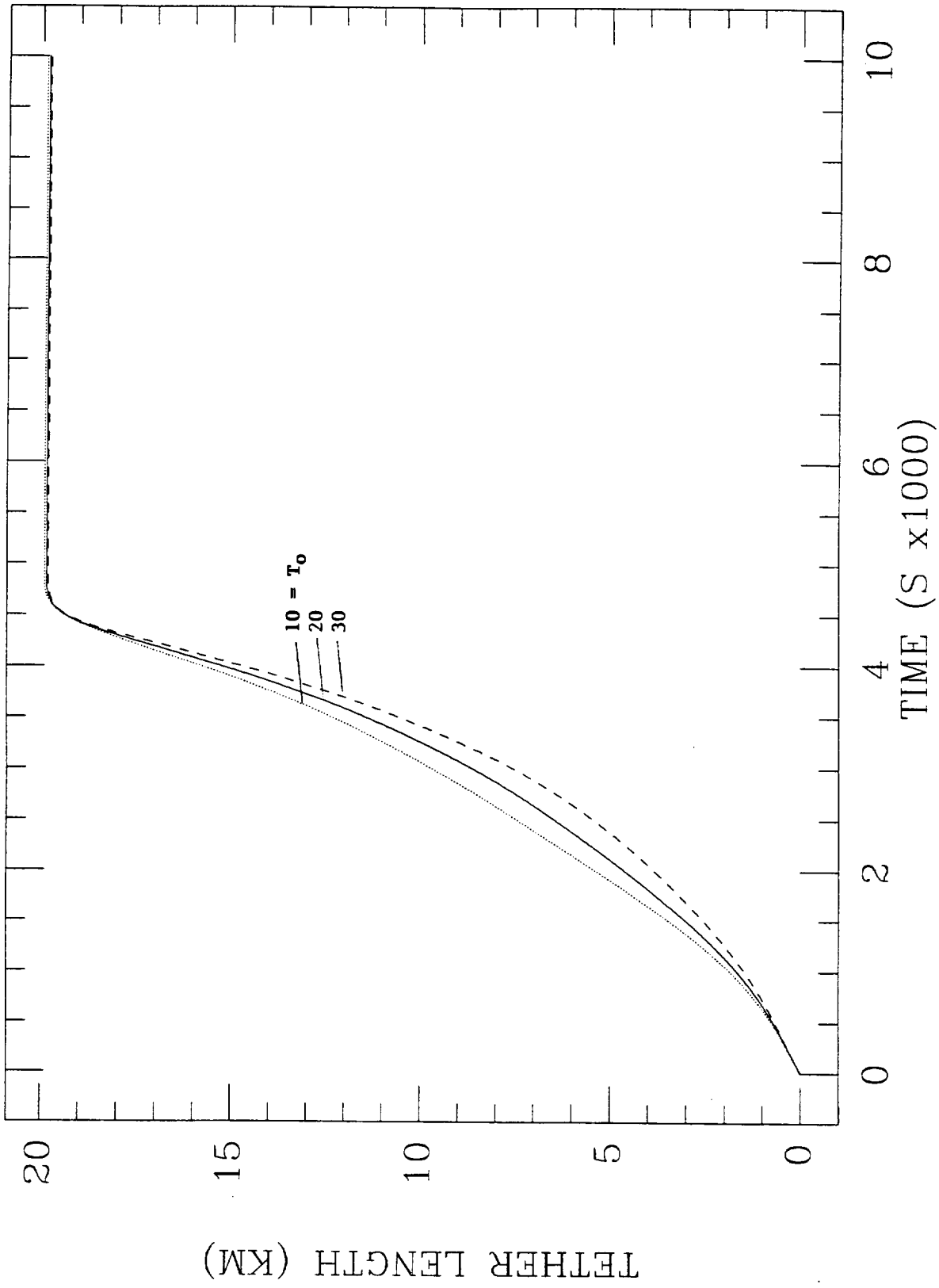


**Fig. 10(c).** Dynamic response of SEDSAT during deployment for reference 39 (see text).

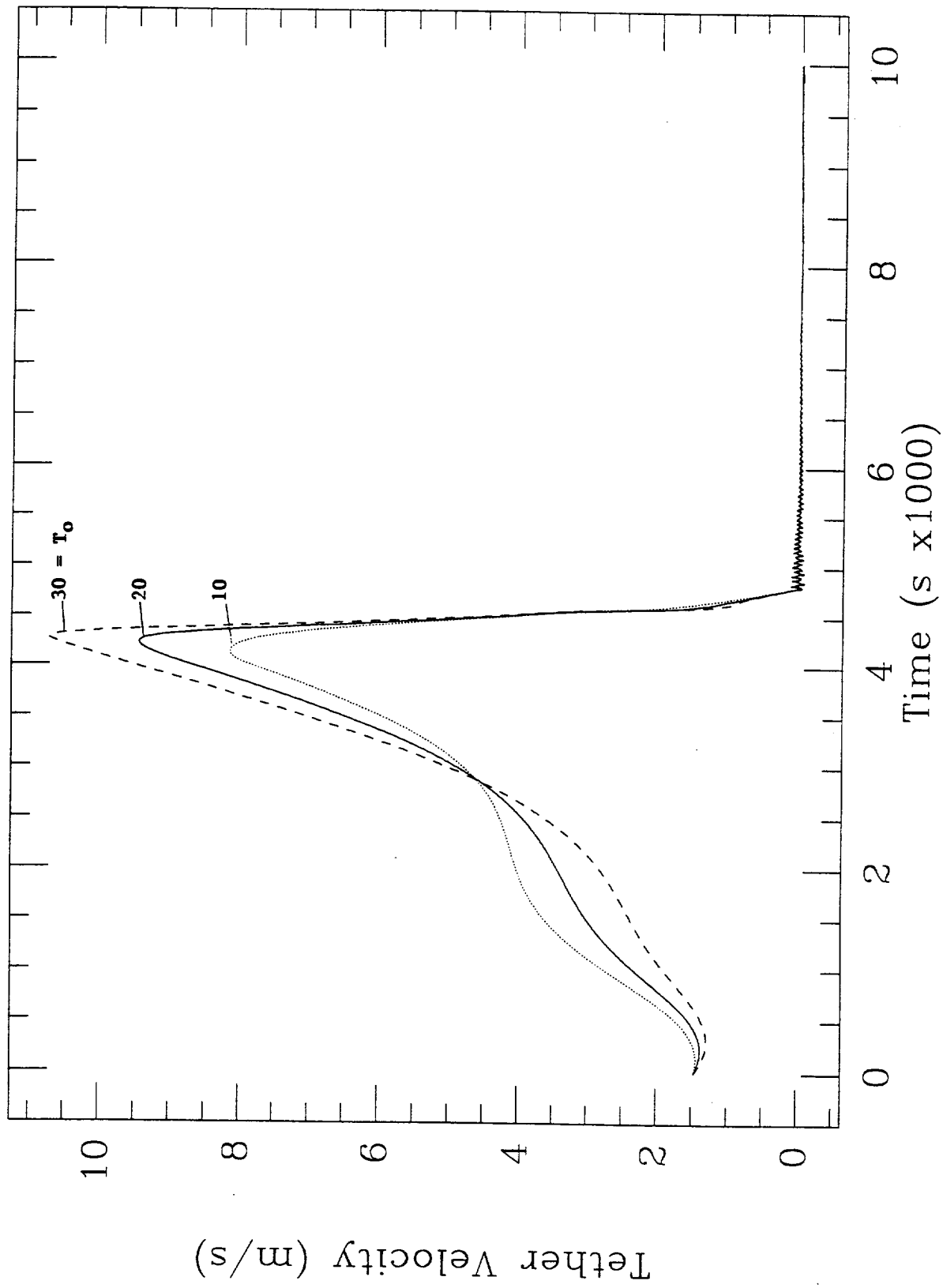


**Fig. 10(d).** Dynamic response of SEDSAT during deployment for reference 39 (see text).

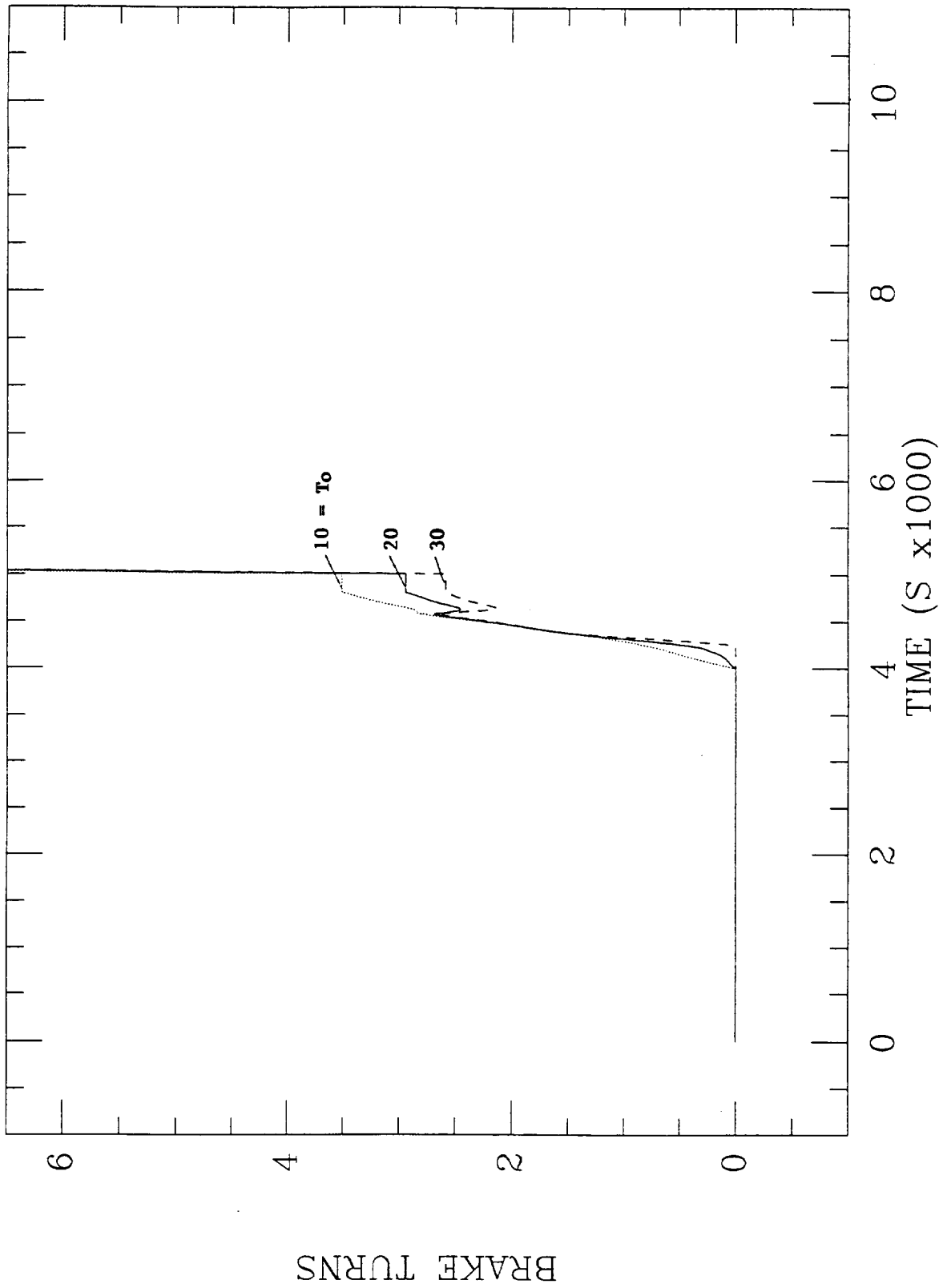


**Fig. 10(e).** Dynamic response of SEDSAT during deployment for reference 39 (see text).

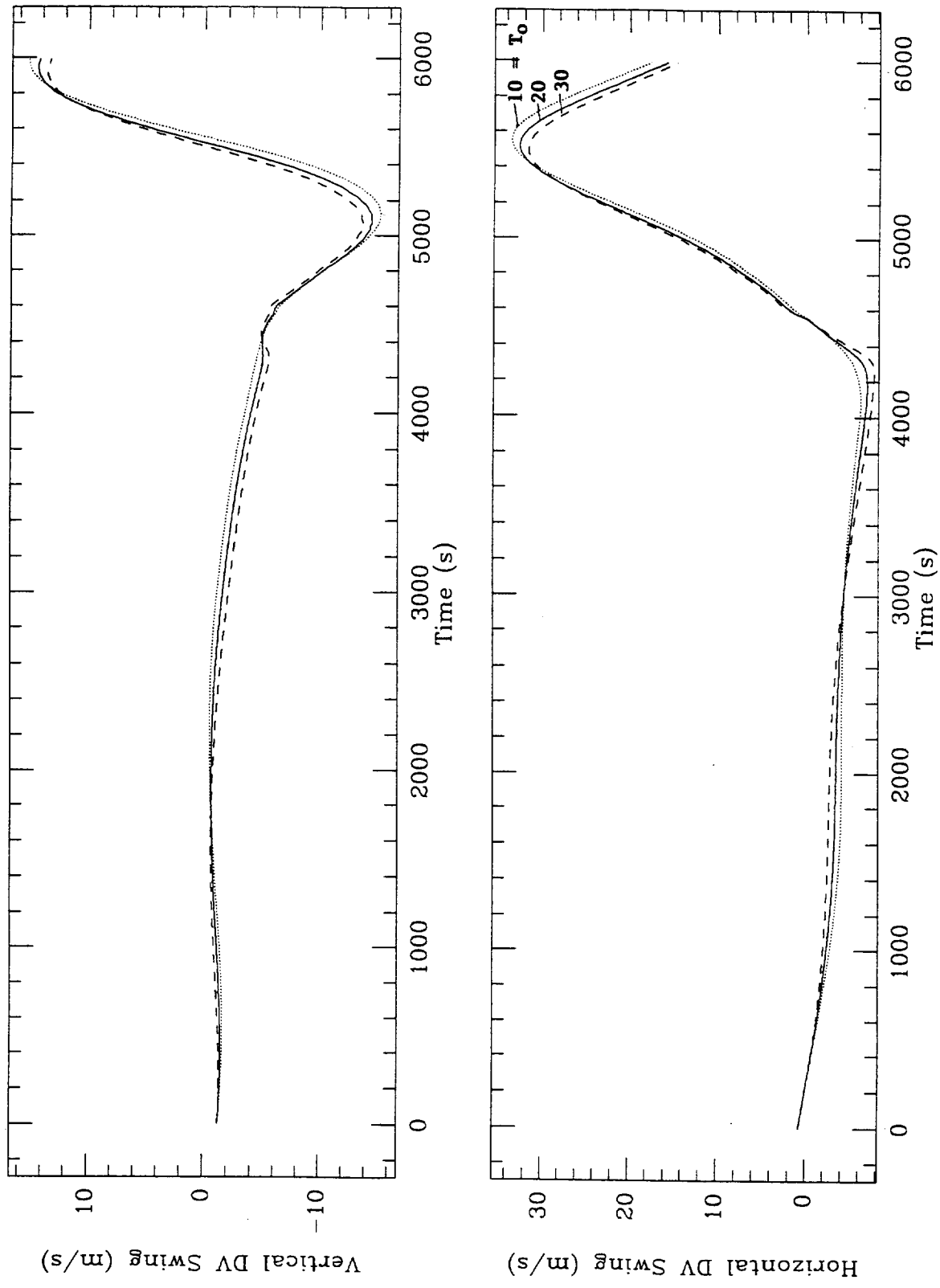


**Fig. 10(f).** Dynamic response of SEDSAT during deployment for reference 39 (see text).

The nominal post-release orbit of the center of mass of the satellite-tether system is about 317kmX535km, with respect to a spherical Earth, after the first tether cut at the Shuttle end. Subsequently, close to a convenient apogee, the tether is cut a second time at the satellite end in order to raise the altitude of the perigee. The tether accounts for about 17% of the mass of the satellite-tether system and its release provides an increase of perigee height of about 13 km after considering that $L_{CM}$ in this case is the distance between the satellite CM and the CM of the satellite-tether system and that the tether is not exactly at apogee when crossing LV for the second time.

In conclusion, the final nominal orbit of the satellite is about 330kmX535km with respect to a spherical Earth. When the apogee altitude is computed with respect to an oblate Earth, its numerical value can vary by about ±9 km with respect to the number quoted above depending on the value of the argument of perigee. With this control law the final tether length of 20 km is reached in 1 hour 20 min while the tether crosses the local vertical 12 min later. Consequently, the satellite with the attached tether is released 5,520 s after the start of deployment from the Shuttle.

The absolute time of the first cut (or equivalently the orbital anomaly) is not critical for SEDSAT because there is no specific requirement on the phase of the final orbit for this mission. However, the sensitivity of the release time to variations of the deployer's model parameters can be more or less important depending on the level of crew and on-board equipment involvement in estimating the tether crossing LV. In the simplest scenario, the LV crossing could be based solely on the deployment start time and, consequently, the insensitivity of the maneuver duration to different deployer's parameters is important for obtaining an accurate ΔV at release. For instance, the timing error associated with the expected variability of the static tension is less than ±20 s.

The hydraulic component (proportional to $\dot{L}^2$) in the deployer's tension model also has an effect on the deployment dynamics and, hence, on the timing and magnitude of ΔV at the crossing of LV. Unfortunately, the ejection angle that nullifies the effect of the hydraulic tension term is on the opposite side of LV with respect to the ejection angle that nullifies the effect of the minimum tension. It can be inferred from Figs. 11(a)-11(b), which show the deployment dynamics for reference profile 39 for different values of the hydraulic tension term, that a variation of the inertia multiplier I of ±25%, with respect to the reference value of 4.1, involves a variation of the timing to cross LV of about ±80 s. The variation of the horizontal component of the swinging ΔV is less than ±1 m/s at the

estimated time of LV crossing. The variation of the vertical component of the swinging $\Delta V$ is about $\pm 4$ m/s at the estimated time of LV crossing. However, a vertical $\Delta V$ produces an increase (or decrease) of the orbital height which is about 1/4 of the effect produced by an horizontal $\Delta V$.

In summary, if the tether cut is determined by the estimated time to cross LV from the start of deployment, the dispersion of the horizontal $\Delta V$ component is minimized. If the same tether cut is effected at the actual crossing of LV, the dispersion of the vertical $\Delta V$ component is minimized. The latter case requires more crew and on-board equipment involvement. The two cases produce comparable dispersion in terms of the height of the final orbit. The former case can produce a slightly different phasing of the initial and final orbit which, however, is not an issue for SEDSAT at present.

The time accuracy at release is definitely important for future missions which are expected to use a SEDS-type deployer for the atmospheric reentry of capsules. In this case the dispersion on the absolute time at release determines to a large extent the dispersion of the reentry capsule footprint. For instance, a timing error of the reentry $\Delta V$ in LEO of $\pm 20$ s implies, approximately, a $\pm 148$ km ($\pm 80$ nmi) error in the length of the footprint. It is worth remembering that the length of the footprint of the *Gemini* capsule was typically $\pm 185$ km ($\pm 100$ nmi) [12].

### 1.5 Conclusions on SEDSAT Control and Dynamics

In 1997, SEDSAT will the deployed on a 20-km-long tether from the Shuttle orbiting on a 297-km circular orbit and released at the time the tether crosses the local vertical. The final tether length is reached in 1 hour 20 min with the deployment control law described in this report. Upon crossing the local vertical, 12 min later, the tether is cut at the Shuttle and, consequently, the satellite with the attached tether is injected into an higher orbit thanks to the librating tether acting as a sling shot. After the (second) tether disconnection from the satellite, close to apogee, a final orbit of about 330kmX535km, with respect to a spherical Earth, is reached. The present estimate for SEDSAT lifetime is approximately 3 years.

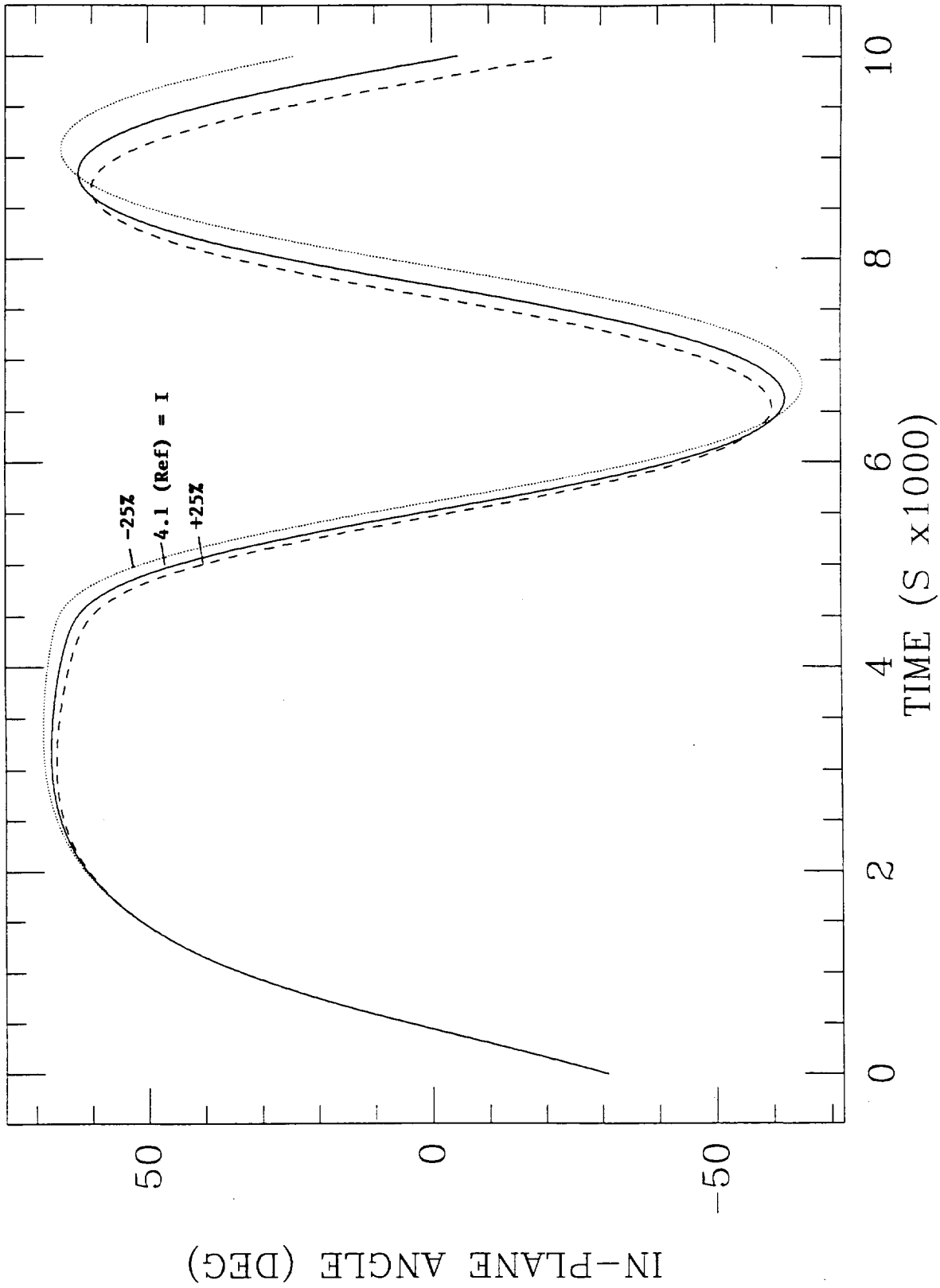


**Fig. 11(b)**. Sensitivity of deployment to Inertia Multiplier I for reference profile 39.

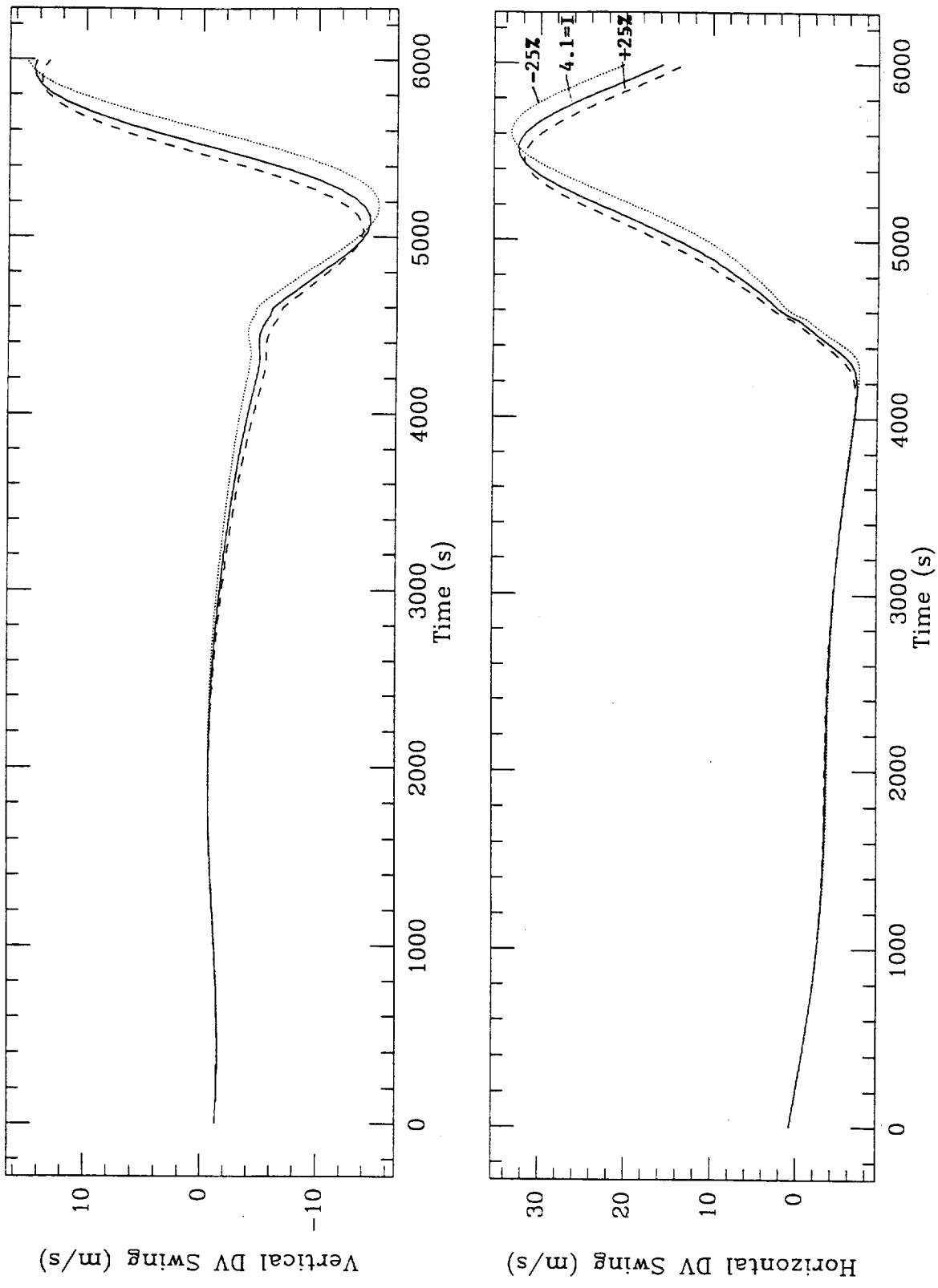


**Fig. 11(b).** Sensitivity of deployment to Inertia Multiplier I for reference profile 39.

## 2.0 Tethered Multi-Probe for Thermospheric Research

In the following we include three papers, authored by scientists of the Smithsonian Astrophysical Observatory, that were presented to the *Fourth International Conference on Tethers in Space* which illustrate respectively: (1) the chemistry of the lower thermosphere and the associated cooling processes; (2) the on-board instrumentation required to conduct the measurements of the cooling processes; and (3) a possible tethered system to carry out those measurements in the altitude range of 110-160 km for the lowest probe and 200-250 for the mother platform.

The cooling processes in the mesosphere and in the lower thermosphere are of particular scientific and also public interest because, according to several scientists, they are related to the increased concentration of "greenhouse gases" in the troposphere and hence to the global warming trend of the troposphere. A tethered system with one or preferably two probes attached to typically a 90-km-long tether linked to a mother platform can uniquely contribute to this exciting field by taking measurements in a region of the Earth's atmosphere that is not accessible to conventional satellites.

**Paper MFUTMS-1**

# ATMOSPHERIC SCIENCE WITH TETHERS: HEATING, COOLING AND CHEMISTRY IN THE LOWER THERMOSPHERE

Kate P. Kirby
Smithsonian Astrophysical Observatory

**Fourth International Conference on Tethers in Space**

Sponsored by National Aeronautics and Space Administration, Smithsonian Astrophysical Observatory, Agenzia Spaziale Italiana, Martin Marietta, Alenia Spazio S.p.A., Science Applications International Corporation

Smithsonian Institution, Washington, DC, 10-14 April 1995

# ATMOSPHERIC SCIENCE WITH TETHERS; HEATING, COOLING AND CHEMISTRY IN THE LOWER THERMOSPHERE

Kate P. Kirby
Smithsonian Astrophysical Observatory
60 Garden Street, Mail Stop 14
Cambridge, MA 02138

## Abstract

Tethered probes offer a unique opportunity for studying the lower thermosphere and ionosphere. An instrument package focussed to provide detailed information on the various cooling processes taking place throughout the thermosphere would enable significant progress in the overall understanding of the energy budget in this region. Cooling processes, intimately linked to the atmospheric chemistry, may be substantially affected by the build-up of greenhouse gases in the atmosphere. Evidence for increased cooling in the upper atmosphere might serve as an early diagnostic of global warming occurring in the lower atmosphere. Enhanced cooling in the upper atmosphere may contribute to increased ozone destruction.

## Introduction

It is an honor to lead off the session on future missions with tethered satellites. It is clear that the opportunities offered for atmospheric science by a tethered instrument package are particularly compelling:

1) The altitudes which can be probed by *in situ* techniques, down to 120 km, are in great need of exploration.

2) The idea of flying smaller, less expensive missions with instrument packages that target important questions but that do not attempt to address all the science has the advantages of flexibility - with faster realization from proposal and design to actual flight.

3) The advantage of multi-probe tethers, in which a number of identical instrument packages are strung out, like pearls on a string, offers a unique opportunity to obtain properties in the atmosphere simultaneously at several different altitudes.

It has been noted that, *"the Earth's mesosphere and lower thermosphere are the least explored regions in the Earth's atmosphere ".*[1] These regions span the altitude range from 60 km to 130 km. Too high to be explored by balloon-borne instruments and too low to be explored *in situ* by satellites, this region of the atmosphere is often referred to as the "ignorosphere".

The purpose of this talk is twofold. First, critical questions are raised regarding cooling processes in the lower thermosphere and mesosphere. It will be shown that these processes are intimately connected to an understanding of the atmospheric chemistry and overall energy budget in these regions. Secondly, it is emphasized that an understanding of cooling processes in the upper atmosphere has direct relevance to two important global change issues: global warming due to the build-up of greenhouse gases from anthropogenic sources, and stratospheric ozone depletion.

Several other papers in these proceedings are complementary to this one. In his paper, *"Spectroscopic Measurements from a Tethered Satellite Platform* (WSCI-5)", Dr. Kelly Chance has described the specific series of measurements which we propose to make to study the cooling mechanisms and has defined the kind of instrument package we are considering. Dr. Enrico Lorenzini and co-workers have described the tether engineering and orbital considerations required for such an atmosphere science mission in their paper, *"Tethered Multi-probe for Thermospheric Research* (Th FUTA-6)".

Heating, Cooling and Chemistry: An Overview

Heating of the upper atmosphere occurs primarily through the absorption of solar radiation at ultraviolet and extreme ultraviolet wavelengths and is mediated by collision between electrons, ions. and neutrals.[2] The process of heating puts energy into the translational degrees of freedom of the gas. This can be done directly by the absorption of radiation to produce fragment species with high kinetic energies - as in photoionization and photodissociation. Examples are given, with the translationally hot species underlined:

$$N_2 + h\nu \rightarrow N_2^+ + \underline{e} \qquad \text{(photoionization)}$$

and

$$O_2 + h\nu \rightarrow \underline{O}\ (^3P) + \underline{O}\ (^3P). \qquad \text{(photoionization)}$$

Heating can also be accomplished indirectly by the absorption of radiation to produce electronically or vibrationally excited species which then collide, converting their internal energy into translational energy of the collision partners. This collision process is called quenching. An example is the photodissociation of molecular oxygen to produce an electronically excited oxygen atom which collides with $N_2$ to heat the gas, in the process de-exciting the oxygen atom

$$O_2 + h\nu \rightarrow O(^3P) + O(^1D)$$

and

$$O(^1D) + N_2 \rightarrow \underline{O}\ (^3P) + \underline{N}_2 .$$

Electronically excited species which are metastable, such as O ($^1$D), have much greater

chemical reactivity than ground state species. With increasing translational energy ground state species such as N($^4$S) and O ($^3$P) become much more chemically reactive because they are able to surmount small endothermicities on the reaction surface. Thus it is clear that absorption of radiation and the consequent heating are primary drivers of the chemistry in the thermosphere.

Even at night time, with no solar radiation present, heating processes such as dissociative recombination occur. Dissociative recombination, the primary electron loss mechanism in the lower thermosphere and ionosphere, takes place when an electron is captured by a molecular ion and the resulting neutral molecule dissociates. Significant kinetic energies can be imparted to the fragments in the process, thereby heating the neutral gas. Examples include:

$$e + O_2^+ \rightarrow \underline{O}\ (^3P) + \underline{O}\ (^3P)\ (+7\ eV)$$

$$e + N_2^+ \rightarrow \underline{N}\ (^4S) + \underline{N}\ (^4S)\ (+6\ eV)$$

Cooling takes place when kinetic energy of the gas is transformed through collisions into internal energy which can then be radiated away to space. An example is the excitation of the v = 1 vibrational mode of NO by collisions with atomic oxygen. The NO then radiates away this energy in the fundamental band (v = 1→0) at 5.3 $\mu$m:

$$O + NO \rightarrow O + NO\ (v = 1)$$
$$NO\ (v = 1) \rightarrow NO\ (v = 0) + h\nu\ (5.3\ \mu m)$$

Nitric oxide is thought to be the major coolant from approximately 120 to 200 km. It is to be noted that the major molecular species in the atmosphere, $N_2$ and $O_2$, are not infrared active. Therefore cooling is predominately accomplished through trace species, such as NO and $CO_2$.

There are strong interconnections between the chemistry and heating and cooling processes which can be best illustrated by an example. It is impossible to show, given the time and space allotted, the full range of the complex chemistry which takes place in this region of the atmosphere, with just four major neutral ingredients: $N_2$, $O_2$, O and He. The following examples are just two out of the five or more major chemical reactions forming the NO molecule:

1) An electronically excited nitrogen atom can react with molecular oxygen to produce NO molecules that are vibrationally excited.

$$N\ (^2D) + O_2 \rightarrow NO^* + O$$

From laboratory experiments it is known that NO is formed in a range of vibrational states up to v = 12.[3] If NO* radiates away the vibrational energy (predominately via $\Delta$v = 1 transitions) NO contributes to cooling. If the NO* is quenched before it radiates, the energy goes into heating the gas, and the formation of NO then results in net heating.

The factors determining whether NO formation results in heating or cooling are: 1) the densities at the altitude at which NO is formed (densities determine the frequency of

collisions and thus the quenching rate); and 2) the radiative transition probabilities or Einstein A-coefficients for radiation of the vibrational energy.

2) Another mechanism for NO formation involves translationally hot nitrogen atoms which react with molecular oxygen to produce NO which is vibrationally and rotationally excited.[4]

$$\underline{N}_{fast}\ (^4S) + O_2 \rightarrow NO^{**} + O$$

It turns out that it matters whether internal energy is manifested as vibration or rotation because the transition probabilities differ by several orders of magnitude. Vibrational transition probabilities are typically almost a thousand times larger than rotational transition probabilities. Thus energy deposited in vibration is more easily radiated , thereby contributing to cooling, whereas energy deposited in rotation is not as easily radiated and may contribute to heating.

Thermospheric/Mesospheric Cooling Processes

The primary cooling processes in the thermosphere and ionosphere are summarized here. Above about 200 km, the oxygen fine-structure transition O ($^3P_1$) → O ($^3P_2$) which radiates at 63 $\mu$m is the major cooling mechanism. The fine structure levels of atomic oxygen are thermally populated. Between approximately 120 to 200 km, the fundamental band ($v = 1 \rightarrow 0$) of NO, radiating at 5.3 $\mu$m, is the major cooling mechanism. Below approximately 120 km the $\nu_2$ vibrational bending mode is the predominant coolant, radiating at 15 $\mu$m. The $CO_2$ is excited by collisions with atomic oxygen.

There are major uncertainties, however, regarding these mechanisms. Thus a tether probe instrument package targeted to measure spectroscopic emission of the major coolants has tremendous potential.

The NO density is not well-known, with some models disagreeing with others by as much as an order of magnitude. The formation mechanisms for NO are still in some doubt. Is the cooling accomplished primarily by $v = 1 \rightarrow 0$ transitions excited by collisions with atomic oxygen, or does the chemistry contribute substantially to the cooling via $\Delta v = 1$ transitions of higher-lying vibrational levels populated in the formation process ($v = 4 \rightarrow 3$, $3 \rightarrow 2$, $2 \rightarrow 1$, etc.)?

The $CO_2$ density is not well-known in the lower thermosphere and ionosphere. The rate coefficient for the excitation of the $\nu_2$ bending mode of $CO_2$ by collisions with atomic oxygen is very uncertain. The is a factor of 6 difference between measurements carried out in the laboratory and emission measurements made in the atmosphere.[6,7]

There may be additional cooling mechanisms involving other constituents that have not been considered. For instance, recent data from a rocket experiment (CIRRIS) indicate a significant presence of vibrationally excited CO which had not been seen previously. This may contribute to the cooling. Other recent data show both neutral molecules and molecular ions with

much greater vibrational and rotational excitation than expected.[8] The molecular ion $N_2^+$ was found to have as much as 0.5 eV of vibrational and rotational excitation.

Ultimately, if one could obtain some data down around 90 km and below, one might get closer to solving one of the greatest mysteries regarding the thermal budget of the Earth's atmosphere: the Mesospheric Temperature Anomaly. Whereas at 200 km temperatures may reach 1500 to 2000° K, only 100 km lower at the mesopause (85-90 km) the coldest temperatures in the Earth's atmosphere exist (~130° K). The high temperatures are understood, but the precipitous drop to the very low temperatures at the mesopause remains to the adequately explained. A clear understanding of the various cooling processes in the lower thermosphere will help to explain this phenomenon.

Cooling and Global Change

Cooling processes in the upper atmosphere are linked to two prominent global change issues. A brief review of both the global warming and ozone depletion problems follows.

The Earth's atmosphere, which is approximately 80% $N_2$ and 20% $O_2$, is transparent to much of the solar radiation in the 3200 to 7000 Å region of the spectrum. This solar radiation is largely absorbed by the Earth. In order for the Earth to stay in equilibrium it must reradiate this energy, and since it is at a lower temperature than the sun it radiates at longer wavelengths, in the infrared. Certain molecules such as $H_2O$, $CO_2$, $CH_4$ and the chlorofluorocarbons in the atmosphere absorb this infrared radiation, trapping it and causing the earth's surface and lower atmosphere to heat up. This additional amount of heating makes the Earth habitable for plant and animal life. But increasingly gases, such as carbon dioxide from the burning of fossil fuels and methane from agriculture and raising livestock, are being put into the atmosphere in abundance. These gases will trap more radiation, causing the temperature in the lower part of the atmosphere (the troposphere) to rise. What is known as "Global Warming" results.[9,10]

Extrapolation of recent trends in measured $CO_2$ and $CH_4$ concentrations in the atmosphere predicts a worst-case scenario of $CO_2$ and $CH_4$ concentrations doubling over the next century.

For a doubled $CO_2$ and $CH_4$ atmosphere large computer codes known as General Circulation Models (GCM's) have predicted that temperatures in the lower atmosphere (0 to 15 km) will rise by approximately 1.5 to 4.5° K over the next century. However above 15 km, in the stratosphere, mesosphere, and thermosphere the temperature is not raised but instead is lowered. In the stratosphere, temperatures are predicted to decrease by 6-8° C and in the thermosphere the temperature decreases may be as much as 40-50° C.[11,12] This effect is all due to the fact that $CO_2$ acts as a heat trap in the troposphere and as a coolant throughout the upper atmosphere. Thus significant increases in the $CO_2$ density cause heating in the lower atmosphere and cooling in the upper atmosphere. The extent of the cooling predicted depends critically on the rate coefficient for the $O + CO_2$ excitation of the $\nu_2$ bending mode of $CO_2$ - a parameter which is very uncertain. However, the measurement we propose to undertake with the tether would enable us to quantify this process very accurately.

The predicted magnitude of the temperature decrease in the thermosphere is larger by over

an order of magnitude than the predicted increase in the lower atmosphere that defines the "global warming" problem. If this large temperature decrease could somehow be monitored it could serve as an early detection of global warming beginning in the lower atmosphere - where the effect is much more subtle and therefore difficult to measure. There is some evidence that considerably lower temperatures are already occurring in the mesosphere.[13,14,15]

Cooling of the middle atmosphere, though not as profound as the upper atmosphere, will significantly affect the ozone chemistry. Lower temperatures in the stratosphere may increase the frequency of formation of polar stratospheric clouds that drive the heterogenous chemistry and causes massive destruction of the ozone over Antarctica during the transition from polar winter to spring. Other ozone depletion chemistries taking place on the surface of sulfate aerosols may also be enhanced by lower temperatures. Thus, significant temperature decreases resulting from a build-up of $CO_2$ may further exacerbate ozone destruction. Ozone, itself, is the dominant heat source in the lower stratosphere. Decreasing the amount of ozone will drive temperatures still lower. Unfortunately, these two effects operate together to further increase ozone depletion. Hence, the effect of the build-up of $CO_2$ may be far more serious in the middle and upper atmospheres than in the lower atmosphere.

## CONCLUSIONS

In summary, there are many unknowns regarding the cooling processes in the lower thermosphere which could be explored with a tethered probe and which have important implications for understanding several critical global change issues.

## ACKNOWLEDGEMENTS

I would like to thank my atmospheric chemistry collaborators in this effort,Dr. K. Chance, Prof. A. Dalgarno. Dr. P. Smith, and Dr. R. Sharma. In addition, I thank the tether group at SAO, including Dr. E. Lorenzini, Dr. M. Grossi, and Dr. M. Cosmo. Finally, I would like to acknowledge Prof. I. Shapiro, Director of Harvard-Smithsonian Center for Astrophysics, who brought our groups together.

## REFERENCES

1. Space Science Board, National Academy of Sciences, 1988, report, "Space Science in the 21st Century: Imperatives for the Decades 1995-2015".

2. See, for instance, M. H. Rees, "Physics and Chemistry of the Upper Atmosphere", Cambridge Univ. Press. 1989.

3. J. P. Kennedy, F. P. Del Greco, G. E. Caledonia and B. D. Green, J. Chem. Phys. **69**, 1574 (1978).

4. R. D. Sharma, Y. Sun, and A. Dalgarno, Geophys. Res. Lett. **20**, 2043 (1993).

5. D. S. Pollock, G. B. I. Scott, and L. F. Phillips, Geophys. Res. Lett. **20**, 727 (1993).

6. R. D. Sharma and P. P. Wintersteiner, Geophys. Res. Lett. **17**, 2201 (1990).

7. C. D. Rodgers, F. W. Taylor, A. H. Muggeridge, M. Lopez-Puertas, and M. A. Lopez-Valverde, Geophys. Res. Lett. **19**, 589 (1992).

8. P. S. Armstrong, J. J. Lipson, J. A. Dodd, J. R. Lowell, W. A. M. Blumberg, and R. M. Nadile, Geophys. Res. Lett. **21**, 2425 (1994); R. D. Sharma, private communication.

9. J. F. B. Mitchell, Reviews of Geophysics **27**, 1 (1989).

10. J. Hansen, D. Johnson, A. Lacis, S. Lebedeff, P. Lee, D. Rind, and G. Russell, Science **213**, 957 (1981).

11. H. Rishbeth and R. G. Roble, Planet. Space Sci. **40**, 1011 (1992).

12. R. G. Roble and R. E. Dickinson, Geophys. Res. Lett. **16**, 1441 (1989).

13. A. C. Aikin, M. L. Charin, J. Nash, and D. J. Kendig, Geophys. Res. Lett. **18**, 416 (1991).

14. A. Hauchecorne, M. L. Charin, and P. Keckhut, J. Geophys. Res. **96**, No. D8, 15,297 (1991).

15. M. Gadsden, J. Atm. Terr. Phys. **52**, 247 (1990).

**Paper WSCI-5**

# SPECTROSCOPIC MEASUREMENTS FROM A TETHERED SATELLITE PLATFORM

Kelly V. Chance
Harvard-Smithsonian Center for Astrophysics

**Fourth International Conference on Tethers in Space**

Sponsored by National Aeronautics and Space Administration, Smithsonian Astrophysical Observatory, Agenzia Spaziale Italiana, Martin Marietta, Alenia Spazio S.p.A., Science Applications International Corporation

Smithsonian Institution, Washington, DC, 10-14 April 1995

# SPECTROSCOPIC MEASUREMENTS FROM A TETHERED SATELLITE PLATFORM

K. V. Chance
Harvard-Smithsonian Center for Astrophysics
Cambridge, MA 02138 USA

## Abstract

Spectroscopic measurements of atmospheric emission that can be made from a tethered instrument module are potentially important as direct probes of lower thermospheric and mesospheric cooling and related chemistry. Cooling of the lower thermosphere and mesosphere is closely related to "greenhouse" warming of the lower atmosphere (the troposphere) and may provide an early indication of such warming. This paper presents an instrument concept for a limb-observing spectrometer that would be combined with one or more *in situ* neutral mass spectrometers to perform definitive measurements of all necessary components of the major cooling processes in the lower thermosphere and mesosphere. Spectroscopic emissions would be monitored looking to the Earth's limb to measure the emitted radiation strongly peaked at a range of tangent altitudes at and below the instrument package containing the spectrometer. The instrument candidates for the proposed measurements have good technical heritage although, as noted below, they vary in complexity and in requirements on satellite resources. They are briefly described, followed by notes on the issues of cooling and pointing and description of a straw man instrument package

## Introduction

A tethered satellite system provides a unique opportunity for obtaining measurements in the Earth's lower thermosphere and mesosphere that are complete and definitive in the known processes that control cooling in this part of the atmosphere. The scientific issues that drive the selection of the tether satellite instrument described in this paper are discussed in detail by my colleague Dr. K. Kirby elsewhere in these proceedings.[1] The tethered satellite concept used here is also from a Center for Astrophysics presentation in these proceedings, by E. Lorenzini *et al.*[2] This part of the atmosphere is difficult to measure in detail because it it is well above altitudes that can be explored using balloons or aircraft and below that normally accessible with satellites. Limited measurements have been made using rockets[3] and limb instruments on the space shuttle.[4] However, these have not been able to determine diurnal and latitudinal variations of emission and absolute concentrations of the emitting species. The straw man tethered satellite concept used here consists of an upper platform with a 200 km × 250 km orbit with two tethered probes separated by 5 km and an overall tether length of 90 km.[2] The proposed measurements would include spectroscopic measurements of limb emission, using a spectrometer system developed by the Harvard-Smithsonian Center for Astrophysics, in conjunction with two *in situ* neutral mass spectrometers provided by investigators at another institution (for example, as described in References 5-7).

## Proposed Experiment

**15 $\mu$m $CO_2$ (atmospheric cooling and pointing)** This is a primary measurement of atmospheric cooling. Below about 120 km, infrared emission by $CO_2$, which has been excited by collision with oxygen atoms, is the dominant cooling mechanism in the thermosphere. In the lower atmosphere, various minor isotopic species and hot bands contribute to the radiance, but above about 105 km only the $01^10 \rightarrow 00^00$ band is significant. Also note that above about 110 km the limb radiance becomes optically thin. The appropriate detector technology to use in this $CO_2$ band is HgCdTe operating at 80 K or less. A small linear array of detectors (the SAFIRE instrument proposed a 7 × 15 array) with a monochromator of modest size would be adequate. An additional 15 $\mu$m channel will measure lower altitude $CO_2$ for pointing of the limb spectrometers (see **Pointing**, below).

**5.3 $\mu$m NO (atmospheric cooling)** The cooling lines include both the fundamental band of NO and vibrational hot bands. The best possibility for measurement is a diode-array based spectrometer using a linear array of HgCdTe detectors cooled to 80 K or less. A 200-element array of HIRDLS or AIRS-type detectors operating at 60 K, for example, would be quite adequate. An instrument measuring from about 4.17-6.25 $\mu$m could measure both the NO and the 4.3 $\mu$m $CO_2$ emission mentioned below with resolution which should be adequate to distinguish the overall rotational structure. An alternate approach would be the use of a single detector and a circularly-variable filter (as used in SPIRE[3]). A tradeoff study will need to consider sensitivity vs. the desire to resolve the (non-LTE) rotational structure of the bands to some extent.

**4.3 $\mu$m $CO_2$ (diagnostic)** Measurement of the $30^01 \rightarrow 30^00$ bands permits the monitoring of $CO_2$ density in the solar-illuminated portion of the orbit. These measurements could be made with the same monochromator and detector array as 5.3 $\mu$m NO measurements.

**63 $\mu$m $O^3P$ (atmospheric cooling)** This measurement is more ambitious than the others included here. Although the technical heritage is sound, it would require both a more complex instrument (a metal-mesh Fabry-Perot) and liquid helium-temperature cooling (either from liquid helium or from a multi-stage Stirling/Joule-Thomson mechanical cooler. The best way forward with the spectrometer technology would be to include the group at NASM who have been involved with the long-wavelength spectrometer of ISO, and who have a flight spare of the (fully space-qualified) ISO Fabry-Perot in their possession.

**Detector and instrument cooling** Space qualified Stirling cycle coolers are available which supply 800 mW of cooling at 80 K from 30-35 W input power, operating from -20 to +40 C, and weighing 4.5 kg. Two-stage versions cooling to as low as 30 K are almost space qualified. They supply somewhat less cooling power at just about double the weight and power. Mechanical coolers operating to 4 K are under development. These coolers use a multi-stage Stirling/Joule-Thomson arrangement and give ca. 10 mW of cooling power at 4.2 K for 160 W of input power. Their weight is 16.5 kg. For near-term considerations, the 80 K coolers are a reasonable choice; the 4 K coolers are probably not. Other cooling possibilities for 80 K and below include the two-stage coolers, dewars with liquid nitrogen (77 K), pumped (solid) nitrogen (about 55 K) and solid $H_2$ (14 K) or Ne (25 K). For a short-term (several day) deployment, liquid helium cooling of the gallium-doped germanium photoconductor detector for the $O^3P$ measurements and pumped (solid) nitrogen cooling of the HgCdTe detectors is the baseline.

**Pointing** Pointing for limb emission measurements should be accurate and stable to better than 1°. A horizon sensor detecting $CO_2$ at 40 km, operating at 15 $\mu$m is the baseline for limb pointing. This has worked in the past to well within our requirements (for example in CIRRIS-IA) and is proposed for future space-borne experiments, such as the HIRDLS instrument on Eos.

**Straw man instrument package** With proper choices from the above suggestions we can make *definitive measurements of all necessary components of the major cooling processes in the thermosphere, and thus determine if they are modeled correctly* for the rather extensive range of conditions that the tether experiment can probe. The instrument module which contains the spectrometer would measure from approximately 90 km up to the module height. It would include spectroscopic measurements of (1) the 15 $\mu$m $CO_2$ bands, for atmospheric cooling and pointing; (2) the 5.3 $\mu$m NO and 4.3 $\mu$m $CO_2$ bands; and (3) the 63 $\mu$m atomic fine structure line ($J = 1 \rightarrow 2$) of $O^3P$. Neutral mass spectrometer measurements must include oxygen atoms (mass 16), NO (mass 30), and $CO_2$ (mass 44).

It is amply demonstrated from SPIRE[3] and CIRRUS-1A[4] measurements, SAO measurements of $O^3P$,[8] and ISO characteristics[9] that the proposed measurements are possible given sufficient payload resources. Appropriate detector manufacturers and users are currently being contacted in order to investigate the available performance vs. cooling. This will allow a tradeoff study of size, weight, complexity, etc. to be made on the spectrometer portion of the payload.

**Combining limb and *in situ* measurements** The proposed tethered satellite experiment combines *in situ* measurements of neutral composition with limb measurements of atmospheric emissions. In order to combine such data in a meaningful way, the geometry of the limb measurements must be such that the measurements are essentially local. Figure 1 shows weighting functions for measurement of emission from the 63$\mu$m line of $O^3P$ calculated for various tangent heights from a platform at 200 km altitude. O atom concentrations are taken from the MSIS-86 thermospheric model under conditions of low solar activity.[10] It is apparent from the figure that the sampling in the limb geometry is very strongly peaked near the tangent height, providing measurements that are essentially local in nature. The horizontal smearing from the tangent geometry corresponds to several tens of seconds of *in situ* observing at the orbital velocity of 7.8 km $s^{-1}$.

## CONCLUSIONS

The concept for a tethered aeronomy mission described in this paper and two other Center for Astrophysics papers in these proceedings[1,2] is one wherein an experiment requiring modest resources and using mature technology can produce unique scientific results. These results are of particular interest because of their importance to the issues of global warming and stratospheric ozone photochemistry.

## REFERENCES

1. Kirby, K.P., Atmospheric science with tethers: Heating, cooling and chemistry in the lower thermosphere, *Proceedings of the Fourth International Conference on Tethers in Space* (1995).

2. Lorenzini, E.C., M.L. Cosmo, M.D. Grossi, K. Chance, and J.L. Davis, Tethered multiprobe for thermospheric research, *Proceedings of the Fourth International Conference on Tethers in Space* (1995).

3. Stair, A.T., R.D. Sharma, R.M. Nadile, D.J. Baker, and W.F. Grieder, Observations of limb radiance with cryogenic spectral infrared rocket experiment, *Journal of Geophysical Research* **90**, 9763-9775 (1985).

4. Armstrong, P.S., S.J. Lipson, J.A. Dowd, J.R. Lowell, W.A.M. Blumberg, and R.M. Nadile, Highly rotationally excited NO (v,J) in the thermosphere from CIRRIS 1A limb radiance measurements, *Geophysical Research Letters* **21**, 2425-2428 (1994).

5. Hoffman, J.H., R.R. Hodges, and K.D. Duerksen, Pioneer Venus large probe neutral mass spectrometer, *Journal of Vacuum Science and Technology* **16**, 692-694 (1979).

6. Spencer, N.W., L.E. Wharton, H.B. Niemann, A.E. Hedin, G.R. Carignan, and J.C. Maurer, The Dynamics Explorer Wind And Temperature Spectrometer, *Space Science Instrumentation* **5**, 417-428 (1981).

7. Kayser, D.C., Measurements of the thermospheric meridional wind from the S85-1 spacecraft, *Journal of Geophysical Research* **93**, 9979-9986 (1988).

8. Lin, F.J., K.V. Chance, and W.A. Traub, Atomic oxygen in the lower thermosphere, *Journal of Geophysical Research* **92**, 4325-4336 (1987).

9. Emery, R.J., P.A.R. Ade, I. Furniss, M. Joubert, and P. Saraceno, The long wavelength spectrometer (LWS) for ISO, *SPIE* **589**, 194-200 (1985).

10. Hedin, A.E., MSIS thermospheric model, *Journal of Geophysical Research* **92**, 4649-4662 (1987).

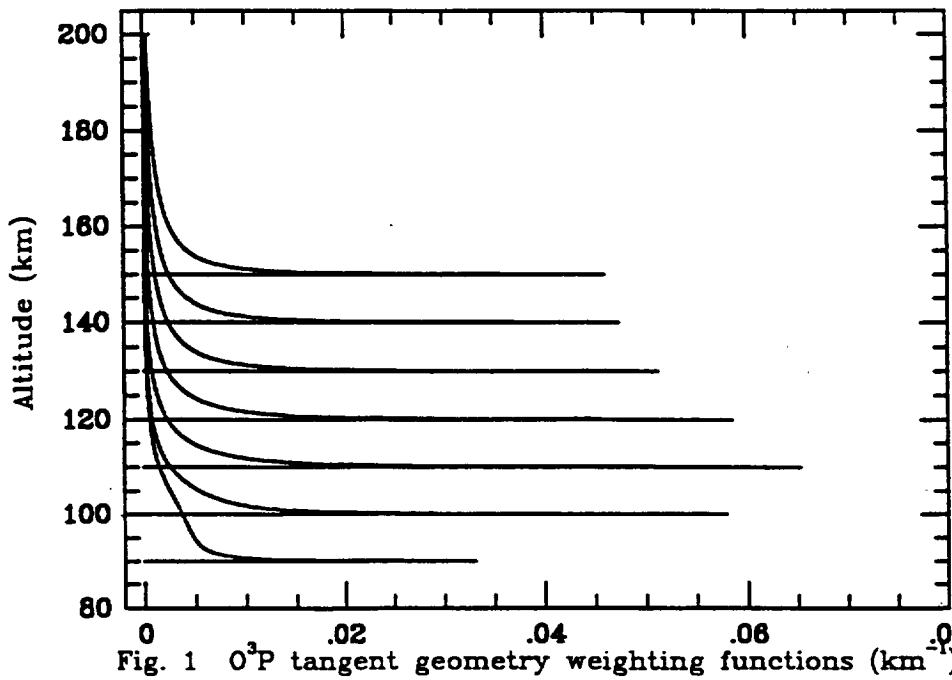


Fig. 1 $O^3P$ tangent geometry weighting functions ($km^{-1}$)

**Paper ThFUTA-6**

# TETHERED MULTI-PROBE FOR THERMOSPHERIC RESEARCH

E.C. Lorenzini, M.L. Cosmo, M.D. Grossi, K. Chance, and J.L. Davis
Harvard-Smithsonian Center for Astrophysics

**Fourth International Conference on Tethers in Space**

Sponsored by National Aeronautics and Space Administration, Smithsonian Astrophysical Observatory, Agenzia Spaziale Italiana, Martin Marietta, Alenia Spazio S.p.A., Science Applications International Corporation

Smithsonian Institution, Washington, DC, 10-14 April 1995

# TETHERED MULTI-PROBE FOR THERMOSPHERIC RESEARCH

E.C. Lorenzini, M.L. Cosmo, M.D. Grossi, K. Chance, and J.L. Davis
Harvard-Smithsonian Center for Astrophysics
Cambridge, Massachusetts, USA

## Abstract

This paper focuses on the dynamics, on-board instrumentation, and science that can be conducted by means of a multi-probe tethered system deployed into the Earth's lower thermosphere. Particular attention is given to the measurement of cooling processes in the lower thermosphere. According to a number of authors, thermospheric cooling may result from an increased concentration of $CO_2$ and $CH_4$ in the atmosphere and, hence, is related to global warming of the troposphere. Since a key issue of low-altitude tethered systems (with one or more probes) is the propellant consumption required for orbital maintenance, simple formulas are derived to estimate the propellant consumption per orbit. The dynamics and thermal requirements of a dual probe system deployed, from a low-eccentricity orbit, into the lower thermosphere is, then, investigated in order to prove the feasibility of such mission with present day tether technology.

## Introduction

Tethered satellites provide a tool for exploring the lower portion of the Earth's thermosphere extending above 90 km of altitude. By means of a tethered system, a probe or a number of vertically spaced probes can be deployed into the relatively dense atmosphere for taking simultaneous, *in-situ* measurements of vertical profiles and spatial gradients of atmospheric quantities in the region of interest.

At a time of increased public concern over the Earth's environment and its future trends, measurements in the lower thermosphere of the predicted effects of increased concentrations of "greenhouse gases" is of great current interest. It is postulated by a number of scientists [1-3], utilizing General Circulation models, that the increased greenhouse gases released into the atmosphere will lead to a global warming of the troposphere (0-10 km) and a stronger global cooling of the mesosphere (50-80 km) and lower thermosphere (above 90 km). The average temperature in the troposphere is estimated to *increase* by 1-5 K in the next century. The temperature effects in the lower thermosphere, according to some authors [1, 2], are amplified with respect to similar effects in the mesosphere [4, 5] with an average *decrease* in temperature of the lower thermosphere predicted to reach 40 K by the mid of the next century. The temperature changes, moreover, would involve changes in the *vertical profiles* of minor atmospheric species like NO, O, $O_3$, $H_2O$, OH, $HO_2$, CO, H in the stratosphere, mesosphere, and lower thermosphere [6, 7]. Computer modeling of global circulation predict relatively steep vertical gradients, especially in the altitude band 100-125 km, of the neutral temperature redistribution and also of the rearranged concentrations of atomic Oxygen and Nitrogen with respect to present day conditions (see Fig. 1 reprinted, with authors' permission, from Ref. [1]). It is also interesting to point out that the vertical temperature redistribution is more influenced by the solar cycle than the latitude-longitude distribution on a constant-pressure surface [1], thereby indicating the importance of taking point and gradient measurements at the above-mentioned altitudes.

A multi-probe tethered system lowered into this region of the atmosphere could measure the horizontal (along a spherical shell) and vertical distributions of minor species concentrations and spectroscopic emissions characteristic of the primary coolant species in these regions. The data so obtained would allow one to develop a more complete and detailed picture of the relevant cooling processes in the upper atmosphere.

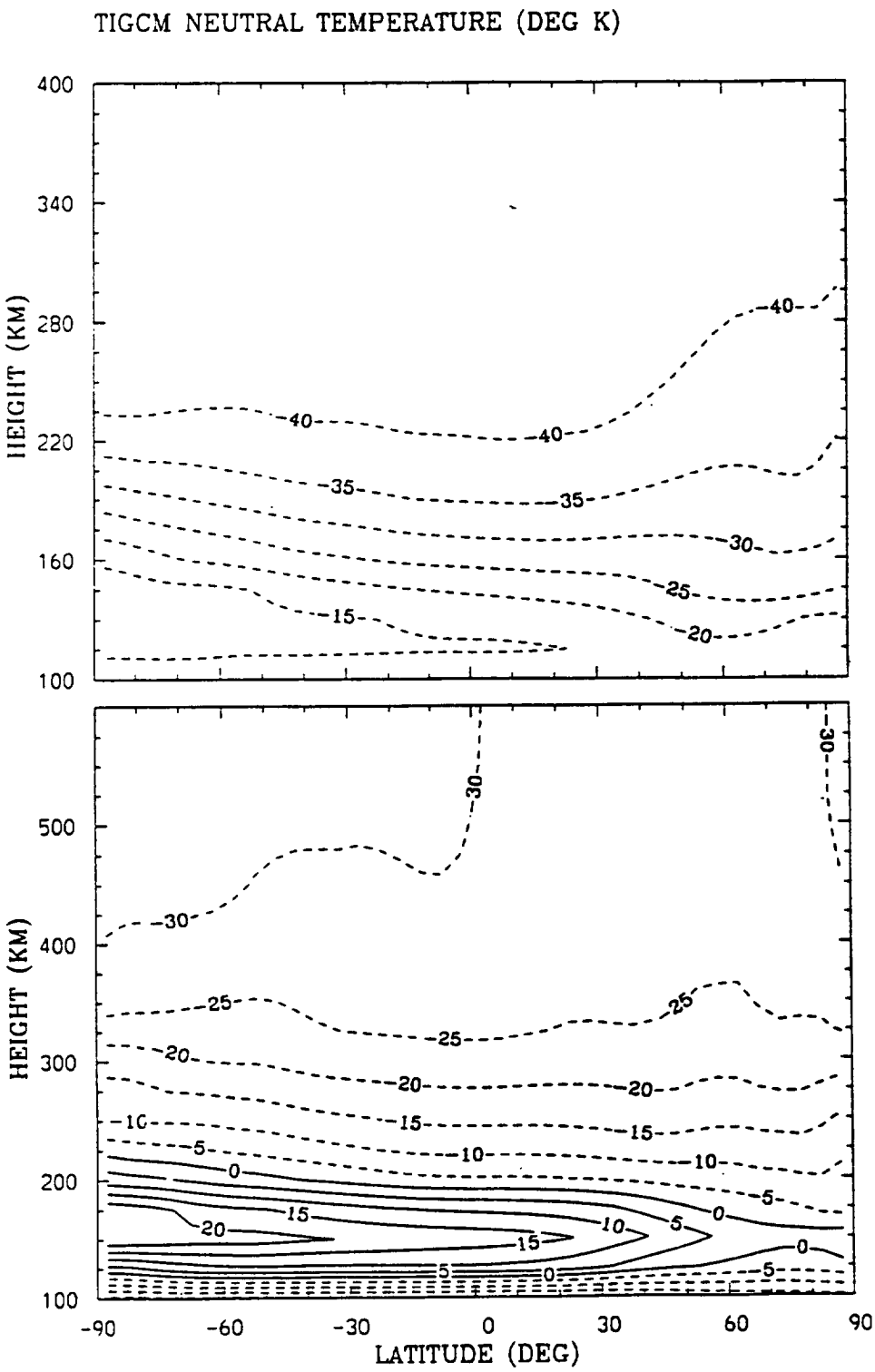


**Fig. 1.** Contours in height and latitude of the zonally averaged field ("doubled $CO_2/CH_4$" - "present conditions" of temperature, $\Delta T$, December solstice at 00 UT. (a) Above: solar minimum (b) Below: solar maximum [Graphs and caption reprinted with authors' permission from Ref. 1].

## Tethered System Dynamics at Low Altitudes

A probe or a number of probes attached along a long tether can be deployed from a mother platform (e.g., the Space Shuttle) into the relatively dense low thermosphere. Several papers and a book (Ref. [8-10] just to mention a few) address the dynamics and stability of single-probe atmospheric tethered systems at low altitudes. Also, the study of several aspects of the dynamics of multi-probe tethered systems has been more recently undertaken by some authors [11, 12]. Only a few key issues, related to multi-probe systems flying at low altitudes, will the addressed in this paper.

It should be pointed out that tethers, on the one hand, do allow the deployment of probes into the relatively dense atmosphere while keeping a large mother platform, like the Shuttle for example, outside of the high drag region. On the other hand, tethers of present day technology have substantial drag areas.

After approximating locally the atmospheric density with an exponential function with reference density and scale height at the bottom tip of the tether and integrating the drag effect over the tether length, the total drag on the tether is readily obtained as follows:

$$D_{tet} = -\frac{1}{2} C_D \bar{\rho} \bar{v}^2 A_T^{eq} \tag{1}$$

where the equivalent drag-force area of a cylindrical tether tether is [13]

$$A_T^{eq} = \bar{H}_s d\left[1 - \exp(-L\cos(\theta)/H_s)\right] \tag{2}$$

In the equations above, $\bar{H}_s$ is the atmospheric scale height, $\bar{\rho}$ the atmospheric density, and $\bar{v}$ the wind velocity (all the barred quantities are computed at the bottom tip of the tether), $L$ and $d$ are the tether length and diameter, respectively, $C_D$ the drag coefficient, and $\theta$ the angle between the tether and the local vertical (LV), which is frequently called the in-plane libration angle. The equations above reduce the tether drag-force contribution to an equivalent drag-force area to be added to the probe at the tether's end.

Figure 2 shows the effective drag-force area per unit diameter (in mm) for a vertical and cylindrical tether vs the altitude of the bottom tip for L = 60 km and L = 80 km and for average atmospheric conditions. A typical diameter of a high-stress, long atmospheric tether is about 0.5 mm and, consequently, the tether contribution to the overall drag force is usually comparable or larger than the contribution of the probe (or probes) attached to it.

A large drag area implies a large propellant consumption for orbital maintenance. After assuming that the tethered system is on an elliptical orbit with small eccentricity $e$, the impulse per orbit per unit drag area $A$ can be computed as follows [14]:

$$I_{A,rev} = 2\pi\sqrt{\mu a} C_D K\left[I_0(b) + 2eI_1(b)\right] \tag{3.1}$$

where

$$K = \rho_p \exp(-b)\left(1 - 2\Omega_E \cos i \Big/ \sqrt{\mu / \alpha^3}\right) \tag{3.2}$$

$$b = ae / H_s \tag{3.3}$$

The symbols in eqns. (3) are as follows: $\mu$ and $\Omega_E$ the Earth's gravitational constant and rotational rate, respectively; $a$ and $e$ the orbit semi-major axis and eccentricity; $C_D$ the drag coefficient; $I_0$ and $I_1$ the modified Bessel functions of order zero and one; $\rho_p$ and $H_s$ the atmospheric density and scale height measured at the perigee of the lowest point in the tethered system.

Consequently, the propellant consumption per orbit per unit drag area is simply:

$$P_{A,rev} = I_{A,rev}/gI_{sp} \tag{4}$$

where $I_{sp}$ is the specific impulse and g the Earth's gravity acceleration.

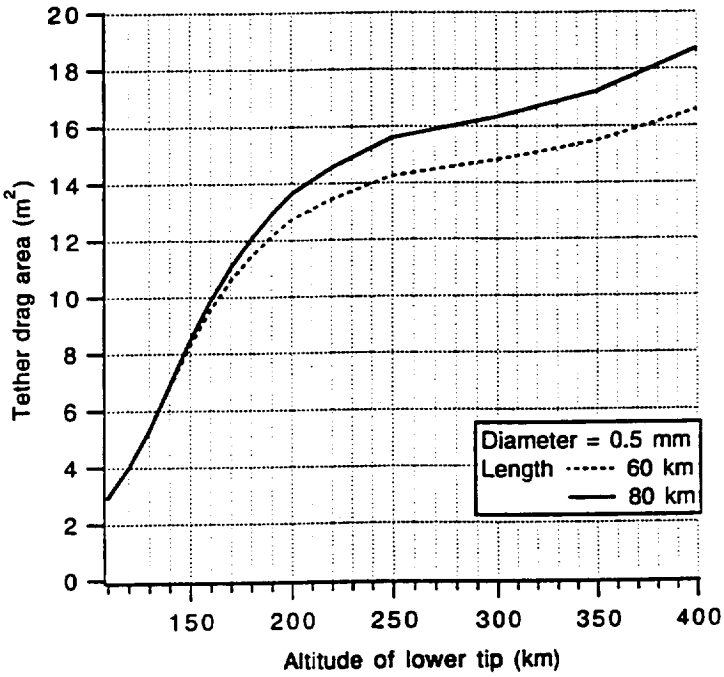


**Fig. 2.** Equivalent drag-force area per unit diameter (in mm) of two vertical and cylindrical tethers vs altitude of the bottom tip for average atmospheric conditions.

Figure 3 shows $P_{A,rev}$ vs the apogee altitude of the bottom tip (or the bottom probe) of a tethered system with a 110 km or a 120 km perigee and a specific impulse of 250 s (an average value for Hydrazine systems). The drag area $A$ mentioned above is the total drag area, i.e., the sum of the equivalent drag-force area of the tether and the overall drag area of the probes. The contribution of additional probes along the tether can be readily computed by scaling the drag area of the higher probes (subscript i, i = 2,...,$n$ where $n$ is the total number of the probes) by the atmospheric density at the tether lowest probe (subscript 1), i.e.,

$$A_i^{eq} = A_1 \rho_i/\rho_1 \qquad i = 2,....,n \tag{5}$$

For example, a system in a *circular orbit* with an 80-km-long, 0.5-mm-diameter tether with two probes of 1-m$^2$ each, separated by one scale height (~8 km in this case), and the lowest probe at 120 km of altitude, would have a total drag area $A$ = 5.37 m$^2$ and require ~16 kg/orbit (or 260 kg/day) of Hydrazine for orbital maintenance. The same propellant consumption is required for an *elliptical orbit* of 110kmx160km (measured at the bottom probe) while for a 110-km *circular orbit* (at the probe) the propellant consumption would be a staggering 68 kg/orbit (or 1105 kg/day). Elliptical orbits appear to

be mandatory, with present day tether technology, for a reasonable mission duration and a perigee altitude of the lowest probe of 110 km.

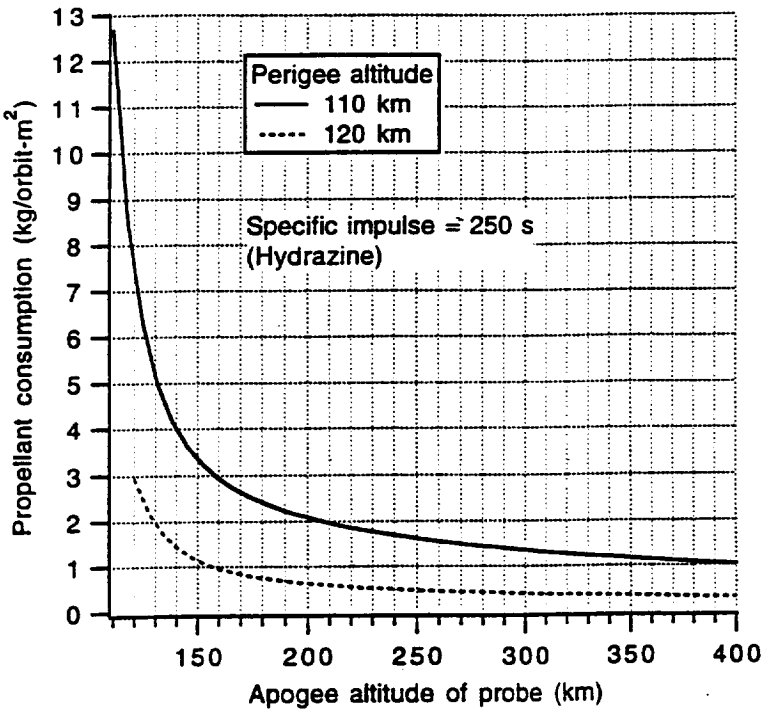


**Fig. 3.** Propellant consumption per orbit per unit drag area vs apogee altitudes of the bottom tip (or the lowest probe) for tethered systems with 110 km and 120 km perigee and a specific impulse of 250 s.

Since the in-plane libration frequency is independent of the mass distribution along the tether, the libratory modes of a multi-probe tethered system have the same frequency as the librations of a single-probe tethered system. Differences in dynamic response between the two arise from the differing lateral modes of the tether which, on the contrary, depend on the mass distribution. We refer to the modes above as *lateral modes* because even if, strictly speaking, any mode involves all the degrees of freedom, in the present case the eigenvectors of specific modes affect only certain degrees of freedom. For a comprehensive treatment of eigenvalues and eigenvectors of multi-body tethered systems see Ref. [12].

In order to exemplify the statements above, the dynamics of a single-probe and a dual-probe system are compared in Figs. 4(a) and 4(b) for the following numerical values: upper platform orbit of 200kmX200km; L = 80 km for the single-probe system; $L_1$ = 72 km and $L_2$ = 8 km (i.e., one atmospheric scale height) for the dual-probe system (L = $L_1$ + $L_2$ = 80 km); tether diameter = 0.5 mm; probe 1 mass = probe 2 mass = 100 kg; probe 1 frontal area = probe 2 frontal area = 1 $m^2$; and orbital inclination = 28.5°. The simulations were carried out with a lumped-mass computer model for tethered systems [11] with an oblate Earth, a non-spherical gravity field, and a Jacchia 77 atmospheric density model. Since the orbit of the mother platform is circular, the in-plane librations are primarily forced by the atmospheric density variations along the orbit associated with the Earth's oblateness and the diurnal bulge.

Figures 5(a)-5(d) show the dynamics of an hypothetical dual-probe system that could accomplish the scientific goals described in the Introduction of this paper. Since an extended orbital coverage at the altitude band of interest is required for global measurements of atmospheric characteristics, an

orbital inclination of 57°, which is the maximum allowed to the Shuttle, has been adopted. Also, a relatively small eccentricity is desirable in order to scan large portions of the Earth's atmosphere near the perigee height. Numerical values of the system parameters are, therefore, as follows: upper platform on a 200kmX250km orbit; tether diameter = 0.5 mm; $L_1$ = 85 km and $L_2$ = 5 km (L = overall length = 90 km); probe 1 mass = probe 2 mass = 100 kg.

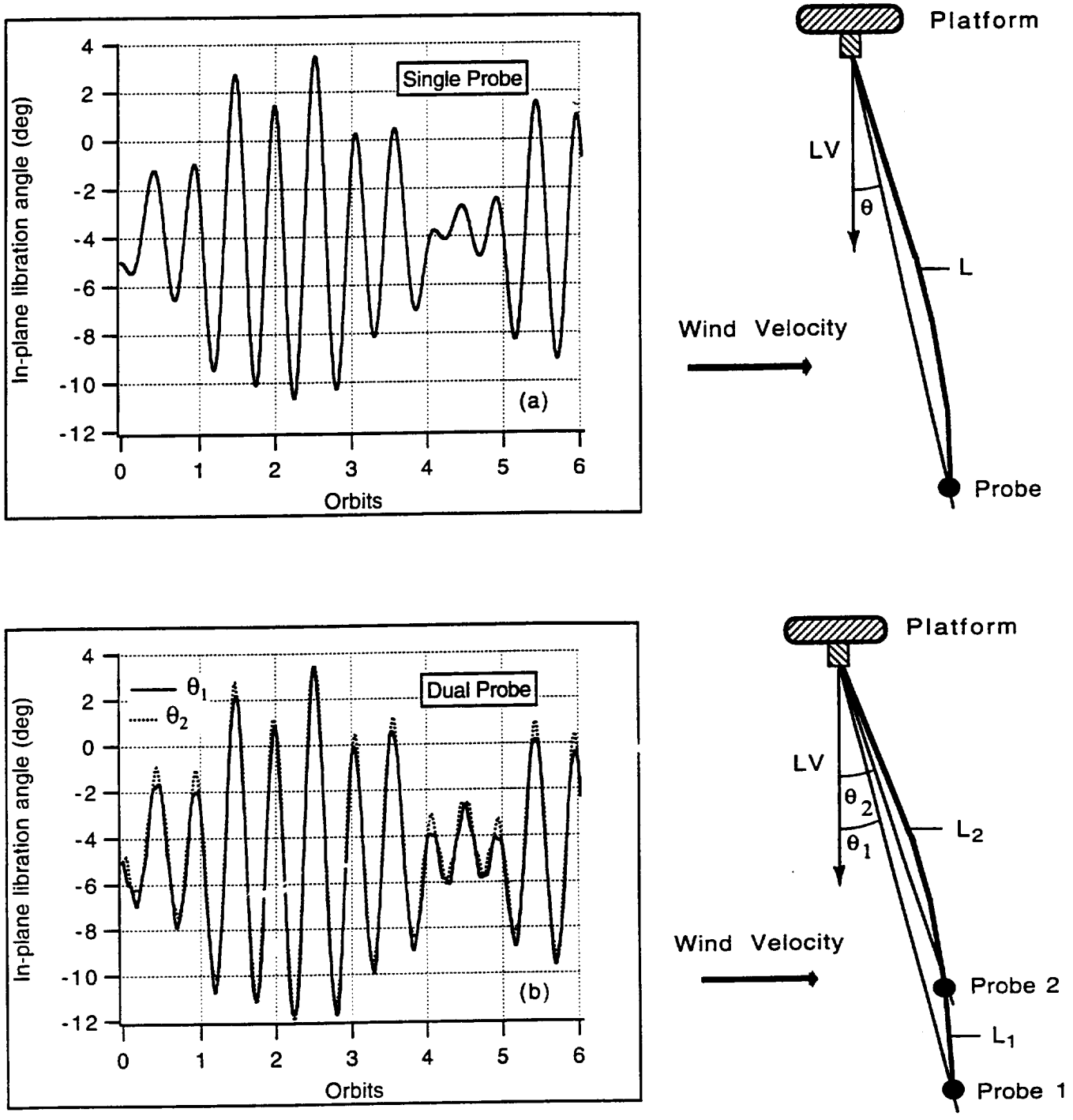


**Figs. 4.** In-plane librations of two 80-km-long tethered systems with an upper platform on a 200-km circular orbit and an overall tether lengths of 80 km (see text): (a) single-probe system; and (b) dual-probe system.

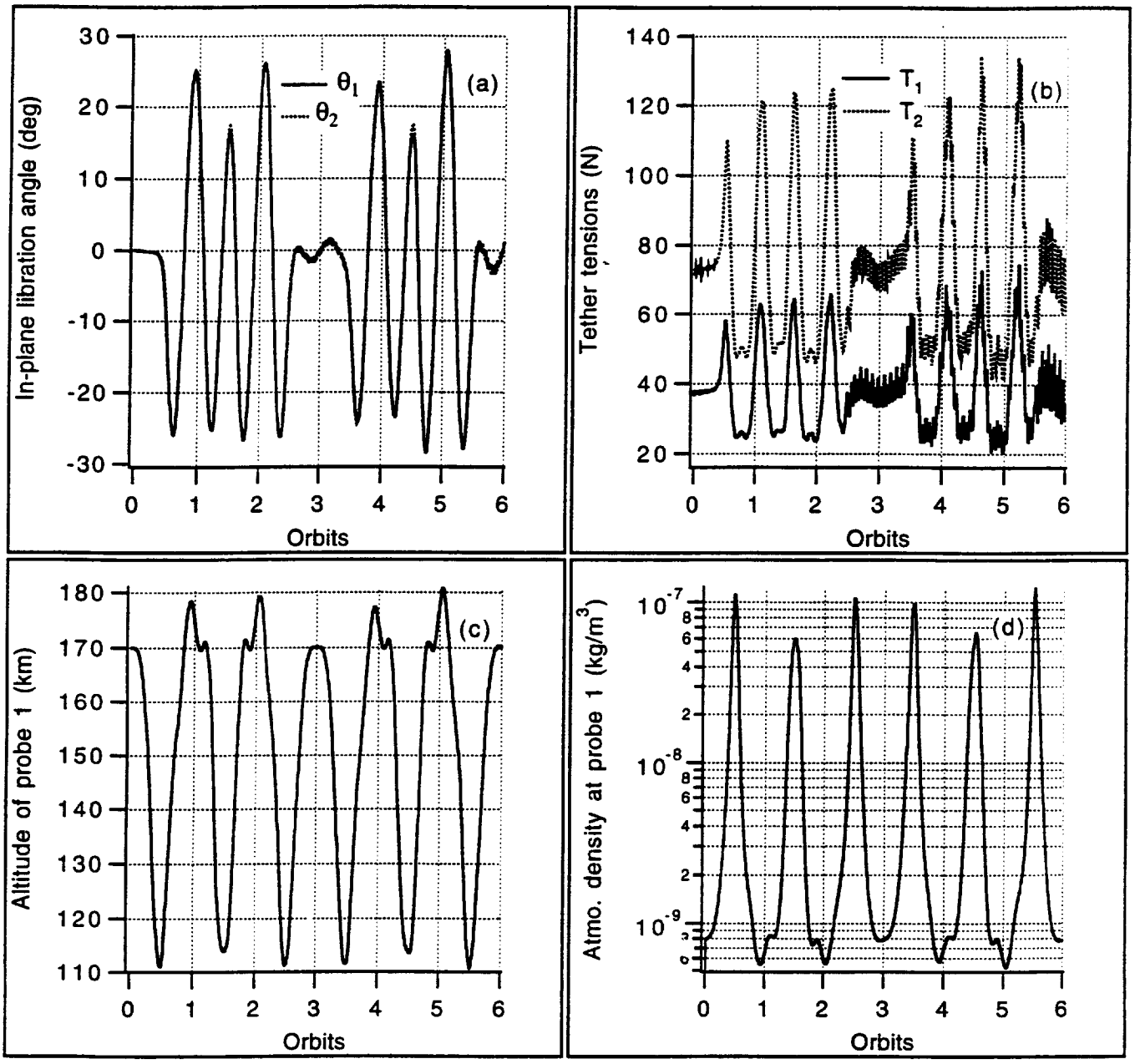


**Figs. 5.** Dynamic response of a tethered system with two probes separated by 5 km, an upper platform in a 200kmX250km orbit and an overall tether length of 90 km: (a) in-plane libration angles ($\theta_1$ lower probe, $\theta_2$ higher probe); (b) tether tensions ($T_1$ lower tether segment, $T_2$ higher tether segment); (c) altitude of lower probe; and (d) atmospheric density at lower probe.

With an elliptical orbit, the amplitudes of in-plane oscillations increase because of the larger altitude variation over one orbit which results in a stronger (than for a circular and inclined orbit) pumping of these oscillations. Masses of the probes can be increased substantially with respect to the values adopted here with no major impact on the system dynamics but with an increase of the propellant consumption due to the required increase of tether diameter. The dynamics of the dual-probe system with a perigee at 110 km of altitude is stable and the most severe system requirement is

the propellant consumption for orbital maintenance. Thanks to the dual probe configuration, the maximum tension in the lower tether segment ($T_1$) is about half the tension in the upper tether segment ($T_2$). Consequently, the diameter of the lower tether segment, which is responsible for a large portion of the drag on the system, can be smaller than the diameter of the upper tether segment, thus reducing the propellant consumption with respect to an equal-diameter-tethers configuration. The tether diameters of the dual-probe system in this paper are 0.3 mm and 0.5 mm (consistent with a safety factor of 4) for the lower and upper tether segments, respectively. The propellant consumption for orbital maintenance for this system is estimated to be about 11 kg/orbit (or equivalently 178 kg/day) of Hydrazine. A several-day-long mission could be handled by the Space Shuttle as a mother platform. Deployment of a low-altitude atmospheric system is also possible from a platform other than the Space Shuttle but mission duration and perigee altitude must be traded off for the propellant available on board. The lifetime without orbital reboosting of a typical low-altitude tethered mission with a perigee of 110 km and low eccentricity will be shorter than one orbit for an hypothetical platform mass of about 2000 kg.

Tether temperature is another concern for low-altitude atmospheric missions. Since the tether is in free molecular flow (at altitudes > 100 km) while the probes are in transitional flow, the tether is exposed to a higher heat flux than the probes. Furthermore, thermal shields can be added to the probes but are not applicable to long, thin tethers. Figure 6 shows the steady state temperature of a tether vs altitude in sunlit and eclipse conditions. In deriving these temperature values, the thermal conduction along the tether itself has been neglected and average values of emissivity and absorbitivity have been adopted. Steady-state temperatures at 120 km of altitude can be handled by conventional tether materials like stainless steel while for the temperatures at 110 km, more advanced tether materials like coated boron fibers, graphite HS, or tungsten should be considered [15]. It should also be pointed out that only the last portion of the tether (with a typical length of one scale height) is subjected to demanding thermal conditions. This last portion must be thin (and, consequently, highly stressed) for reducing the drag area, and thermally resistant for withstanding the high temperatures encountered. The rest of the tether has more relaxed thermal and stress requirements.

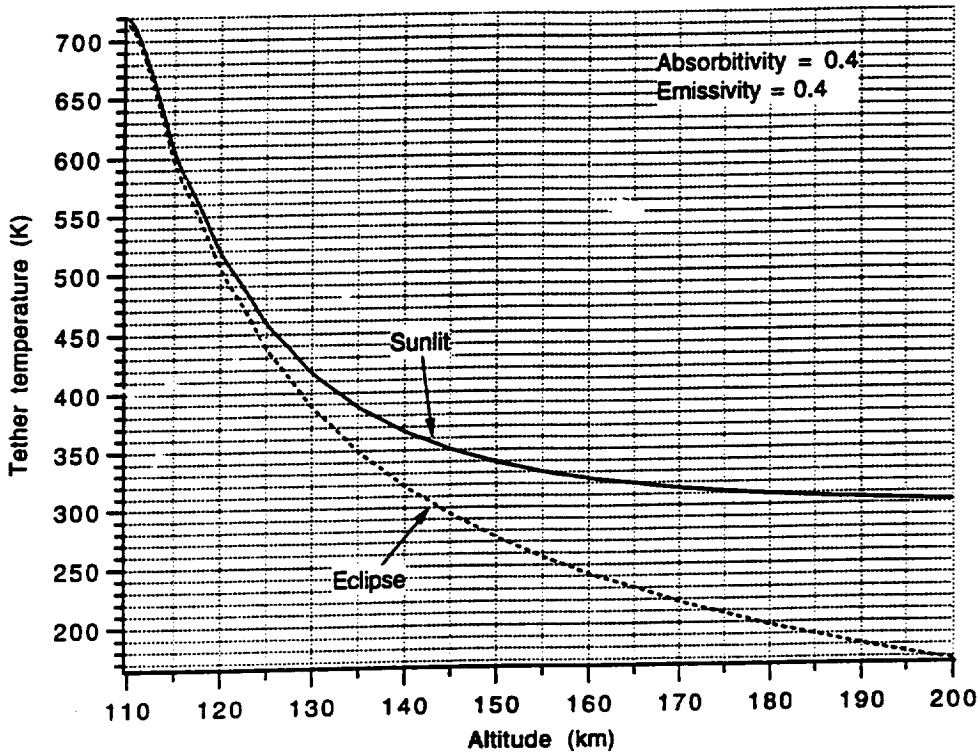


**Fig. 6.** Steady-state temperature of tether vs altitude.

## On-board Instrumentation

In the following we describe briefly the core instrumentation needed for the measurement of thermospheric cooling processes. The Smithsonian Astrophysical Observatory-supplied portion of the atmospheric measurement packages [16] would include an array detector-based limb sounding spectrometer which would measure the 15 micron $CO_2$ bands and the 5.3 micron NO and 4.3 micron $CO_2$ bands. Additionally, we hope to be able to include a far infrared Fabry-Perot instrument for measuring the 63 micron atomic fine structure line ($J = 2 <-- 1$) of $O^3P$.

Detailed measurement of the 15 micron $CO_2$ bands provides a primary measurement of atmospheric cooling. Below about 120 km, infrared emission by $CO_2$, which has been excited by collision with oxygen atoms, is the dominant cooling mechanism in the thermosphere. An additional 15 micron channel will measure lower altitude $CO_2$ for pointing of the limb spectrometers The 5.3 micron NO measurements include both the fundamental band of NO and vibrational hot bands, determining details of the formation of NO from $O_2$ and hot nitrogen atoms. Cooling by emission from the NO fundamental band is the major source of atmospheric cooling from about 120-200 km. Above about 200 km, cooling by the 63 micron emission from the fine structure transition in atomic oxygen dominates the atmospheric cooling. When complemented by mass spectrometric measurements, these emission measurements will provide definitive data on the major cooling processes in the thermosphere.

Additional instrumentation on board the probes could include GPS receivers for accurate position determination and accelerometers and tether-attachment tensiometers for measuring drag-induced dynamical perturbations and atmospheric density.

## Conclusions

Limb observations of characteristic spectroscopic emissions as well as in-situ measurements of the concentrations of trace constituents which perform the primary cooling in the thermosphere and ionosphere can be carried out by means of a multi-probe tethered system deployed into the Earth's lower thermosphere. These measurements are of particular importance in exploring the effect of the build-up of $CO_2$ on the temperature structure of the upper atmosphere. A multi-probe tethered system is uniquely suitable for reaching the required low altitudes and taking simultaneous vertically-spaced measurements with a global coverage of the Earth at the altitudes of interest. A perigee altitude as low as 110 km, for the lowest probe, can be maintained for several days with a small-eccentricity orbit and a system deployed from a platform with a substantial propellant supply (e.g., the Space Shuttle). Alternatively, a circular orbit of 120 km, for the lowest probe, could be sustained for an equivalent duration and propellant consumption. Tether temperature and dynamic stability requirements for this system can be met with presently available tether materials and tested tether control technology. Future improvements in tether materials could further improve the present scenario.

## Acknowledgments

The authors are grateful to: Kate Kirby, Alexander Dalgarno, Peter L. Smith, Irwin Shapiro, Wesley Traub, George Victor of the Smithsonian Astrophysical Observatory, and Ramesh Sharma of the Air Force Geophysical Laboratory for the fruitful discussions on thermospheric and mesospheric physics; and Charles Rupp of NASA Marshall Space Flight Center for his advice on multi-probe dynamics and technology. This research was supported in part by NASA Marshall Space Flight Center Grant NAG8-1046.

## References

1. Rishbeth, H., and R.G. Roble, "Cooling of the Upper Atmosphere by Enhanced Greenhouse Gases--Modelling of Thermospheric and Ionospheric Effects." Planetary Space Sciences, Vol. 40, No. 7, pp. 1011-1026, 1992.

2. Cicerone, R.J., "Greenhouse cooling high up." Nature, Vol. 344, 104, 1990.

3. Kirby, K. "Atmospheric Science with Tethers: Heating, Cooling and Chemistry in the Lower Thermosphere." Proceedings of the *Fourth International Conference on Tethers in Space*, 10-14 April 1995, Washington, DC, NASA Publication, 1995.

4. Roble, R.G., and R.E. Dickinson, "How will changes in carbon dioxide and methane modify the mean structure of the mesosphere and thermosphere?" Geophysical Research Letters, Vol. 16, p. 1441, 1989.

5. Aikin, A.C., M.L. Chanin, J. Nash, and D.J. Kendig, "Temperature Trends in the Lower Mesosphere." Geophysical Research Letters, Vol. 18, No. 3, pp. 416-419, 1991.

6. Roble, R.G., "Greenhouse cooling of the Upper Atmosphere." EOS Transactions, American Geophysical Union, pp. 92-93, February 23, 1993.

7. Brasseur, G., and M.H. Hitchman, "Stratospheric response to trace gas perturbations: Changes in ozone and temperature distributions." Science, Vol. 240, p. 634, 1988.

8. Spencer, T.M., "Atmospheric Perturbations and Control of a Shuttle Tethered Satellite." Proceedings of the IFAC Space Symposium, Oxford, England, July 1979, Paper 79-165.

9. Onoda, J., and N. Watanabe, "Tethered Subsatellite Swinging from Atmospheric Gradients." Journal of Guidance, Control, and Dynamics, Vol. 11, No. 5, pp. 477-479, 1988.

10. Beletski, V.V., and E.M. Levin, "Dynamics of Space Tether Systems." Advances in the Astronautical Sciences, Vol. 83, pp. 199-266, American Astronautical Society Publication, Univelt, 1993.

11. Lorenzini, E. C., M. Cosmo, S. Vetrella, and A. Moccia, "Dynamics and Control of the Tether Elevator/Crawler System," Journal of Guidance, Control, and Dynamics, Vol. 12, No. 3, May-June 1989.

12. Keshmiri, M., and A.K. Misra, "A General Formulation for N-body Tethered Satellite System Dynamics." Proceedings of the AAS/AIAA Astrodynamics Specialists Conference, Victoria, Canada, 16-19 August 1993, Paper AAS 93-700.

13. Lorenzini, E.C., C. Borgonovi, and M.L. Cosmo, "Passive Stabilization of Small Satellites." Proceedings of the 45-th Congress of the International Astronautical Federation, 9-14 October 1994, Jerusalem, Israel, Paper IAF-94-A.3.026.

14. E.C. Lorenzini, M L. Cosmo, G.G. Gullahorn, R. D. Estes, and M.D. Grossi, "Analytical Investigation of the Dynamics of Tethered Constellation in Earth Orbit (Phase II)." Smithsonian Astrophysical Observatory Final Report, NASA/MSFC Contract NAS8-36606, May 1994.

15. Scala, E., "Tethers in Space and Micrometeoroids." Proceedings of the Third International Conference on Tethers in Space - *Tethers in Space Towards Flight,* San Francisco, CA, 17-19 May 1989, 372-378, AIAA 1989.

16. Chance, K., "Spectroscopic Measurements from a Tethered Satellite Platform." Proceedings of the *Fourth International Conference on Tethers in Space*, 10-14 April 1995, Washington, DC, NASA Publication, 1995.

## 3.0 Analysis of SEDS-II Satellite Flight Data

A paper, presented at the *Fourth International Conference on Tethers in Space*, is included in the following to illustrate the results of the analysis of the acceleration levels and dynamic noise on-board the SEDS-II end-mass.

**Paper WSEDSP-5**

# ACCELERATION LEVELS AND DYNAMIC NOISE ON SEDS END-MASS

M.L. Cosmo, E.C. Lorenzini, and G.E. Gullahorn
Harvard-Smithsonian Center for Astrophysics

**Fourth International Conference on Tethers in Space**

Sponsored by National Aeronautics and Space Administration,
Smithsonian Astrophysical Observatory, Agenzia Spaziale Italiana, Martin Marietta,
Alenia Spazio S.p.A., Science Applications International Corporation

Smithsonian Institution, Washington, DC, 10-14 April 1995

# ACCELERATION LEVELS AND DYNAMIC NOISE ON SEDS END-MASS

M.L. Cosmo, E.C. Lorenzini, G.E. Gullahorn
Smithsonian Astrophysical Observatory
Cambridge, MA 02138, USA

## ABSTRACT

Spaceborne tethers offer a unique transportation capability for instrumented probes attached to orbiting platforms (e.g. Space Station) or access to otherwise inaccessible flight regions (e.g. Lower Thermosphere).

SEDS flights have provided the scientific community with a wealth of data. In this paper the authors focus their attention on the acceleration levels on board the tethered end-mass and how they are affected by the tether motions and environmental perturbations. The absence of any damping device gives a realistic picture of a typical "tethered environment" as well as pinpoint its limits or suggest necessary modifications.

Simplified models have been developed in order to understand the features observed in the acceleration spectra. A good agreement has been found between the observations and the theory.

## INTRODUCTION

The successful flights of the Small Expendable Deployer System (SEDS) have demonstrated the capability of tethers in space transportation. Long tethers can trawl deep into the Earth's lower atmosphere to perform continuous "in-situ" measurements of chemical species[2] and remote sensing of the Earth's' gravity gradient [6,8] . Moreover, space tethers might of insulate experiments from a "noisy" (e.g. high dynamic activity) and/or contaminated environment [9,11] when a "quiet" acceleration envelope is needed.

In this paper we concentrate on the spectral contents of the accelerations on board SEDS-2 and estimate the dynamic noise. We have approached the problem by separating the various contributions to the acceleration levels in three groups, namely the tether, the platforms' dynamics and the environmental perturbations.

## THE "TETHER" ENVIRONMENT

Let us consider the two-dimensional equations of motion for a dumbbell system orbiting the earth at a constant rate $\Omega$ under the hypotheses of small librations and massless tether

$$\begin{aligned} \ddot{\vartheta} + 2\frac{\dot{l}}{l}(\dot{\vartheta} - \Omega) + 3\Omega^2 \frac{\sin 2\vartheta}{2} &= \frac{T_D}{ml} \\ \ddot{l} - l(\dot{\vartheta} - \Omega)^2 - l\Omega^2(3\cos^2\vartheta - 1) &= \frac{(D-T)}{m} \end{aligned} \qquad (1)$$

where:

$\vartheta$ = angle between line connecting end masses and local vertical (i.e. in-plane angle)
$l$ = tether length
T = tether tension
D = perturbing acceleration
$T_D$ = generalized perturbing torque
m = equivalent mass

In the absence of perturbations, the specific forces measured onboard a tethered platform are -T along the tether and zero in the perpendicular direction. Namely, the axis along the libration is in "free-fall" , while the other is affected by a "bias" term . Consequently the knowledge of the tether direction with respect to the end-mass is necessary in order to make acceleration measurements onboard a tethered satellite. Furthermore, the influence of the tether must be carefully characterized as a perturbation in order to discriminate it from the other accelerations.

Tethers have a wide spectrum of oscillations. Under the hypotheses of small angles, the in-plane and out-of-plane libration frequencies are $\sqrt{3}\Omega$ and $2\Omega$, respectively. The lateral (i.e. "string") and longitudinal oscillations frequencies $\omega_n/2\pi$ can be computed by solving the equation:

$$z_n tg z_n = \frac{\mu l}{M}$$
$$z_n = l\omega_n \sqrt{\frac{\mu}{Y}} \qquad (2)$$

where:

$\mu$ = tether linear density
$l$ = tether length
$M$ = equivalent mass
Y = EA for longitudinal modes = product between the tether Young's modulus and the cross section area
or

= T for lateral modes = tether tension (assumed constant along tether)

The spring-mass frequency of the two body system connected by a massless tether is

$$f = \frac{1}{2\pi}\sqrt{\frac{EA}{lM}} \qquad (3)$$

As we shall discuss later on. there are various sources of external perturbation that can deposit energy in these modes. Tethers can naturally abate only perturbations acting along the longitudinal direction through structural damping. All other modes, once excited. cannot be damped naturally unless specific control strategies are applied [4,9].

## SEDS-2 FLIGHT

Both SEDS flights were equipped with a 3-axis accelerometer. The data were analyzed in order to estimate the natural acceleration environment of a tethered platform, without any stabilization device.

Figure 1 shows a schematic of the end-mass with the body reference frame and the location of the instruments [10]. The end-mass properties are given in Table 1 and the characteristics of the accelerometers are given in Table 2.

| Table 1. SEDS-2 End-Mass Characteristics | |
|---|---|
| Mass (kg) | 25.9 |
| Moments of Inertia (kg-$m^2$) | X) 0.285; Y) 0.464; Z) 0.545 |
| Accel. X Location wrt CM (m) | X)-$1.90 \times 10^{-3}$; Y)-$1.84 \times 10^{-2}$; Z)-$8.1 \times 10^{-3}$ |
| Accel. Y " | X)-$1.84 \times 10^{-2}$; Y) $1.68 \times 10^{-3}$; Z) $2.85 \times 10^{-2}$ |
| Accel. Z " | X) $1.82 \times 10^{-2}$; Y) $1.97 \times 10^{-2}$ ; Z) $6.88 \times 10^{-3}$ |
| Tether Attachment Point Location wrt CM (m) | X) 0.165; Y) 0.184; Z) -$8.86 \times 10^{-3}$ |

| Table 2. Accelerometer Characteristics | |
|---|---|
| Type | Sundstrand QA 2000-030 |
| Range | 1)1 mg; 2) 5 mg; 3) 50 mg |
| Resolution | 1) 8 μg 2) 40 μg; 3) 400 μg |
| Sampling Rate | 8 Hz |

SEDS second flight provided about 8 hours of data during station keeping before the onboard battery exhausted its energy. The following analysis will focus on this set of data because of the stationarity of this phase.

In both flights, the analysis of the magnetometer data showed that the end-mass spun around the tether axis [1]. In the second flight the spin rate increased until it reached 35 °/s ($\simeq$ 6 rpm)at about 26000 seconds, as shown in figure 2. Note that the time is counted from the ejection of the end-mass from the Delta II stage. The end of the deployment was reached at about 6600 seconds.

The frequencies of SEDS-2 are given in Table 3 and the mass properties adopted are:

$\mu = 3.3 \times 10^{-4}$ Kg/m
$l = 20$ Km
M = 26 Kg
EA = 15,000 N
$\Omega = 1.14 \times 10^{-3}$ rad/s

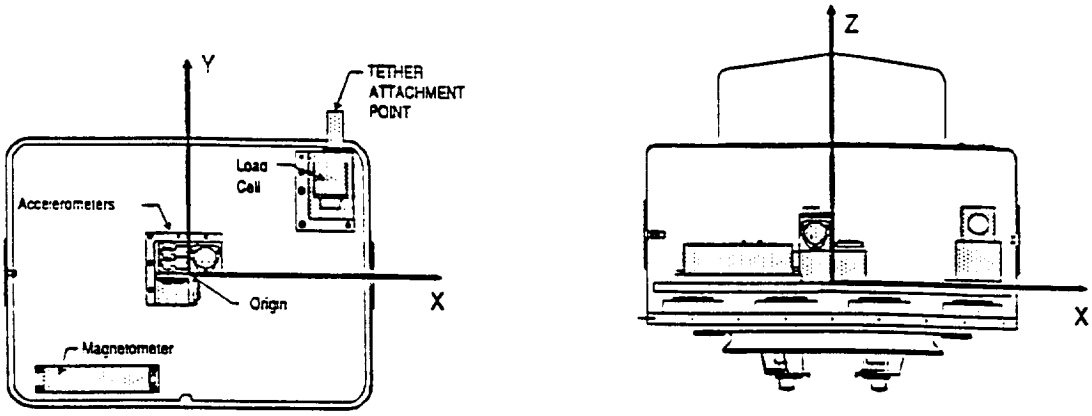


Figure 1. SEDS end-mass schematic

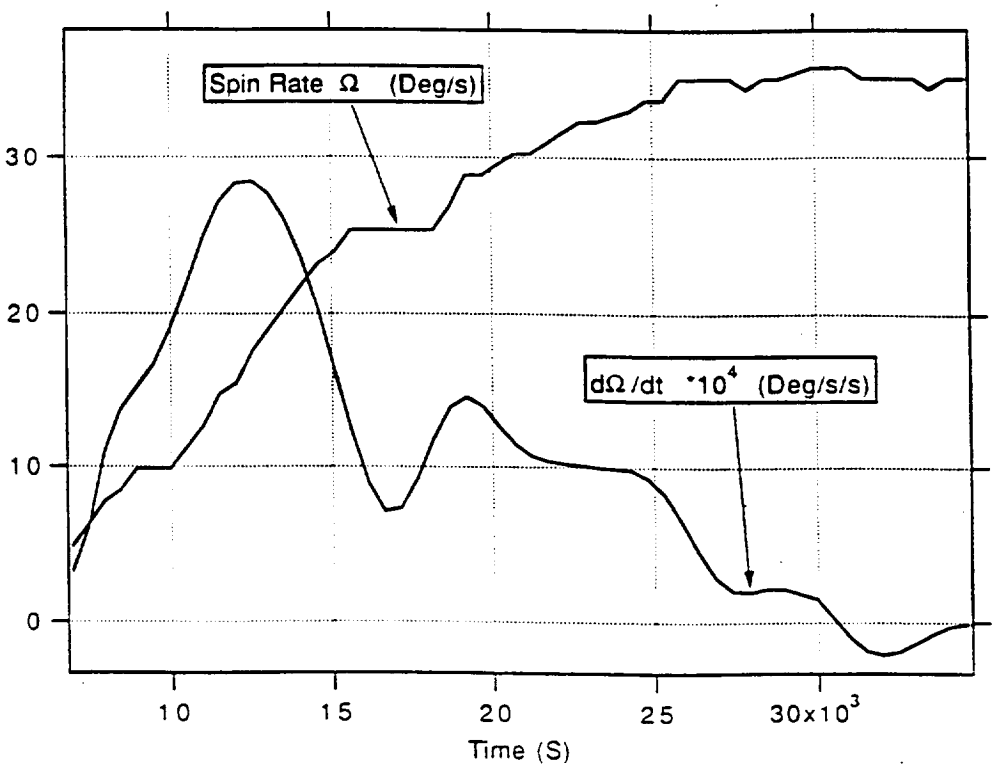


Figure 2. End-mass spin and spin rate during station keeping.

| Table 3. SEDS-2 Natural Frequencies (Hz) | |
|---|---|
| In-plane libration | $3.15 \times 10^{-4}$ |
| Out-of-plane libration | $3.64 \times 10^{-4}$ |
| Spring mass | $2.70 \times 10^{-2}$ |
| Longitudinal Modes | |
| 1st Mode | 0.17 |
| 2nd Mode | 0.34 |
| 3rd Mode | 0.50 |
| Lateral Modes | |
| 1st Mode | $1.91 \times 10^{-3}$ |
| 2nd Mode | $3.82 \times 10^{-3}$ |
| 3rd Mode | $5.72 \times 10^{-3}$ |

To compute the lateral frequencies we used the mean value of the tension provided by the load cells at the satellite attachment point (≈ 1.96 N). The tension acting on the end mass is shown in figure 3.

## END-MASSES RIGID BODY MOTION

In order to understand the dynamic coupling between tether and end-platforms we computed the attitude frequencies of the end-mass and the Delta's second stage.

As stated earlier the end-mass spun around the tether at increasing rate throughout the whole mission. Therefore, we erected a new body frame by aligning the new x axis ("yaw" axis) with the tether attachment point.

The new inertia matrix is:

$$\begin{vmatrix} 0.38 & 0.089 & 0.006 \\ 0.089 & 0.36 & -0.0032 \\ 0.006 & -0.0032 & 0.54 \end{vmatrix}$$

Rewriting the Euler's equations in the new reference frame and assuming that the rate around the x axis is constant and equal to the spin rate, under the hypotheses of small angular displacements around the other two axes. we obtain:

$$f_{pitch} = 0.15 \text{ Hz}$$
$$f_{roll} = 0.17 \text{ Hz}$$

By comparing the end-mass attitude frequencies with SEDS-2 natural frequencies (Table 3) we notice that these frequencies are very similar to the longitudinal modes. A

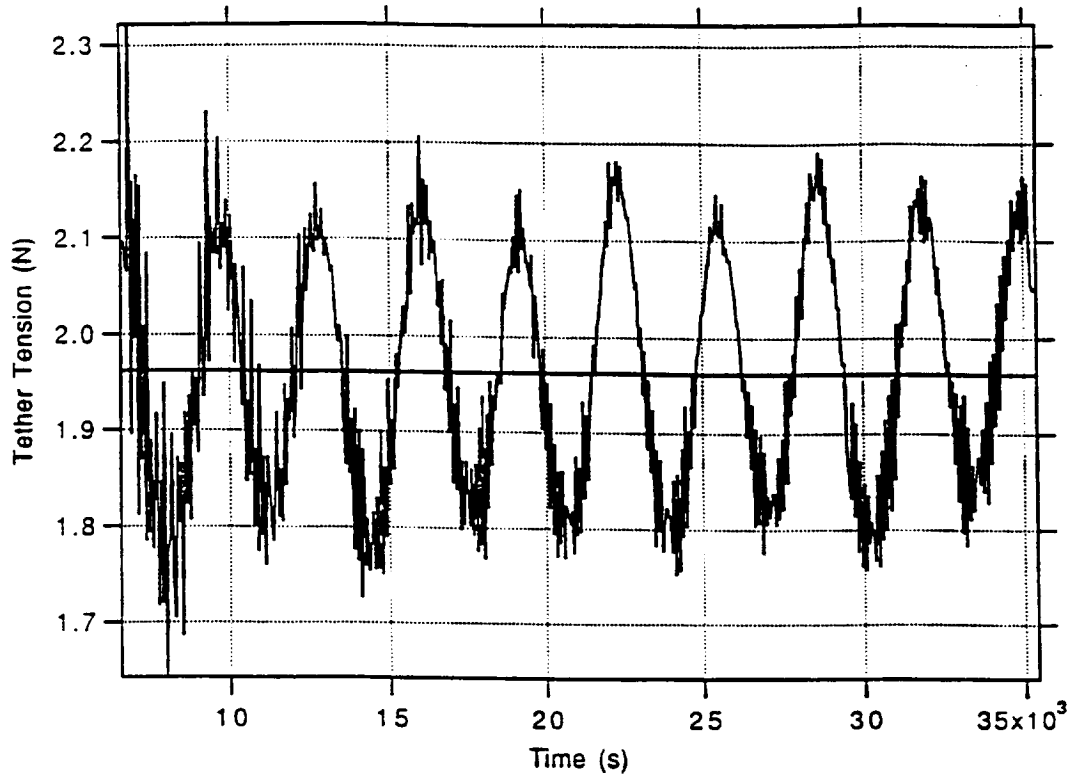


Figure 3. Tension modulus during station keeping

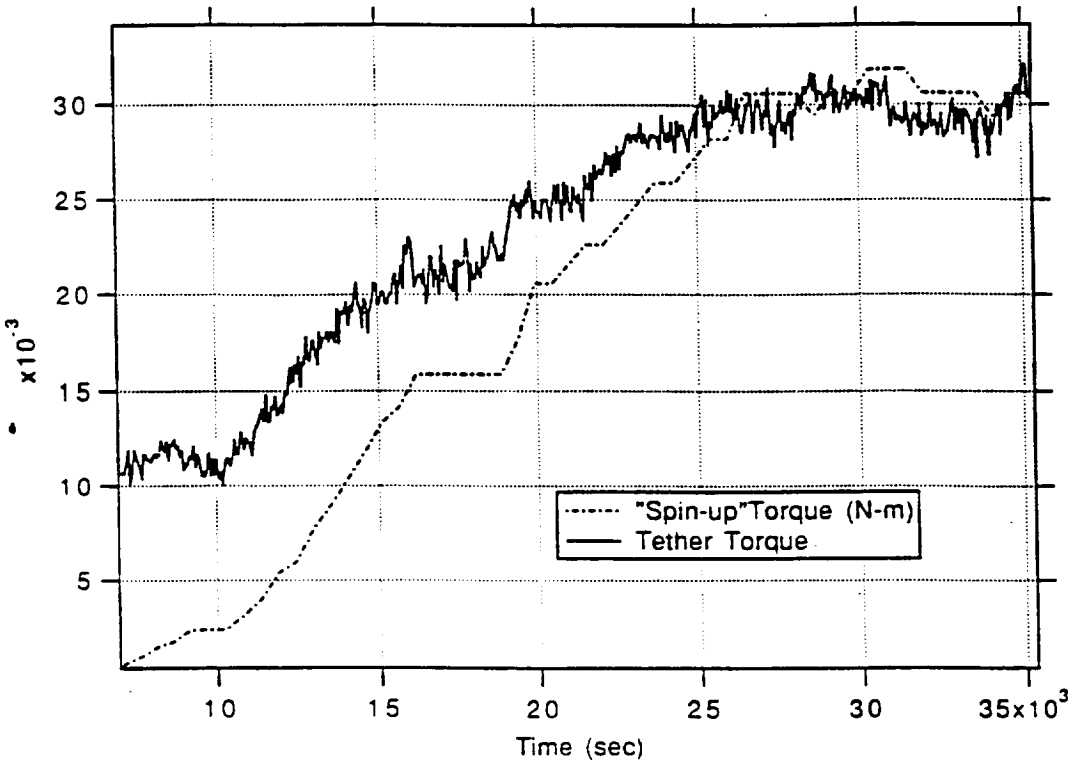


Figure 4. Comparison of tether torque and "spin-up" torque

resonance between tether modes and end-mass attitude frequencies could explain the increase in spin rate observed during the mission.

To this end we compared the modulus of the tether torque as measured by the load cells to the modulus of the torque necessary to "spin-up" the end mass obtained from the magnetometer data. By assuming that the end-mass is rotating only around the x axis ($\omega_X = \Omega$ and $\omega_Y \approx \omega_Z \approx 0$) we can rewrite the Euler equations as

$$M_X \approx I_{XX}\, d\Omega/dt$$
$$M_Y \approx -I_{XY}\, d\Omega/dt + I_{XZ}\, \Omega^2$$
$$M_Z \approx -I_{XZ}\, d\Omega/dt - I_{XY}\, \Omega^2$$

where $M_X$, $M_Y$ and $M_Z$ are the torques required to spin-up the end mass. The comparison between the modulus of the "spin up" torque and the torque computed by the load cells data is shown in Figure 4. It can be noticed that, within the simplifications of our assumptions, the moduli are similar thus suggesting the torque required was mainly provided by the tether itself.

The Delta attitude frequencies were computed by adopting the inertia and geometric properties as reported in reference 5.

$$f_{pitch} = 5.7 \times 10^{-3}\ Hz$$
$$f_{roll} = 8.9 \times 10^{-3}\ Hz$$

## ENVIRONMENTAL PERTURBATIONS

On the one hand, a thorough characterization of the environmental perturbations and their spectra is necessary in order to understand their influence on the system dynamics. On the other hand. SEDS flight instrumentation was intended only to assess the overall dynamic scenario. Consequently, this section will only briefly overview some of the external perturbation that may affect the acceleration environment onboard a tethered satellite.

The disturbances transmitted through the tether from the deployer to the satellite are not negligible. As already stated, only longitudinal perturbations can be naturally damped. The analysis of the damping mechanisms as well as their coupling to other modes are beyond the scope of this paper. As we shall see in the next section, the influence of the deployer motions on the acceleration levels of SEDS-2 end-mass is very significant.

Atmospheric drag is the main perturbation acting on satellites in LEO. For tethered satellites this influence is amplified because of their large exposed area. The mean atmospheric structure at a certain altitude is governed by factors like the type of heating processes taking place. At low thermospheric altitudes the mean atmospheric structure is dominated by semi-diurnal variations, as shown in figure 5 (from reference 7), with density variations of up to 30% in one orbit. Moreover, density variations due to transport processes can cause the mean density to vary up to one order of magnitude.

The observed density variations $\Delta\rho/\rho$ for some atmospheric processes are as follows [7]:

| | |
|---|---|
| Gravity Waves | 5-20% |
| Tides | 10-20% |
| Geomagnetic Storms | 20-40% |
| Winds | 20-30% |

The occurrence of these phenomena and their frequencies vary with geomagnetic activity. altitude. latitude and local time [13] and it is hard to define a time scale for each variation.

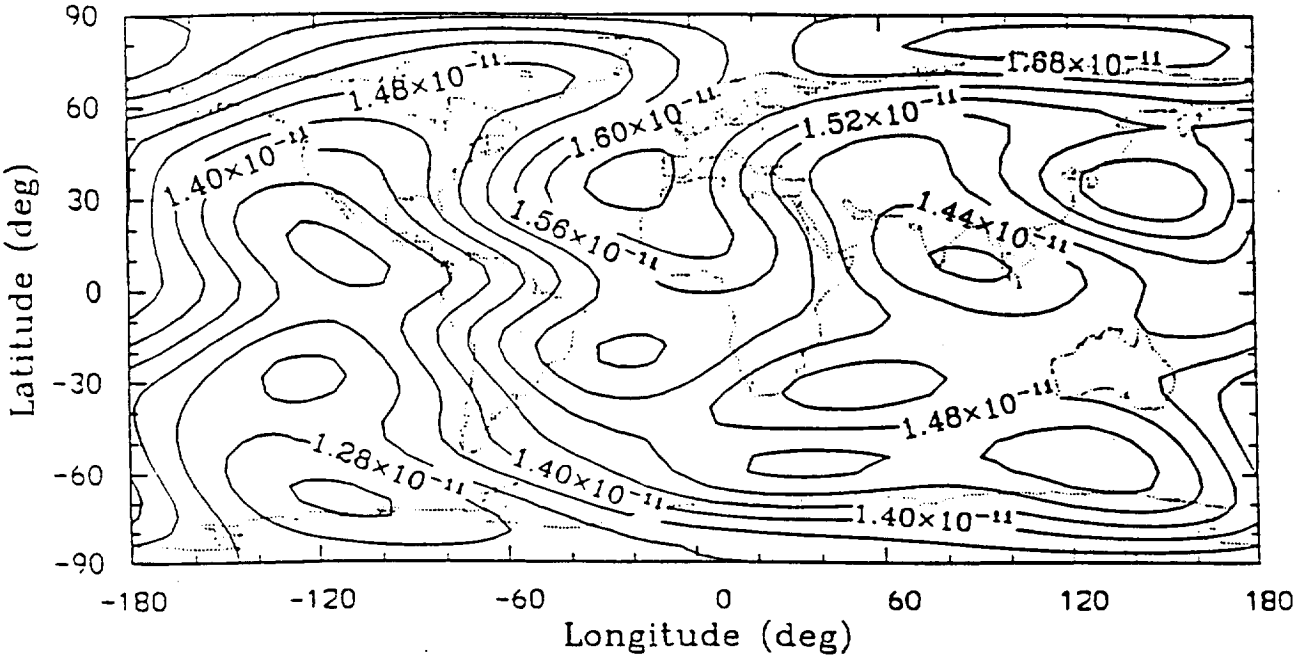


Figure 5. Modeled mean atmospheric density at 120 km altitude ($A_p$=12 and $F_{10.7}$=180 (from ref. 7)

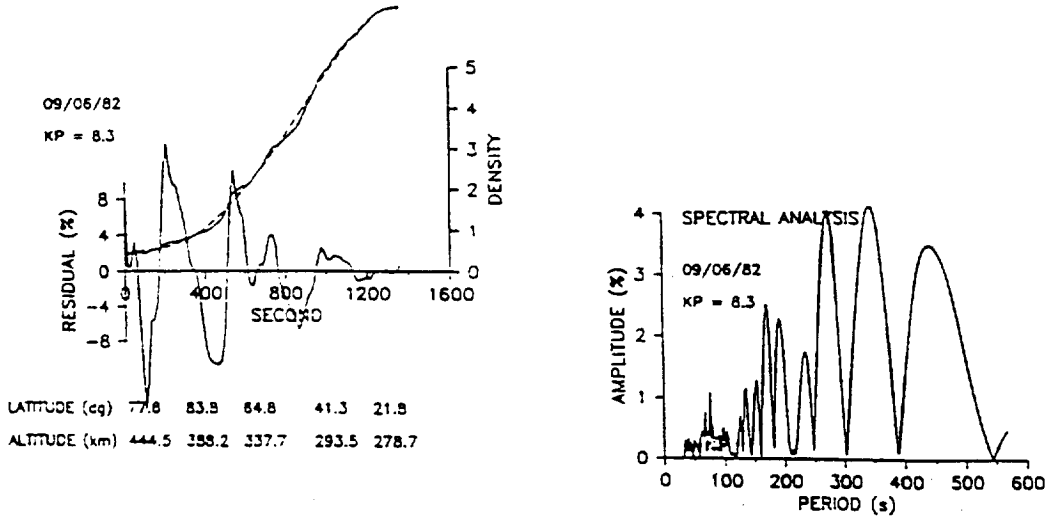


Figure 6. Fluctuations of total density for DE-2 measurements with respect to polynomial fitting and spectral analysis (from ref. 13)

Figure 6 depicts the fluctuations in total density experienced by the Dynamics Explorer-2 (DE-2) during a period of high solar activity. The spectral analysis shows that some atmospheric variations have periods similar to the lateral modes of tethered satellites (e.g. $\approx 10^2$ seconds). Most of these perturbations are going to act in a direction perpendicular to the tether line, therefore the lateral frequencies are going to be excited.

Thermal variations also play a major role causing the tether to expand and contract with a noticeable influence on the onboard accelerations levels. The main input in the tether thermal budget is the solar radiation. Variation in the total solar irradiance at various time scales are the subject of extensive studies. The variability on solar activity time scales (days or months), which are of interests for our missions, account to up 0.25% of the total irradiance (3.5 $W/m^2$) . Variability at shorter time scales (minutes and hours), caused by solar oscillations do not appear to be very significant. "5-minutes" oscillations, for instance, are 3 ppm of the total irradiance signal. At present, our analysis of SEDS-2 data has not been able to detect any acceleration variation caused by thermal excursion.

## FLIGHT DATA

In this paragraph we will present the results of the analysis of SEDS-2 accelerometers data. In our analysis we try to utilize our understanding of the tether dynamics and the influence of external perturbations in order to obtain an estimate of the acceleration environment onboard a tethered satellite.

We numerically computed the power spectra of the onboard accelerations by adopting the classical "periodogram" estimation [12]. In order to keep the uncertainty of our estimates within a reasonable range we block-averaged the original data set at the expense of a reduced frequency resolution [3,12]. Since the orientation of the end-mass is not accurately known[1], we chose to estimate the moduli of the accelerations. This choice is not going to give the lowest noise since the data will be altered by the rotational dynamics.

The first set of data were taken two, four and six orbits since ejection, respectively. The spectra are shown in figure 7a, 7b and 7c. The data were averaged at 0.25 seconds and we took 8192 data samples divided in two blocks. The range between $10^{-3}$ and $10^{-2}$ Hz shows two distinct peaks. The first peak is given by the system libration. Our analysis has shown that the tether final in-plane libration was ~4 deg. The second peak at $7.5 \times 10^{-3}$ Hz is comparable to the Delta attitude frequencies. The discrepancy may be attributed to different values of the Delta's moments of inertia. Since the Delta's attitude was not controlled, the peak height is practically constant with time. In the $10^{-2}$ and $10^{-1}$Hz range there is a peak of 0.9 $m/s^2/\sqrt{Hz}$ which is very close to the theoretical spring-mass frequency. As figure 7b and 7c show this peak decreases with time suggesting that the mode has been damped. Another explanation of these peaks could be given by the coupling between the Delta attitude and the tether lateral modes. As time progresses some peaks disappear or merge like the harmonic at $1.25 \times 10^{-2}$ and $1.6 \times 10^{-2}$ Hz. The power spectrum in the frequency range between $10^{-1}$ and 1 Hz decreases inversely with the frequency at the beginning of the station keeping and stabilizes at about $10^{-3}$ $m/s^2/\sqrt{Hz}$ after 6 orbits. The coupling between end-mass modes and tether modes plays the major role in this frequency range.

Figure 8 shows the spectra of the x and z acceleration components. The z axis was mostly perpendicular to the spin axis and this explains the lower noise at low frequencies. On the other hand, the end-mass attitude frequencies are now more discernible in the 0.1-2 Hz range. The dynamic noise in this range is practically the same for both axis. The spectra of the two acceleration components in the $10^{-3}$-$10^{-1}$ Hz range, differ by an order of magnitude. By assuming that the end-mass and the delta attitudes were stabilized, like it would be the case in a scientific mission, we could extrapolate that the dynamic noise would tend to $5 \times 10^{-4}$ $m/s^2/\sqrt{Hz}$.

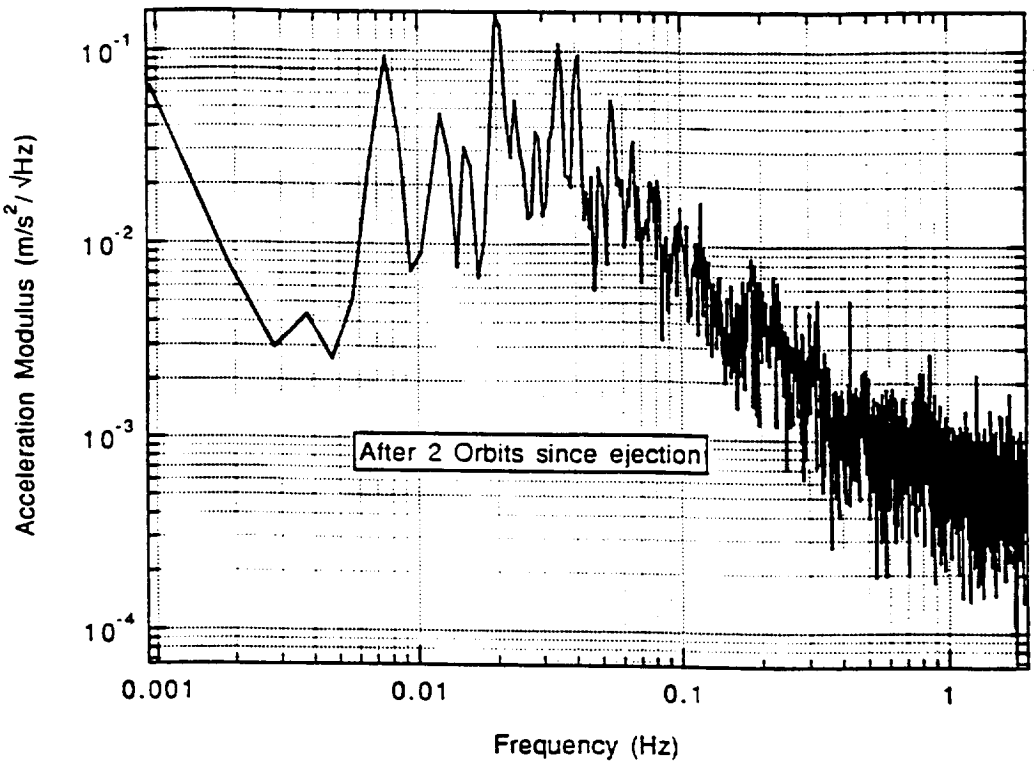


Figure 7a. Power spectrum of end-mass acceleration modulus
(2 orbits since ejection)

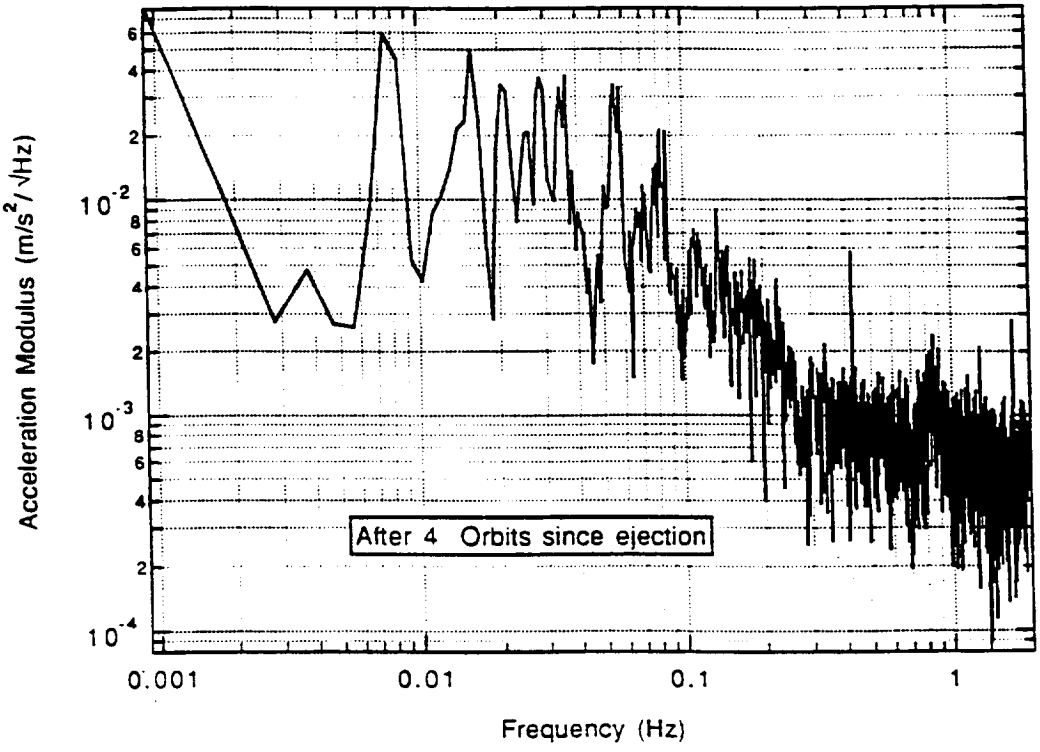


Figure 7b. Power spectrum of end-mass acceleration modulus
(4 orbits since ejection)

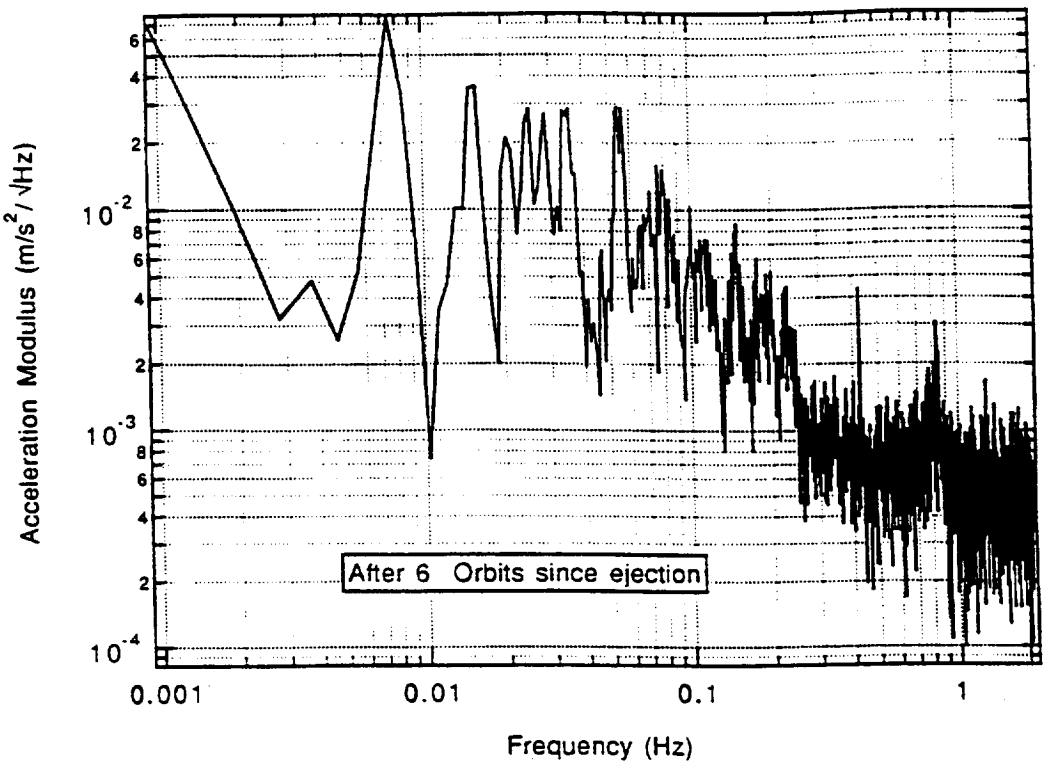


Figure 7c. Power spectrum of end-mass acceleration modulus (6 orbits since ejection)

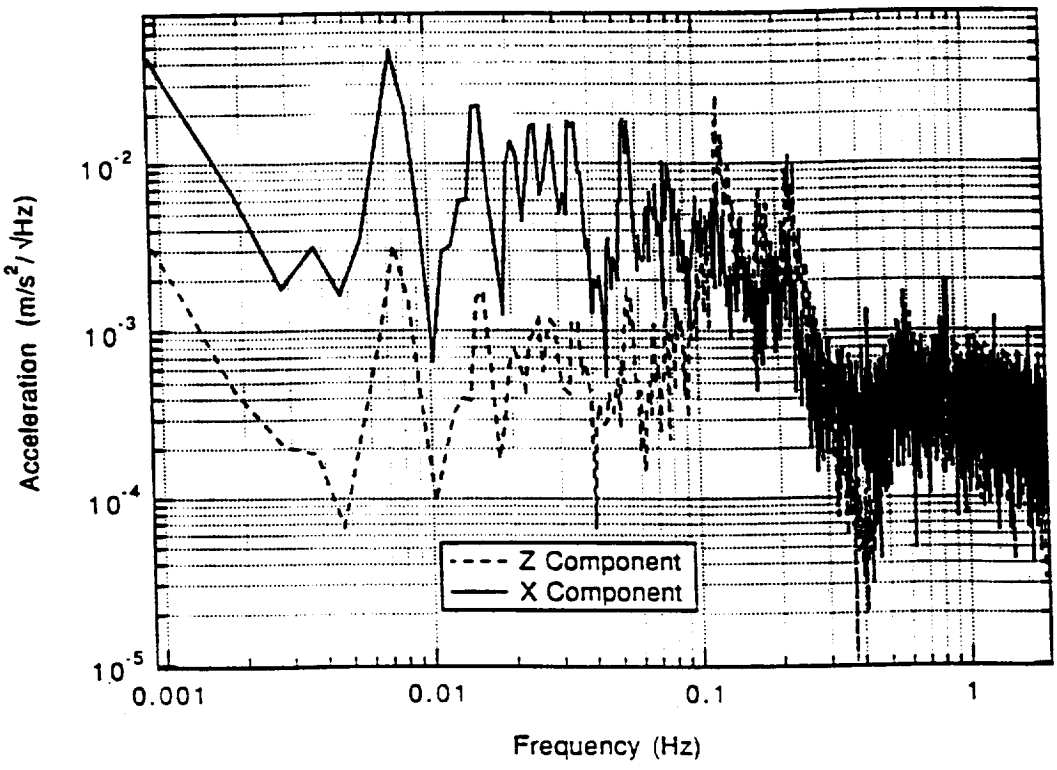


Figure 8. Power spectrum of end-mass acceleration x and z components (6 orbits since ejection)

## CONCLUSIONS

This paper has analyzed the acceleration levels onboard SEDS-2 end-mass in order to assess the influence of the tether and the environmental perturbations on an hypothetical scientific platform. The estimation of the accelerations' power spectra has yielded a residual noise level of about $5 \times 10^{-4}$ $m/s^2/\sqrt{Hz}$. This value, however, cannot be generalized to all types of tethered satellites since some of the observed features are strictly related to SEDS-2 dynamics. Actually, some of the modes, like the longitudinal waves propagating through the tether from the deployer or the system's librations, can be actively damped. On the other hand, there are environmental perturbations like atmospheric density variations that are going to excite some tether oscillation modes which are very difficult to abate. Therefore, a thorough characterization of the "tether environment" and its dependence on environmental perturbations must be performed on a case by case basis in order to meet the missions' scientific objectives.

## ACKNOWLEDGMENTS

Support for this paper has been provided by grant NAG8-1046 from NASA Marshall Space Flight Center and NASA Langley Research Center. M.C. would also like to acknowledge the useful advice received by P. Ciarpallini, A.Diaferio, S.Fineschi and L.Strachan.

## REFERENCES

1. M.Cosmo, G.E. Gullahorn, E.C. Lorenzini, M. Grassi. Analysis of SEDS-1 dynamics from on board instrumentation. AIAA Space Programs and Technology Conference and Exhibit, Huntsville, Alabama, Sept 23, 1993
2. A.Dalgarno, W.B.Hanson, N.W.Spencer, E.R. Schmerling. The Atmosphere Explorer mission. *Radio Science*, **8**, No.4, pp263-266, April 1973
3. J.C. Hardin. Introduction to time series analysis. NASA Reference Publication 1145, 1986
4. X. He and D. Powell, Tether Damping in Space. *J. Guidance Control Dynamics*, **13**, PP. 104-112, 1990
5. J.Glaese. SEDS-2 DRM, Release 2. Logicon Control Dynamics Report to NASA/MSFC, February, 1994
6. W.D. Kahn and F.O. Von Bun. Error analysis for a gravity gradiometer mission. *IEEE Trans. Geosci. Remote Sensing*, **GE-23**, 527, 1985
7. T.L. Killeen, A.G. Burns, R.M. Johnson, F.A. Marcos. Modeling and prediction of density changes and winds affecting spacecraft trajectories. In Enviromental Effects on spacecraft positioning and trajectories, A. Vallance Jones, ed., AGU Geophysical Monograph 73, pp. 83-110, 1993
8. E.C. Lorenzini, G.E. Gullahorn, and F.Fuligni. Recent developments in gravity gradiometry from the Space-Shuttle-borne tethered satellite system. *J. Appl. Phys.* **63**(1), pp.216-223, 1988
9. E.C. Lorenzini and M.L. Cosmo. Wave propagation in the Tether/Crawler System. *Acta Astronautica*, **21** No. 8, pp.545-552, 1990
10. L.T. Melfi, K.H. Crumbly, G.M. Wood, N.C. Coffey, J.K.Diamond, T.D. Finley, J.K. Quinn, J.E. Price, R.D. Rhew, J.H. Stadler, W.J. Webster, D.T. Fralick, R.A. Marshall, W.G. Nagurny, W.J. Scott. Engineering performance of the SEDS tethered end mass payload. AIAA Space Programs and Technology Conference and Exhibit. Huntsville, Alabama, Sept 23, 1993
11. P. Musi, M.Martino, S.Bergamaschi and P.Zanetti. Micro-g noise levels measured on board tethered satellite during STS-46 mission. Proceedings of the International Round Table on Tethers in Space, ESA WPP-081, ESTEC, Noordwijk, The Netherlands, Sept. 28-30, pp. 452-463, 1994
12. W.H.Press, B.P.Flannery, S.A.Teukolsky, W.T. Vetterling. Numerical Recipes: The art of scientific computing. Cambridge University Press, 1986

13. P.Touboul, A.Bernard, F.Barlier, and C.Berger. Air drag effects on gradiometer measurements. *Manuscripta Geodaetica*, **16**, pp. 73-91, 1991
14. R.C.Willson. Results of space-based total solar irradiance experiments. P. Foukal, ed., Proceedings of the Workshop on Solar Radiative Output Variations at NCAR, Boulder , CO, Nov 9-11, 1987

## 4.0 Acknowledgments

We would like to acknowledge that the work on the sensitivity of SEDSAT deployment was done by Prof. Jesus Pelaez while visiting the Smithsonian Astrophysical Observatory from the Politechnical University of Madrid in Spain with financial support from his home institution. We would also like to thank Kate Kirby and Kelly Chance of the Smithsonian Astrophysical Observatory for the great contributions to the *Fourth International Conference on Tethers in Space* which are represented in this report by their two papers presented at that conference.

## 5.0 References

1. Kaplan, M.H., "Modern Spacecraft Dynamics and Control." p. 112, Wiley, 1976.

2. E.C. Lorenzini, D.K. Mowery, and C.C. Rupp, "SEDS-II Deployment Control Law and Mission Design." Proceedings of the *Fourth International Conference on Tethers in Space*, 10-14 April 1995, Washington, DC, Science and Technology Corporation, Hampton, Virginia.

3. Carroll, A.J., "SEDS Deployer Design and Flight Performance," Proceedings of the AIAA Space Programs and Technology Conference Exhibit, 21-23 September 1993, Huntsville, Alabama, AIAA paper 93-4764.

4. Lorenzini, E.C., M.L. Cosmo, and G.E. Gullahorn, "Tethered Systems Dynamics and Flight Data Analysis." Smithsonian astrophysical Observatory Annual Report, NASA/MSFC Grant NAG8-1046, April 1995 (in print).

5. Wertz, R., and W.J. Larson (Eds.), "Space Mission Analysis and Design." p. 127, Kluwer Academic Publisher, 1991.

6. Carroll, J. A., " Users Guide to SEDS, The Small Expendable-Tether Deployment System," Tether Applications, La Jolla, CA, April 1990.

7. Lallman, F., "Tethered Satellite System - Independent Fresh Look" Presentation NASA Langley Research Center, February 8, 1984.

8. Pelaez, J., "On the Dynamics of the Deployment of a Tether from an Orbiter." Proceedings of the *International Round Table on Tethers in Space*, 28-30 September 1994, ESA/ESTEC, Noordwijk, The Netherlands.

9. E.C. Lorenzini, M.L. Cosmo, G.G. Gullahorn, R. D. Estes, and M.D. Grossi, "Analytical Investigation of the Dynamics of Tethered Constellation in Earth Orbit (Phase II)." Smithsonian Astrophysical Observatory Final Report, NASA/MSFC Contract NAS8-36606, May 1994.

10. Lorenzini, E. C., M. Cosmo, S. Vetrella, and A. Moccia, "Dynamics and Control of the Tether Elevator/Crawler System," Journal of Guidance, Control, and Dynamics, Vol. 12, No. 3, May-June 1989.

11. Bortolami, S.B., E.C. Lorenzini, C.C. Rupp, and F. Angrilli, "Control Law for the Deployment of SEDS-II" Advances in the Astronautical Sciences, *Astrodynamics 1993*, Vol. 85, 733-748, AAS 1993.

12. Griffin, M.D., and J.R. French, "Space Vehicle Design." p. 252, AIAA Education Series, 1991.

**Appendix A**

1) REFERENCE TABLE FOR SEDSAT_REF39

2) LIST OF CONTROL LAW PARAMETERS FOR SEDSAT_REF39

REFERENCE TABLE FOR SEDSAT_REF39

Note: Only the last three columns of this file are incorporated in the flight reference table.

| Time (s) | Length (m) | Speed (m/s) | Turns | TurnRate | Brake Turns |
|---|---|---|---|---|---|
| 0.00 | 0.500 | 1.470 | 3. | 2.106 | 0.000 |
| 8.00 | 12.090 | 1.463 | 20. | 2.097 | 0.000 |
| 16.00 | 23.665 | 1.457 | 37. | 2.088 | 0.000 |
| 24.00 | 35.223 | 1.450 | 53. | 2.079 | 0.000 |
| 32.00 | 46.762 | 1.444 | 70. | 2.071 | 0.000 |
| 40.00 | 58.278 | 1.438 | 86. | 2.063 | 0.000 |
| 48.00 | 69.771 | 1.433 | 103. | 2.056 | 0.000 |
| 56.00 | 81.238 | 1.427 | 119. | 2.049 | 0.000 |
| 64.00 | 92.677 | 1.422 | 136. | 2.042 | 0.000 |
| 72.00 | 104.080 | 1.417 | 152. | 2.035 | 0.000 |
| 80.00 | 115.460 | 1.412 | 168. | 2.029 | 0.000 |
| 88.00 | 126.800 | 1.408 | 185. | 2.023 | 0.000 |
| 96.00 | 138.110 | 1.404 | 201. | 2.017 | 0.000 |
| 104.00 | 149.370 | 1.400 | 217. | 2.012 | 0.000 |
| 112.00 | 160.590 | 1.396 | 233. | 2.007 | 0.000 |
| 120.00 | 171.770 | 1.392 | 249. | 2.003 | 0.000 |
| 128.00 | 182.910 | 1.389 | 265. | 1.998 | 0.000 |
| 136.00 | 193.990 | 1.385 | 281. | 1.994 | 0.000 |
| 144.00 | 205.050 | 1.383 | 297. | 1.990 | 0.000 |
| 152.00 | 216.070 | 1.380 | 313. | 1.987 | 0.000 |
| 160.00 | 227.070 | 1.377 | 329. | 1.984 | 0.000 |
| 168.00 | 238.050 | 1.375 | 345. | 1.981 | 0.000 |
| 176.00 | 249.020 | 1.373 | 361. | 1.979 | 0.000 |
| 184.00 | 259.970 | 1.371 | 376. | 1.977 | 0.000 |
| 192.00 | 270.910 | 1.370 | 392. | 1.975 | 0.000 |
| 200.00 | 281.840 | 1.368 | 408. | 1.974 | 0.000 |
| 208.00 | 292.770 | 1.367 | 424. | 1.973 | 0.000 |
| 216.00 | 303.700 | 1.367 | 439. | 1.972 | 0.000 |
| 224.00 | 314.630 | 1.366 | 455. | 1.972 | 0.000 |
| 232.00 | 325.570 | 1.366 | 471. | 1.972 | 0.000 |
| 240.00 | 336.520 | 1.366 | 487. | 1.973 | 0.000 |
| 248.00 | 347.490 | 1.366 | 503. | 1.974 | 0.000 |
| 256.00 | 358.470 | 1.367 | 518. | 1.975 | 0.000 |
| 264.00 | 369.470 | 1.368 | 534. | 1.977 | 0.000 |
| 272.00 | 380.500 | 1.369 | 550. | 1.979 | 0.000 |
| 280.00 | 391.540 | 1.370 | 566. | 1.981 | 0.000 |
| 288.00 | 402.590 | 1.372 | 582. | 1.984 | 0.000 |
| 296.00 | 413.650 | 1.374 | 598. | 1.987 | 0.000 |
| 304.00 | 424.720 | 1.376 | 614. | 1.991 | 0.000 |
| 312.00 | 435.810 | 1.378 | 630. | 1.995 | 0.000 |
| 320.00 | 446.900 | 1.381 | 646. | 1.999 | 0.000 |
| 328.00 | 458.010 | 1.384 | 662. | 2.004 | 0.000 |
| 336.00 | 469.130 | 1.387 | 679. | 2.009 | 0.000 |
| 344.00 | 480.250 | 1.390 | 695. | 2.015 | 0.000 |
| 352.00 | 491.390 | 1.394 | 711. | 2.021 | 0.000 |
| 360.00 | 502.540 | 1.398 | 727. | 2.027 | 0.000 |
| 368.00 | 513.690 | 1.403 | 743. | 2.034 | 0.000 |
| 376.00 | 524.860 | 1.407 | 759. | 2.041 | 0.000 |
| 384.00 | 536.030 | 1.412 | 776. | 2.049 | 0.000 |
| 392.00 | 547.210 | 1.417 | 792. | 2.057 | 0.000 |
| 400.00 | 558.400 | 1.423 | 808. | 2.066 | 0.000 |
| 408.00 | 569.640 | 1.429 | 824. | 2.075 | 0.000 |
| 416.00 | 580.990 | 1.435 | 841. | 2.084 | 0.000 |
| 424.00 | 592.440 | 1.441 | 857. | 2.093 | 0.000 |
| 432.00 | 603.970 | 1.447 | 874. | 2.103 | 0.000 |
| 440.00 | 615.590 | 1.453 | 891. | 2.113 | 0.000 |
| 448.00 | 627.290 | 1.460 | 908. | 2.123 | 0.000 |
| 456.00 | 639.070 | 1.467 | 925. | 2.134 | 0.000 |

| | | | | | |
|---|---|---|---|---|---|
| 464.00 | 650.910 | 1.474 | 943. | 2.145 | 0.000 |
| 472.00 | 662.820 | 1.481 | 960. | 2.156 | 0.000 |
| 480.00 | 674.790 | 1.489 | 977. | 2.168 | 0.000 |
| 488.00 | 686.810 | 1.497 | 995. | 2.180 | 0.000 |
| 496.00 | 698.870 | 1.505 | 1012. | 2.192 | 0.000 |
| 504.00 | 710.980 | 1.513 | 1030. | 2.205 | 0.000 |
| 512.00 | 723.120 | 1.521 | 1048. | 2.218 | 0.000 |
| 520.00 | 735.290 | 1.530 | 1065. | 2.232 | 0.000 |
| 528.00 | 747.490 | 1.539 | 1083. | 2.245 | 0.000 |
| 536.00 | 759.710 | 1.549 | 1101. | 2.260 | 0.000 |
| 544.00 | 772.030 | 1.559 | 1119. | 2.275 | 0.000 |
| 552.00 | 784.460 | 1.568 | 1137. | 2.289 | 0.000 |
| 560.00 | 797.000 | 1.578 | 1155. | 2.304 | 0.000 |
| 568.00 | 809.650 | 1.588 | 1174. | 2.319 | 0.000 |
| 576.00 | 822.400 | 1.597 | 1193. | 2.334 | 0.000 |
| 584.00 | 835.250 | 1.607 | 1211. | 2.350 | 0.000 |
| 592.00 | 848.200 | 1.618 | 1230. | 2.365 | 0.000 |
| 600.00 | 861.240 | 1.628 | 1249. | 2.381 | 0.000 |
| 608.00 | 874.360 | 1.638 | 1269. | 2.397 | 0.000 |
| 616.00 | 887.570 | 1.649 | 1288. | 2.413 | 0.000 |
| 624.00 | 900.860 | 1.660 | 1307. | 2.430 | 0.000 |
| 632.00 | 914.220 | 1.671 | 1327. | 2.446 | 0.000 |
| 640.00 | 927.660 | 1.682 | 1347. | 2.464 | 0.000 |
| 648.00 | 941.160 | 1.693 | 1366. | 2.481 | 0.000 |
| 656.00 | 954.730 | 1.704 | 1386. | 2.499 | 0.000 |
| 664.00 | 968.350 | 1.716 | 1406. | 2.517 | 0.000 |
| 672.00 | 982.050 | 1.728 | 1426. | 2.535 | 0.000 |
| 680.00 | 995.860 | 1.740 | 1447. | 2.554 | 0.000 |
| 688.00 | 1009.800 | 1.752 | 1467. | 2.572 | 0.000 |
| 696.00 | 1023.800 | 1.764 | 1488. | 2.591 | 0.000 |
| 704.00 | 1038.000 | 1.776 | 1508. | 2.610 | 0.000 |
| 712.00 | 1052.200 | 1.788 | 1529. | 2.628 | 0.000 |
| 720.00 | 1066.600 | 1.801 | 1550. | 2.647 | 0.000 |
| 728.00 | 1081.100 | 1.813 | 1572. | 2.666 | 0.000 |
| 736.00 | 1095.600 | 1.825 | 1593. | 2.685 | 0.000 |
| 744.00 | 1110.300 | 1.837 | 1615. | 2.704 | 0.000 |
| 752.00 | 1125.100 | 1.849 | 1637. | 2.723 | 0.000 |
| 760.00 | 1140.000 | 1.862 | 1658. | 2.742 | 0.000 |
| 768.00 | 1154.900 | 1.874 | 1680. | 2.761 | 0.000 |
| 776.00 | 1170.000 | 1.887 | 1703. | 2.781 | 0.000 |
| 784.00 | 1185.100 | 1.899 | 1725. | 2.800 | 0.000 |
| 792.00 | 1200.400 | 1.912 | 1747. | 2.820 | 0.000 |
| 800.00 | 1215.700 | 1.925 | 1770. | 2.840 | 0.000 |
| 808.00 | 1231.100 | 1.938 | 1793. | 2.860 | 0.000 |
| 816.00 | 1246.600 | 1.950 | 1816. | 2.880 | 0.000 |
| 824.00 | 1262.300 | 1.963 | 1839. | 2.900 | 0.000 |
| 832.00 | 1278.000 | 1.976 | 1862. | 2.920 | 0.000 |
| 840.00 | 1293.900 | 1.989 | 1886. | 2.940 | 0.000 |
| 848.00 | 1309.800 | 2.002 | 1909. | 2.961 | 0.000 |
| 856.00 | 1325.900 | 2.015 | 1933. | 2.981 | 0.000 |
| 864.00 | 1342.100 | 2.028 | 1957. | 3.001 | 0.000 |
| 872.00 | 1358.300 | 2.041 | 1981. | 3.022 | 0.000 |
| 880.00 | 1374.700 | 2.053 | 2005. | 3.042 | 0.000 |
| 888.00 | 1391.200 | 2.066 | 2030. | 3.062 | 0.000 |
| 896.00 | 1407.800 | 2.079 | 2054. | 3.083 | 0.000 |
| 904.00 | 1424.500 | 2.092 | 2079. | 3.103 | 0.000 |
| 912.00 | 1441.300 | 2.105 | 2104. | 3.123 | 0.000 |
| 920.00 | 1458.200 | 2.118 | 2129. | 3.144 | 0.000 |
| 928.00 | 1475.200 | 2.131 | 2154. | 3.164 | 0.000 |
| 936.00 | 1492.300 | 2.143 | 2180. | 3.184 | 0.000 |
| 944.00 | 1509.500 | 2.156 | 2205. | 3.205 | 0.000 |
| 952.00 | 1526.800 | 2.169 | 2231. | 3.225 | 0.000 |
| 960.00 | 1544.200 | 2.181 | 2257. | 3.245 | 0.000 |
| 968.00 | 1561.700 | 2.194 | 2283. | 3.265 | 0.000 |
| 976.00 | 1579.300 | 2.206 | 2309. | 3.286 | 0.000 |
| 984.00 | 1597.000 | 2.219 | 2335. | 3.306 | 0.000 |

| | | | | | |
|---|---|---|---|---|---|
| 992.00 | 1614.800 | 2.231 | 2362. | 3.326 | 0.000 |
| 1000.00 | 1632.700 | 2.244 | 2389. | 3.346 | 0.000 |
| 1008.00 | 1650.700 | 2.257 | 2415. | 3.366 | 0.000 |
| 1016.00 | 1668.800 | 2.269 | 2442. | 3.386 | 0.000 |
| 1024.00 | 1687.000 | 2.281 | 2470. | 3.407 | 0.000 |
| 1032.00 | 1705.300 | 2.294 | 2497. | 3.427 | 0.000 |
| 1040.00 | 1723.700 | 2.306 | 2524. | 3.447 | 0.000 |
| 1048.00 | 1742.200 | 2.319 | 2552. | 3.467 | 0.000 |
| 1056.00 | 1760.800 | 2.331 | 2580. | 3.487 | 0.000 |
| 1064.00 | 1779.500 | 2.343 | 2608. | 3.507 | 0.000 |
| 1072.00 | 1798.400 | 2.355 | 2636. | 3.527 | 0.000 |
| 1080.00 | 1817.300 | 2.368 | 2665. | 3.547 | 0.000 |
| 1088.00 | 1836.300 | 2.379 | 2693. | 3.567 | 0.000 |
| 1096.00 | 1855.400 | 2.391 | 2722. | 3.586 | 0.000 |
| 1104.00 | 1874.500 | 2.403 | 2750. | 3.606 | 0.000 |
| 1112.00 | 1893.800 | 2.415 | 2779. | 3.625 | 0.000 |
| 1120.00 | 1913.100 | 2.427 | 2808. | 3.645 | 0.000 |
| 1128.00 | 1932.600 | 2.438 | 2838. | 3.664 | 0.000 |
| 1136.00 | 1952.100 | 2.450 | 2867. | 3.683 | 0.000 |
| 1144.00 | 1971.700 | 2.461 | 2896. | 3.702 | 0.000 |
| 1152.00 | 1991.400 | 2.473 | 2926. | 3.721 | 0.000 |
| 1160.00 | 2011.200 | 2.484 | 2956. | 3.740 | 0.000 |
| 1168.00 | 2031.200 | 2.495 | 2986. | 3.759 | 0.000 |
| 1176.00 | 2051.200 | 2.506 | 3016. | 3.778 | 0.000 |
| 1184.00 | 2071.300 | 2.517 | 3046. | 3.797 | 0.000 |
| 1192.00 | 2091.500 | 2.528 | 3077. | 3.815 | 0.000 |
| 1200.00 | 2111.800 | 2.539 | 3107. | 3.834 | 0.000 |
| 1208.00 | 2132.200 | 2.550 | 3138. | 3.852 | 0.000 |
| 1216.00 | 2152.700 | 2.561 | 3169. | 3.871 | 0.000 |
| 1224.00 | 2173.200 | 2.572 | 3200. | 3.889 | 0.000 |
| 1232.00 | 2193.800 | 2.583 | 3231. | 3.908 | 0.000 |
| 1240.00 | 2214.500 | 2.593 | 3263. | 3.926 | 0.000 |
| 1248.00 | 2235.300 | 2.604 | 3294. | 3.944 | 0.000 |
| 1256.00 | 2256.200 | 2.614 | 3326. | 3.962 | 0.000 |
| 1264.00 | 2277.100 | 2.625 | 3358. | 3.980 | 0.000 |
| 1272.00 | 2298.100 | 2.635 | 3389. | 3.998 | 0.000 |
| 1280.00 | 2319.200 | 2.645 | 3421. | 4.015 | 0.000 |
| 1288.00 | 2340.400 | 2.655 | 3454. | 4.033 | 0.000 |
| 1296.00 | 2361.600 | 2.665 | 3486. | 4.050 | 0.000 |
| 1304.00 | 2383.000 | 2.675 | 3518. | 4.068 | 0.000 |
| 1312.00 | 2404.400 | 2.685 | 3551. | 4.085 | 0.000 |
| 1320.00 | 2426.000 | 2.695 | 3584. | 4.102 | 0.000 |
| 1328.00 | 2447.600 | 2.705 | 3617. | 4.120 | 0.000 |
| 1336.00 | 2469.300 | 2.714 | 3650. | 4.137 | 0.000 |
| 1344.00 | 2491.100 | 2.724 | 3683. | 4.154 | 0.000 |
| 1352.00 | 2513.000 | 2.733 | 3716. | 4.171 | 0.000 |
| 1360.00 | 2534.900 | 2.743 | 3750. | 4.187 | 0.000 |
| 1368.00 | 2556.900 | 2.752 | 3783. | 4.204 | 0.000 |
| 1376.00 | 2578.900 | 2.761 | 3817. | 4.221 | 0.000 |
| 1384.00 | 2601.000 | 2.771 | 3851. | 4.238 | 0.000 |
| 1392.00 | 2623.200 | 2.780 | 3885. | 4.254 | 0.000 |
| 1400.00 | 2645.500 | 2.789 | 3919. | 4.271 | 0.000 |
| 1408.00 | 2667.800 | 2.798 | 3953. | 4.287 | 0.000 |
| 1416.00 | 2690.200 | 2.807 | 3987. | 4.303 | 0.000 |
| 1424.00 | 2712.600 | 2.816 | 4022. | 4.320 | 0.000 |
| 1432.00 | 2735.200 | 2.825 | 4056. | 4.336 | 0.000 |
| 1440.00 | 2757.800 | 2.833 | 4091. | 4.352 | 0.000 |
| 1448.00 | 2780.500 | 2.842 | 4126. | 4.368 | 0.000 |
| 1456.00 | 2803.300 | 2.851 | 4161. | 4.383 | 0.000 |
| 1464.00 | 2826.200 | 2.859 | 4196. | 4.399 | 0.000 |
| 1472.00 | 2849.100 | 2.867 | 4231. | 4.415 | 0.000 |
| 1480.00 | 2872.100 | 2.876 | 4267. | 4.430 | 0.000 |
| 1488.00 | 2895.200 | 2.884 | 4303. | 4.446 | 0.000 |
| 1496.00 | 2918.300 | 2.892 | 4338. | 4.461 | 0.000 |
| 1504.00 | 2941.500 | 2.900 | 4374. | 4.477 | 0.000 |
| 1512.00 | 2964.700 | 2.908 | 4410. | 4.492 | 0.000 |

| | | | | | |
|---|---|---|---|---|---|
| 1520.00 | 2988.000 | 2.917 | 4446. | 4.508 | 0.000 |
| 1528.00 | 3011.300 | 2.925 | 4482. | 4.523 | 0.000 |
| 1536.00 | 3034.700 | 2.933 | 4518. | 4.538 | 0.000 |
| 1544.00 | 3058.200 | 2.941 | 4554. | 4.554 | 0.000 |
| 1552.00 | 3081.700 | 2.948 | 4591. | 4.569 | 0.000 |
| 1560.00 | 3105.400 | 2.956 | 4627. | 4.584 | 0.000 |
| 1568.00 | 3129.000 | 2.964 | 4664. | 4.599 | 0.000 |
| 1576.00 | 3152.800 | 2.972 | 4701. | 4.614 | 0.000 |
| 1584.00 | 3176.600 | 2.979 | 4738. | 4.629 | 0.000 |
| 1592.00 | 3200.400 | 2.987 | 4775. | 4.643 | 0.000 |
| 1600.00 | 3224.400 | 2.994 | 4812. | 4.658 | 0.000 |
| 1608.00 | 3248.400 | 3.002 | 4850. | 4.673 | 0.000 |
| 1616.00 | 3272.500 | 3.009 | 4887. | 4.687 | 0.000 |
| 1624.00 | 3296.600 | 3.016 | 4925. | 4.702 | 0.000 |
| 1632.00 | 3320.700 | 3.024 | 4962. | 4.716 | 0.000 |
| 1640.00 | 3345.000 | 3.031 | 5000. | 4.731 | 0.000 |
| 1648.00 | 3369.200 | 3.038 | 5038. | 4.746 | 0.000 |
| 1656.00 | 3393.600 | 3.046 | 5076. | 4.760 | 0.000 |
| 1664.00 | 3418.000 | 3.053 | 5114. | 4.775 | 0.000 |
| 1672.00 | 3442.400 | 3.060 | 5152. | 4.789 | 0.000 |
| 1680.00 | 3466.900 | 3.067 | 5191. | 4.804 | 0.000 |
| 1688.00 | 3491.400 | 3.074 | 5229. | 4.818 | 0.000 |
| 1696.00 | 3516.100 | 3.081 | 5268. | 4.833 | 0.000 |
| 1704.00 | 3540.700 | 3.088 | 5307. | 4.847 | 0.000 |
| 1712.00 | 3565.500 | 3.095 | 5345. | 4.862 | 0.000 |
| 1720.00 | 3590.300 | 3.102 | 5384. | 4.876 | 0.000 |
| 1728.00 | 3615.100 | 3.109 | 5423. | 4.890 | 0.000 |
| 1736.00 | 3640.000 | 3.116 | 5463. | 4.905 | 0.000 |
| 1744.00 | 3665.000 | 3.123 | 5502. | 4.919 | 0.000 |
| 1752.00 | 3690.000 | 3.130 | 5541. | 4.933 | 0.000 |
| 1760.00 | 3715.100 | 3.137 | 5581. | 4.948 | 0.000 |
| 1768.00 | 3740.200 | 3.144 | 5621. | 4.962 | 0.000 |
| 1776.00 | 3765.400 | 3.150 | 5660. | 4.976 | 0.000 |
| 1784.00 | 3790.600 | 3.157 | 5700. | 4.990 | 0.000 |
| 1792.00 | 3815.900 | 3.164 | 5740. | 5.005 | 0.000 |
| 1800.00 | 3841.200 | 3.171 | 5780. | 5.019 | 0.000 |
| 1808.00 | 3866.600 | 3.178 | 5820. | 5.034 | 0.000 |
| 1816.00 | 3892.100 | 3.184 | 5861. | 5.048 | 0.000 |
| 1824.00 | 3917.600 | 3.191 | 5901. | 5.063 | 0.000 |
| 1832.00 | 3943.100 | 3.198 | 5942. | 5.077 | 0.000 |
| 1840.00 | 3968.700 | 3.205 | 5982. | 5.092 | 0.000 |
| 1848.00 | 3994.400 | 3.211 | 6023. | 5.106 | 0.000 |
| 1856.00 | 4020.100 | 3.218 | 6064. | 5.121 | 0.000 |
| 1864.00 | 4045.900 | 3.225 | 6105. | 5.136 | 0.000 |
| 1872.00 | 4071.700 | 3.232 | 6146. | 5.151 | 0.000 |
| 1880.00 | 4097.600 | 3.239 | 6188. | 5.166 | 0.000 |
| 1888.00 | 4123.500 | 3.246 | 6229. | 5.180 | 0.000 |
| 1896.00 | 4149.500 | 3.253 | 6270. | 5.195 | 0.000 |
| 1904.00 | 4175.600 | 3.260 | 6312. | 5.210 | 0.000 |
| 1912.00 | 4201.700 | 3.266 | 6354. | 5.225 | 0.000 |
| 1920.00 | 4227.900 | 3.273 | 6396. | 5.240 | 0.000 |
| 1928.00 | 4254.100 | 3.280 | 6438. | 5.256 | 0.000 |
| 1936.00 | 4280.400 | 3.287 | 6480. | 5.271 | 0.000 |
| 1944.00 | 4306.700 | 3.294 | 6522. | 5.286 | 0.000 |
| 1952.00 | 4333.100 | 3.301 | 6564. | 5.301 | 0.000 |
| 1960.00 | 4359.500 | 3.308 | 6607. | 5.317 | 0.000 |
| 1968.00 | 4386.000 | 3.315 | 6649. | 5.332 | 0.000 |
| 1976.00 | 4412.500 | 3.322 | 6692. | 5.348 | 0.000 |
| 1984.00 | 4439.100 | 3.329 | 6735. | 5.363 | 0.000 |
| 1992.00 | 4465.800 | 3.336 | 6778. | 5.378 | 0.000 |
| 2000.00 | 4492.500 | 3.343 | 6821. | 5.394 | 0.000 |
| 2008.00 | 4519.200 | 3.350 | 6864. | 5.410 | 0.000 |
| 2016.00 | 4546.000 | 3.357 | 6907. | 5.426 | 0.000 |
| 2024.00 | 4572.900 | 3.364 | 6951. | 5.442 | 0.000 |
| 2032.00 | 4599.900 | 3.372 | 6995. | 5.458 | 0.000 |
| 2040.00 | 4626.900 | 3.379 | 7038. | 5.474 | 0.000 |

| | | | | | |
|---|---|---|---|---|---|
| 2048.00 | 4654.000 | 3.386 | 7082. | 5.491 | 0.000 |
| 2056.00 | 4681.100 | 3.394 | 7126. | 5.507 | 0.000 |
| 2064.00 | 4708.300 | 3.401 | 7170. | 5.524 | 0.000 |
| 2072.00 | 4735.600 | 3.409 | 7215. | 5.541 | 0.000 |
| 2080.00 | 4762.900 | 3.417 | 7259. | 5.558 | 0.000 |
| 2088.00 | 4790.300 | 3.424 | 7304. | 5.575 | 0.000 |
| 2096.00 | 4817.700 | 3.432 | 7348. | 5.593 | 0.000 |
| 2104.00 | 4845.200 | 3.440 | 7393. | 5.610 | 0.000 |
| 2112.00 | 4872.700 | 3.448 | 7438. | 5.627 | 0.000 |
| 2120.00 | 4900.300 | 3.456 | 7483. | 5.645 | 0.000 |
| 2128.00 | 4928.000 | 3.464 | 7528. | 5.663 | 0.000 |
| 2136.00 | 4955.600 | 3.471 | 7574. | 5.680 | 0.000 |
| 2144.00 | 4983.400 | 3.479 | 7619. | 5.698 | 0.000 |
| 2152.00 | 5011.300 | 3.487 | 7665. | 5.716 | 0.000 |
| 2160.00 | 5039.200 | 3.496 | 7710. | 5.735 | 0.000 |
| 2168.00 | 5067.200 | 3.504 | 7756. | 5.753 | 0.000 |
| 2176.00 | 5095.300 | 3.512 | 7803. | 5.772 | 0.000 |
| 2184.00 | 5123.500 | 3.521 | 7849. | 5.791 | 0.000 |
| 2192.00 | 5151.700 | 3.529 | 7895. | 5.810 | 0.000 |
| 2200.00 | 5180.000 | 3.538 | 7942. | 5.830 | 0.000 |
| 2208.00 | 5208.300 | 3.547 | 7989. | 5.849 | 0.000 |
| 2216.00 | 5236.800 | 3.556 | 8036. | 5.869 | 0.000 |
| 2224.00 | 5265.300 | 3.565 | 8083. | 5.889 | 0.000 |
| 2232.00 | 5293.800 | 3.573 | 8130. | 5.909 | 0.000 |
| 2240.00 | 5322.500 | 3.582 | 8177. | 5.929 | 0.000 |
| 2248.00 | 5351.100 | 3.592 | 8225. | 5.950 | 0.000 |
| 2256.00 | 5379.900 | 3.601 | 8272. | 5.970 | 0.000 |
| 2264.00 | 5408.700 | 3.610 | 8320. | 5.991 | 0.000 |
| 2272.00 | 5437.500 | 3.619 | 8368. | 6.012 | 0.000 |
| 2280.00 | 5466.500 | 3.628 | 8416. | 6.033 | 0.000 |
| 2288.00 | 5495.500 | 3.638 | 8464. | 6.054 | 0.000 |
| 2296.00 | 5524.700 | 3.648 | 8513. | 6.076 | 0.000 |
| 2304.00 | 5553.900 | 3.658 | 8562. | 6.098 | 0.000 |
| 2312.00 | 5583.200 | 3.668 | 8611. | 6.120 | 0.000 |
| 2320.00 | 5612.600 | 3.678 | 8660. | 6.143 | 0.000 |
| 2328.00 | 5642.100 | 3.688 | 8709. | 6.166 | 0.000 |
| 2336.00 | 5671.700 | 3.698 | 8758. | 6.189 | 0.000 |
| 2344.00 | 5701.400 | 3.708 | 8808. | 6.212 | 0.000 |
| 2352.00 | 5731.100 | 3.719 | 8858. | 6.236 | 0.000 |
| 2360.00 | 5760.900 | 3.730 | 8908. | 6.260 | 0.000 |
| 2368.00 | 5790.800 | 3.740 | 8958. | 6.284 | 0.000 |
| 2376.00 | 5820.800 | 3.751 | 9009. | 6.308 | 0.000 |
| 2384.00 | 5850.800 | 3.762 | 9059. | 6.332 | 0.000 |
| 2392.00 | 5880.900 | 3.773 | 9110. | 6.357 | 0.000 |
| 2400.00 | 5911.100 | 3.784 | 9161. | 6.382 | 0.000 |
| 2408.00 | 5941.300 | 3.795 | 9212. | 6.407 | 0.000 |
| 2416.00 | 5971.700 | 3.806 | 9263. | 6.432 | 0.000 |
| 2424.00 | 6002.100 | 3.818 | 9314. | 6.458 | 0.000 |
| 2432.00 | 6032.700 | 3.829 | 9366. | 6.484 | 0.000 |
| 2440.00 | 6063.400 | 3.841 | 9418. | 6.511 | 0.000 |
| 2448.00 | 6094.300 | 3.853 | 9471. | 6.538 | 0.000 |
| 2456.00 | 6125.200 | 3.865 | 9523. | 6.565 | 0.000 |
| 2464.00 | 6156.200 | 3.877 | 9576. | 6.593 | 0.000 |
| 2472.00 | 6187.300 | 3.890 | 9629. | 6.620 | 0.000 |
| 2480.00 | 6218.500 | 3.902 | 9682. | 6.648 | 0.000 |
| 2488.00 | 6249.800 | 3.915 | 9735. | 6.677 | 0.000 |
| 2496.00 | 6281.200 | 3.928 | 9789. | 6.706 | 0.000 |
| 2504.00 | 6312.700 | 3.940 | 9843. | 6.735 | 0.000 |
| 2512.00 | 6344.200 | 3.953 | 9896. | 6.764 | 0.000 |
| 2520.00 | 6375.900 | 3.967 | 9951. | 6.794 | 0.000 |
| 2528.00 | 6407.600 | 3.980 | 10005. | 6.824 | 0.000 |
| 2536.00 | 6439.400 | 3.993 | 10060. | 6.854 | 0.000 |
| 2544.00 | 6471.300 | 4.006 | 10114. | 6.884 | 0.000 |
| 2552.00 | 6503.400 | 4.020 | 10169. | 6.915 | 0.000 |
| 2560.00 | 6535.600 | 4.034 | 10225. | 6.947 | 0.000 |
| 2568.00 | 6567.900 | 4.048 | 10281. | 6.979 | 0.000 |

| | | | | | |
|---|---|---|---|---|---|
| 2576.00 | 6600.400 | 4.062 | 10337. | 7.011 | 0.000 |
| 2584.00 | 6633.000 | 4.076 | 10393. | 7.043 | 0.000 |
| 2592.00 | 6665.700 | 4.091 | 10449. | 7.076 | 0.000 |
| 2600.00 | 6698.600 | 4.106 | 10506. | 7.110 | 0.000 |
| 2608.00 | 6731.500 | 4.120 | 10563. | 7.143 | 0.000 |
| 2616.00 | 6764.600 | 4.135 | 10621. | 7.178 | 0.000 |
| 2624.00 | 6797.800 | 4.150 | 10678. | 7.212 | 0.000 |
| 2632.00 | 6831.100 | 4.166 | 10736. | 7.247 | 0.000 |
| 2640.00 | 6864.500 | 4.181 | 10795. | 7.282 | 0.000 |
| 2648.00 | 6897.900 | 4.197 | 10853. | 7.318 | 0.000 |
| 2656.00 | 6931.500 | 4.212 | 10911. | 7.354 | 0.000 |
| 2664.00 | 6965.200 | 4.228 | 10970. | 7.390 | 0.000 |
| 2672.00 | 6999.000 | 4.244 | 11029. | 7.427 | 0.000 |
| 2680.00 | 7032.900 | 4.260 | 11089. | 7.464 | 0.000 |
| 2688.00 | 7067.100 | 4.277 | 11149. | 7.502 | 0.000 |
| 2696.00 | 7101.300 | 4.293 | 11209. | 7.540 | 0.000 |
| 2704.00 | 7135.800 | 4.310 | 11269. | 7.578 | 0.000 |
| 2712.00 | 7170.300 | 4.327 | 11330. | 7.617 | 0.000 |
| 2720.00 | 7205.100 | 4.344 | 11391. | 7.657 | 0.000 |
| 2728.00 | 7239.900 | 4.361 | 11453. | 7.697 | 0.000 |
| 2736.00 | 7275.000 | 4.378 | 11515. | 7.737 | 0.000 |
| 2744.00 | 7310.100 | 4.396 | 11577. | 7.778 | 0.000 |
| 2752.00 | 7345.400 | 4.414 | 11639. | 7.819 | 0.000 |
| 2760.00 | 7380.800 | 4.432 | 11702. | 7.861 | 0.000 |
| 2768.00 | 7416.400 | 4.450 | 11765. | 7.903 | 0.000 |
| 2776.00 | 7452.000 | 4.468 | 11828. | 7.946 | 0.000 |
| 2784.00 | 7487.800 | 4.486 | 11892. | 7.989 | 0.000 |
| 2792.00 | 7523.700 | 4.505 | 11956. | 8.033 | 0.000 |
| 2800.00 | 7559.700 | 4.524 | 12020. | 8.076 | 0.000 |
| 2808.00 | 7595.900 | 4.543 | 12085. | 8.121 | 0.000 |
| 2816.00 | 7632.200 | 4.562 | 12150. | 8.166 | 0.000 |
| 2824.00 | 7668.800 | 4.581 | 12216. | 8.211 | 0.000 |
| 2832.00 | 7705.500 | 4.600 | 12281. | 8.258 | 0.000 |
| 2840.00 | 7742.400 | 4.620 | 12348. | 8.304 | 0.000 |
| 2848.00 | 7779.500 | 4.640 | 12414. | 8.351 | 0.000 |
| 2856.00 | 7816.800 | 4.660 | 12482. | 8.399 | 0.000 |
| 2864.00 | 7854.200 | 4.680 | 12549. | 8.447 | 0.000 |
| 2872.00 | 7891.800 | 4.700 | 12617. | 8.496 | 0.000 |
| 2880.00 | 7929.500 | 4.721 | 12685. | 8.545 | 0.000 |
| 2888.00 | 7967.400 | 4.742 | 12754. | 8.595 | 0.000 |
| 2896.00 | 8005.500 | 4.762 | 12823. | 8.645 | 0.000 |
| 2904.00 | 8043.700 | 4.784 | 12892. | 8.696 | 0.000 |
| 2912.00 | 8082.000 | 4.805 | 12962. | 8.748 | 0.000 |
| 2920.00 | 8120.500 | 4.826 | 13032. | 8.799 | 0.000 |
| 2928.00 | 8159.100 | 4.848 | 13103. | 8.852 | 0.000 |
| 2936.00 | 8197.800 | 4.870 | 13173. | 8.905 | 0.000 |
| 2944.00 | 8236.800 | 4.892 | 13245. | 8.958 | 0.000 |
| 2952.00 | 8276.000 | 4.914 | 13316. | 9.013 | 0.000 |
| 2960.00 | 8315.300 | 4.936 | 13389. | 9.067 | 0.000 |
| 2968.00 | 8354.900 | 4.959 | 13461. | 9.123 | 0.000 |
| 2976.00 | 8394.700 | 4.982 | 13535. | 9.179 | 0.000 |
| 2984.00 | 8434.700 | 5.004 | 13608. | 9.235 | 0.000 |
| 2992.00 | 8474.900 | 5.028 | 13683. | 9.293 | 0.000 |
| 3000.00 | 8515.300 | 5.051 | 13757. | 9.351 | 0.000 |
| 3008.00 | 8555.900 | 5.074 | 13833. | 9.409 | 0.000 |
| 3016.00 | 8596.600 | 5.098 | 13908. | 9.468 | 0.000 |
| 3024.00 | 8637.500 | 5.122 | 13984. | 9.528 | 0.000 |
| 3032.00 | 8678.600 | 5.146 | 14061. | 9.588 | 0.000 |
| 3040.00 | 8719.900 | 5.170 | 14138. | 9.649 | 0.000 |
| 3048.00 | 8761.300 | 5.194 | 14215. | 9.711 | 0.000 |
| 3056.00 | 8802.900 | 5.219 | 14293. | 9.773 | 0.000 |
| 3064.00 | 8844.700 | 5.244 | 14371. | 9.836 | 0.000 |
| 3072.00 | 8886.600 | 5.269 | 14450. | 9.900 | 0.000 |
| 3080.00 | 8928.800 | 5.294 | 14529. | 9.964 | 0.000 |
| 3088.00 | 8971.200 | 5.319 | 14609. | 10.029 | 0.000 |
| 3096.00 | 9013.800 | 5.345 | 14689. | 10.094 | 0.000 |

| | | | | | |
|---|---|---|---|---|---|
| 3104.00 | 9056.700 | 5.370 | 14771. | 10.161 | 0.000 |
| 3112.00 | 9099.800 | 5.396 | 14852. | 10.228 | 0.000 |
| 3120.00 | 9143.100 | 5.422 | 14934. | 10.296 | 0.000 |
| 3128.00 | 9186.700 | 5.448 | 15017. | 10.364 | 0.000 |
| 3136.00 | 9230.400 | 5.475 | 15100. | 10.433 | 0.000 |
| 3144.00 | 9274.400 | 5.501 | 15184. | 10.503 | 0.000 |
| 3152.00 | 9318.600 | 5.528 | 15269. | 10.574 | 0.000 |
| 3160.00 | 9363.000 | 5.555 | 15354. | 10.645 | 0.000 |
| 3168.00 | 9407.500 | 5.582 | 15439. | 10.717 | 0.000 |
| 3176.00 | 9452.300 | 5.610 | 15525. | 10.790 | 0.000 |
| 3184.00 | 9497.300 | 5.637 | 15612. | 10.864 | 0.000 |
| 3192.00 | 9542.400 | 5.665 | 15699. | 10.939 | 0.000 |
| 3200.00 | 9587.700 | 5.693 | 15786. | 11.014 | 0.000 |
| 3208.00 | 9633.300 | 5.721 | 15875. | 11.090 | 0.000 |
| 3216.00 | 9679.100 | 5.749 | 15964. | 11.167 | 0.000 |
| 3224.00 | 9725.200 | 5.778 | 16053. | 11.244 | 0.000 |
| 3232.00 | 9771.500 | 5.806 | 16143. | 11.323 | 0.000 |
| 3240.00 | 9818.100 | 5.835 | 16234. | 11.402 | 0.000 |
| 3248.00 | 9864.900 | 5.864 | 16326. | 11.482 | 0.000 |
| 3256.00 | 9912.000 | 5.893 | 16418. | 11.563 | 0.000 |
| 3264.00 | 9959.300 | 5.922 | 16511. | 11.645 | 0.000 |
| 3272.00 | 10007.000 | 5.951 | 16605. | 11.728 | 0.000 |
| 3280.00 | 10055.000 | 5.981 | 16700. | 11.811 | 0.000 |
| 3288.00 | 10103.000 | 6.011 | 16795. | 11.896 | 0.000 |
| 3296.00 | 10151.000 | 6.041 | 16890. | 11.981 | 0.000 |
| 3304.00 | 10199.000 | 6.071 | 16985. | 12.067 | 0.000 |
| 3312.00 | 10248.000 | 6.101 | 17083. | 12.154 | 0.000 |
| 3320.00 | 10297.000 | 6.132 | 17180. | 12.243 | 0.000 |
| 3328.00 | 10346.000 | 6.163 | 17278. | 12.331 | 0.000 |
| 3336.00 | 10395.000 | 6.194 | 17376. | 12.421 | 0.000 |
| 3344.00 | 10445.000 | 6.225 | 17477. | 12.513 | 0.000 |
| 3352.00 | 10495.000 | 6.256 | 17577. | 12.605 | 0.000 |
| 3360.00 | 10545.000 | 6.287 | 17678. | 12.697 | 0.000 |
| 3368.00 | 10595.000 | 6.319 | 17779. | 12.791 | 0.000 |
| 3376.00 | 10646.000 | 6.350 | 17883. | 12.886 | 0.000 |
| 3384.00 | 10697.000 | 6.382 | 17986. | 12.982 | 0.000 |
| 3392.00 | 10748.000 | 6.414 | 18090. | 13.079 | 0.000 |
| 3400.00 | 10800.000 | 6.446 | 18196. | 13.177 | 0.000 |
| 3408.00 | 10852.000 | 6.479 | 18303. | 13.276 | 0.000 |
| 3416.00 | 10904.000 | 6.511 | 18410. | 13.376 | 0.000 |
| 3424.00 | 10956.000 | 6.544 | 18516. | 13.477 | 0.000 |
| 3432.00 | 11008.000 | 6.576 | 18624. | 13.579 | 0.000 |
| 3440.00 | 11061.000 | 6.609 | 18733. | 13.682 | 0.000 |
| 3448.00 | 11114.000 | 6.643 | 18843. | 13.787 | 0.000 |
| 3456.00 | 11167.000 | 6.676 | 18953. | 13.893 | 0.000 |
| 3464.00 | 11221.000 | 6.709 | 19066. | 14.000 | 0.000 |
| 3472.00 | 11275.000 | 6.743 | 19179. | 14.109 | 0.000 |
| 3480.00 | 11329.000 | 6.777 | 19292. | 14.218 | 0.000 |
| 3488.00 | 11383.000 | 6.811 | 19405. | 14.328 | 0.000 |
| 3496.00 | 11437.000 | 6.845 | 19519. | 14.440 | 0.000 |
| 3504.00 | 11492.000 | 6.879 | 19635. | 14.552 | 0.000 |
| 3512.00 | 11548.000 | 6.913 | 19754. | 14.667 | 0.000 |
| 3520.00 | 11603.000 | 6.948 | 19871. | 14.782 | 0.000 |
| 3528.00 | 11659.000 | 6.982 | 19990. | 14.899 | 0.000 |
| 3536.00 | 11715.000 | 7.017 | 20110. | 15.017 | 0.000 |
| 3544.00 | 11771.000 | 7.052 | 20230. | 15.136 | 0.000 |
| 3552.00 | 11828.000 | 7.087 | 20352. | 15.257 | 0.000 |
| 3560.00 | 11885.000 | 7.122 | 20475. | 15.379 | 0.000 |
| 3568.00 | 11942.000 | 7.157 | 20598. | 15.503 | 0.000 |
| 3576.00 | 11999.000 | 7.193 | 20722. | 15.628 | 0.000 |
| 3584.00 | 12057.000 | 7.228 | 20848. | 15.755 | 0.000 |
| 3592.00 | 12115.000 | 7.264 | 20975. | 15.883 | 0.000 |
| 3600.00 | 12173.000 | 7.300 | 21102. | 16.013 | 0.000 |
| 3608.00 | 12231.000 | 7.336 | 21229. | 16.144 | 0.000 |
| 3616.00 | 12290.000 | 7.372 | 21359. | 16.277 | 0.000 |
| 3624.00 | 12349.000 | 7.408 | 21490. | 16.411 | 0.000 |

| | | | | | |
|---|---|---|---|---|---|
| 3632.00 | 12409.000 | 7.445 | 21623. | 16.547 | 0.000 |
| 3640.00 | 12468.000 | 7.481 | 21754. | 16.684 | 0.000 |
| 3648.00 | 12528.000 | 7.517 | 21888. | 16.823 | 0.000 |
| 3656.00 | 12589.000 | 7.554 | 22025. | 16.964 | 0.000 |
| 3664.00 | 12649.000 | 7.590 | 22160. | 17.106 | 0.000 |
| 3672.00 | 12710.000 | 7.627 | 22298. | 17.250 | 0.000 |
| 3680.00 | 12771.000 | 7.664 | 22436. | 17.396 | 0.000 |
| 3688.00 | 12833.000 | 7.701 | 22577. | 17.544 | 0.000 |
| 3696.00 | 12895.000 | 7.738 | 22719. | 17.694 | 0.000 |
| 3704.00 | 12957.000 | 7.775 | 22861. | 17.846 | 0.000 |
| 3712.00 | 13019.000 | 7.813 | 23003. | 18.000 | 0.000 |
| 3720.00 | 13082.000 | 7.850 | 23149. | 18.156 | 0.000 |
| 3728.00 | 13145.000 | 7.888 | 23295. | 18.315 | 0.000 |
| 3736.00 | 13208.000 | 7.926 | 23441. | 18.475 | 0.000 |
| 3744.00 | 13271.000 | 7.964 | 23588. | 18.637 | 0.000 |
| 3752.00 | 13335.000 | 8.002 | 23738. | 18.802 | 0.000 |
| 3760.00 | 13399.000 | 8.041 | 23889. | 18.969 | 0.000 |
| 3768.00 | 13463.000 | 8.079 | 24040. | 19.137 | 0.000 |
| 3776.00 | 13528.000 | 8.117 | 24195. | 19.308 | 0.000 |
| 3784.00 | 13593.000 | 8.155 | 24350. | 19.481 | 0.000 |
| 3792.00 | 13658.000 | 8.193 | 24505. | 19.657 | 0.000 |
| 3800.00 | 13723.000 | 8.231 | 24661. | 19.834 | 0.000 |
| 3808.00 | 13789.000 | 8.270 | 24821. | 20.014 | 0.000 |
| 3816.00 | 13855.000 | 8.308 | 24981. | 20.196 | 0.000 |
| 3824.00 | 13922.000 | 8.346 | 25144. | 20.382 | 0.000 |
| 3832.00 | 13989.000 | 8.384 | 25308. | 20.570 | 0.000 |
| 3840.00 | 14056.000 | 8.423 | 25473. | 20.760 | 0.000 |
| 3848.00 | 14124.000 | 8.461 | 25641. | 20.954 | 0.000 |
| 3856.00 | 14193.000 | 8.499 | 25812. | 21.152 | 0.000 |
| 3864.00 | 14261.000 | 8.537 | 25982. | 21.350 | 0.000 |
| 3872.00 | 14330.000 | 8.576 | 26155. | 21.553 | 0.000 |
| 3880.00 | 14400.000 | 8.614 | 26331. | 21.760 | 0.000 |
| 3888.00 | 14469.000 | 8.652 | 26506. | 21.968 | 0.000 |
| 3896.00 | 14539.000 | 8.691 | 26684. | 22.181 | 0.000 |
| 3904.00 | 14609.000 | 8.729 | 26863. | 22.397 | 0.000 |
| 3912.00 | 14679.000 | 8.768 | 27043. | 22.615 | 0.000 |
| 3920.00 | 14749.000 | 8.806 | 27224. | 22.837 | 0.000 |
| 3928.00 | 14819.000 | 8.845 | 27406. | 23.062 | 0.000 |
| 3936.00 | 14890.000 | 8.883 | 27592. | 23.291 | 0.000 |
| 3944.00 | 14961.000 | 8.922 | 27779. | 23.524 | 0.000 |
| 3952.00 | 15032.000 | 8.960 | 27967. | 23.761 | 0.000 |
| 3960.00 | 15104.000 | 8.998 | 28158. | 24.003 | 0.000 |
| 3968.00 | 15176.000 | 9.037 | 28351. | 24.248 | 0.000 |
| 3976.00 | 15248.000 | 9.075 | 28544. | 24.497 | 0.000 |
| 3984.00 | 15321.000 | 9.114 | 28742. | 24.752 | 0.000 |
| 3992.00 | 15394.000 | 9.152 | 28941. | 25.012 | 0.000 |
| 4000.00 | 15467.000 | 9.190 | 29141. | 25.275 | 0.000 |
| 4008.00 | 15541.000 | 9.227 | 29345. | 25.541 | 0.024 |
| 4016.00 | 15615.000 | 9.262 | 29551. | 25.805 | 0.050 |
| 4024.00 | 15689.000 | 9.293 | 29758. | 26.066 | 0.075 |
| 4032.00 | 15763.000 | 9.323 | 29966. | 26.324 | 0.101 |
| 4040.00 | 15838.000 | 9.349 | 30178. | 26.581 | 0.128 |
| 4048.00 | 15913.000 | 9.372 | 30392. | 26.834 | 0.155 |
| 4056.00 | 15988.000 | 9.392 | 30608. | 27.084 | 0.183 |
| 4064.00 | 16063.000 | 9.409 | 30825. | 27.328 | 0.211 |
| 4072.00 | 16139.000 | 9.422 | 31046. | 27.569 | 0.240 |
| 4080.00 | 16214.000 | 9.431 | 31267. | 27.802 | 0.269 |
| 4088.00 | 16289.000 | 9.436 | 31489. | 28.029 | 0.299 |
| 4096.00 | 16365.000 | 9.438 | 31715. | 28.250 | 0.329 |
| 4104.00 | 16440.000 | 9.435 | 31941. | 28.462 | 0.359 |
| 4112.00 | 16516.000 | 9.427 | 32171. | 28.668 | 0.390 |
| 4120.00 | 16591.000 | 9.415 | 32400. | 28.861 | 0.422 |
| 4128.00 | 16667.000 | 9.398 | 32634. | 29.048 | 0.453 |
| 4136.00 | 16742.000 | 9.376 | 32867. | 29.222 | 0.485 |
| 4144.00 | 16817.000 | 9.349 | 33101. | 29.384 | 0.518 |
| 4152.00 | 16891.000 | 9.317 | 33335. | 29.531 | 0.550 |

| | | | | | |
|---|---|---|---|---|---|
| 4160.00 | 16966.000 | 9.279 | 33574. | 29.669 | 0.584 |
| 4168.00 | 17040.000 | 9.236 | 33811. | 29.790 | 0.617 |
| 4176.00 | 17113.000 | 9.187 | 34048. | 29.894 | 0.651 |
| 4184.00 | 17187.000 | 9.132 | 34290. | 29.987 | 0.685 |
| 4192.00 | 17259.000 | 9.072 | 34527. | 30.058 | 0.719 |
| 4200.00 | 17332.000 | 9.005 | 34770. | 30.116 | 0.753 |
| 4208.00 | 17404.000 | 8.933 | 35012. | 30.156 | 0.788 |
| 4216.00 | 17475.000 | 8.855 | 35253. | 30.174 | 0.823 |
| 4224.00 | 17545.000 | 8.772 | 35493. | 30.172 | 0.858 |
| 4232.00 | 17615.000 | 8.682 | 35734. | 30.152 | 0.893 |
| 4240.00 | 17684.000 | 8.587 | 35975. | 30.111 | 0.929 |
| 4248.00 | 17752.000 | 8.487 | 36215. | 30.048 | 0.965 |
| 4256.00 | 17820.000 | 8.381 | 36457. | 29.968 | 1.001 |
| 4264.00 | 17886.000 | 8.270 | 36694. | 29.861 | 1.037 |
| 4272.00 | 17952.000 | 8.154 | 36933. | 29.737 | 1.073 |
| 4280.00 | 18017.000 | 8.033 | 37172. | 29.592 | 1.109 |
| 4288.00 | 18081.000 | 7.908 | 37409. | 29.426 | 1.145 |
| 4296.00 | 18143.000 | 7.779 | 37640. | 29.235 | 1.182 |
| 4304.00 | 18205.000 | 7.646 | 37875. | 29.028 | 1.218 |
| 4312.00 | 18266.000 | 7.509 | 38107. | 28.803 | 1.255 |
| 4320.00 | 18325.000 | 7.370 | 38335. | 28.554 | 1.291 |
| 4328.00 | 18384.000 | 7.228 | 38565. | 28.293 | 1.328 |
| 4336.00 | 18441.000 | 7.084 | 38789. | 28.010 | 1.365 |
| 4344.00 | 18497.000 | 6.938 | 39011. | 27.712 | 1.401 |
| 4352.00 | 18552.000 | 6.790 | 39232. | 27.401 | 1.438 |
| 4360.00 | 18606.000 | 6.642 | 39451. | 27.078 | 1.475 |
| 4368.00 | 18658.000 | 6.493 | 39664. | 26.738 | 1.511 |
| 4376.00 | 18710.000 | 6.344 | 39880. | 26.393 | 1.548 |
| 4384.00 | 18760.000 | 6.196 | 40089. | 26.035 | 1.584 |
| 4392.00 | 18809.000 | 6.048 | 40296. | 25.670 | 1.621 |
| 4400.00 | 18856.000 | 5.902 | 40496. | 25.295 | 1.657 |
| 4408.00 | 18903.000 | 5.756 | 40698. | 24.921 | 1.694 |
| 4416.00 | 18949.000 | 5.612 | 40899. | 24.541 | 1.733 |
| 4424.00 | 18993.000 | 5.469 | 41092. | 24.149 | 1.773 |
| 4432.00 | 19036.000 | 5.326 | 41283. | 23.748 | 1.815 |
| 4440.00 | 19078.000 | 5.184 | 41471. | 23.339 | 1.858 |
| 4448.00 | 19119.000 | 5.042 | 41656. | 22.919 | 1.903 |
| 4456.00 | 19159.000 | 4.900 | 41839. | 22.489 | 1.949 |
| 4464.00 | 19197.000 | 4.759 | 42014. | 22.043 | 1.996 |
| 4472.00 | 19235.000 | 4.617 | 42191. | 21.591 | 2.045 |
| 4480.00 | 19271.000 | 4.476 | 42360. | 21.123 | 2.094 |
| 4488.00 | 19307.000 | 4.336 | 42531. | 20.650 | 2.145 |
| 4496.00 | 19341.000 | 4.195 | 42694. | 20.162 | 2.196 |
| 4504.00 | 19374.000 | 4.056 | 42853. | 19.665 | 2.249 |
| 4512.00 | 19406.000 | 3.918 | 43009. | 19.160 | 2.302 |
| 4520.00 | 19436.000 | 3.780 | 43156. | 18.643 | 2.356 |
| 4528.00 | 19466.000 | 3.645 | 43305. | 18.126 | 2.411 |
| 4536.00 | 19495.000 | 3.510 | 43449. | 17.604 | 2.467 |
| 4544.00 | 19522.000 | 3.378 | 43585. | 17.074 | 2.523 |
| 4552.00 | 19549.000 | 3.248 | 43722. | 16.547 | 2.579 |
| 4560.00 | 19574.000 | 3.120 | 43850. | 16.015 | 2.636 |
| 4568.00 | 19599.000 | 2.994 | 43979. | 15.488 | 2.693 |
| 4576.00 | 19622.000 | 2.871 | 44098. | 14.958 | 2.751 |
| 4584.00 | 19645.000 | 2.751 | 44219. | 14.436 | 2.809 |
| 4592.00 | 19666.000 | 2.634 | 44329. | 13.913 | 2.867 |
| 4600.00 | 19687.000 | 2.519 | 44441. | 13.398 | 2.925 |
| 4608.00 | 19706.000 | 2.408 | 44542. | 12.886 | 2.983 |
| 4616.00 | 19725.000 | 2.299 | 44644. | 12.383 | 3.041 |
| 4624.00 | 19743.000 | 2.194 | 44741. | 11.886 | 3.099 |
| 4632.00 | 19760.000 | 2.091 | 44833. | 11.395 | 3.157 |
| 4640.00 | 19777.000 | 1.992 | 44926. | 10.916 | 3.215 |
| 4648.00 | 19792.000 | 1.895 | 45009. | 10.439 | 3.272 |
| 4656.00 | 19807.000 | 1.801 | 45092. | 9.973 | 3.329 |
| 4664.00 | 19821.000 | 1.709 | 45169. | 9.513 | 3.385 |
| 4672.00 | 19834.000 | 1.620 | 45242. | 9.059 | 3.441 |
| 4680.00 | 19847.000 | 1.533 | 45315. | 8.615 | 3.496 |

| | | | | | |
|---|---|---|---|---|---|
| 4688.00 | 19859.000 | 1.449 | 45382. | 8.176 | 3.551 |
| 4696.00 | 19870.000 | 1.367 | 45444. | 7.743 | 3.605 |
| 4704.00 | 19881.000 | 1.286 | 45507. | 7.316 | 3.658 |
| 4712.00 | 19891.000 | 1.207 | 45564. | 6.894 | 3.710 |
| 4720.00 | 19900.000 | 1.130 | 45615. | 6.476 | 3.762 |
| 4728.00 | 19909.000 | 1.055 | 45667. | 6.062 | 3.812 |
| 4736.00 | 19917.000 | 0.980 | 45713. | 5.651 | 3.861 |
| 4744.00 | 19925.000 | 0.907 | 45759. | 5.243 | 3.909 |
| 4752.00 | 19932.000 | 0.834 | 45800. | 4.835 | 3.956 |
| 4760.00 | 19938.000 | 0.762 | 45835. | 4.427 | 4.002 |
| 4768.00 | 19944.000 | 0.690 | 45870. | 4.018 | 4.046 |
| 4776.00 | 19949.000 | 0.618 | 45899. | 3.606 | 4.089 |
| 4784.00 | 19954.000 | 0.545 | 45928. | 3.191 | 4.131 |
| 4792.00 | 19958.000 | 0.472 | 45951. | 2.767 | 4.171 |
| 4800.00 | 19961.000 | 0.398 | 45969. | 2.333 | 4.209 |
| 4808.00 | 19964.000 | 0.322 | 45987. | 1.891 | 4.243 |
| 4816.00 | 19966.000 | 0.248 | 45998. | 1.455 | 4.270 |
| 4824.00 | 19968.000 | 0.177 | 46010. | 1.039 | 4.290 |
| 4832.00 | 19969.000 | 0.113 | 46016. | 0.663 | 4.303 |
| 4840.00 | 19970.000 | 0.058 | 46022. | 0.344 | 4.310 |
| 4848.00 | 19970.000 | 0.017 | 46022. | 0.099 | 4.311 |
| 4856.00 | 19970.000 | 0.000 | 46022. | 0.000 | 4.311 |
| 4864.00 | 19970.000 | 0.000 | 46022. | 0.000 | 4.311 |
| 4872.00 | 19970.000 | 0.000 | 46022. | 0.000 | 4.311 |
| 4880.00 | 19970.000 | 0.000 | 46022. | 0.000 | 4.311 |
| 4888.00 | 19970.000 | 0.000 | 46022. | 0.000 | 4.311 |
| 4896.00 | 19970.000 | 0.000 | 46022. | 0.000 | 4.311 |
| 4904.00 | 19970.000 | 0.000 | 46022. | 0.000 | 4.311 |
| 4912.00 | 19970.000 | 0.000 | 46022. | 0.000 | 4.311 |
| 4920.00 | 19970.000 | 0.000 | 46022. | 0.000 | 4.311 |
| 4928.00 | 19970.000 | 0.000 | 46022. | 0.000 | 4.311 |
| 4936.00 | 19970.000 | 0.000 | 46022. | 0.000 | 4.311 |
| 4944.00 | 19970.000 | 0.000 | 46022. | 0.000 | 4.311 |
| 4952.00 | 19970.000 | 0.000 | 46022. | 0.000 | 4.311 |
| 4960.00 | 19970.000 | 0.000 | 46022. | 0.000 | 4.311 |
| 4968.00 | 19970.000 | 0.000 | 46022. | 0.000 | 4.311 |
| 4976.00 | 19970.000 | 0.000 | 46022. | 0.000 | 4.311 |
| 4984.00 | 19970.000 | 0.000 | 46022. | 0.000 | 4.311 |
| 4992.00 | 19970.000 | 0.000 | 46022. | 0.000 | 4.311 |
| 5000.00 | 19970.000 | 0.000 | 46022. | 0.000 | 4.311 |
| 5008.00 | 19970.000 | 0.000 | 46022. | 0.000 | 4.311 |
| 5016.00 | 19970.000 | 0.000 | 46022. | 0.000 | 4.311 |
| 5024.00 | 19970.000 | 0.000 | 46022. | 0.000 | 4.311 |
| 5032.00 | 19970.000 | 0.000 | 46022. | 0.000 | 4.311 |
| 5040.00 | 19970.000 | 0.000 | 46022. | 0.000 | 4.311 |
| 5048.00 | 19970.000 | 0.000 | 46022. | 0.000 | 4.311 |
| 5056.00 | 19970.000 | 0.000 | 46022. | 0.000 | 4.311 |
| 5064.00 | 19970.000 | 0.000 | 46022. | 0.000 | 4.311 |
| 5072.00 | 19970.000 | 0.000 | 46022. | 0.000 | 4.311 |
| 5080.00 | 19970.000 | 0.000 | 46022. | 0.000 | 4.311 |
| 5088.00 | 19970.000 | 0.000 | 46022. | 0.000 | 4.311 |
| 5096.00 | 19970.000 | 0.000 | 46022. | 0.000 | 4.311 |
| 5104.00 | 19970.000 | 0.000 | 46022. | 0.000 | 4.311 |
| 5112.00 | 19970.000 | 0.000 | 46022. | 0.000 | 4.311 |
| 5120.00 | 19970.000 | 0.000 | 46022. | 0.000 | 4.311 |
| 5128.00 | 19970.000 | 0.000 | 46022. | 0.000 | 4.311 |
| 5136.00 | 19970.000 | 0.000 | 46022. | 0.000 | 4.311 |
| 5144.00 | 19970.000 | 0.000 | 46022. | 0.000 | 4.311 |
| 5152.00 | 19970.000 | 0.000 | 46022. | 0.000 | 4.311 |
| 5160.00 | 19970.000 | 0.000 | 46022. | 0.000 | 4.311 |
| 5168.00 | 19970.000 | 0.000 | 46022. | 0.000 | 4.311 |
| 5176.00 | 19970.000 | 0.000 | 46022. | 0.000 | 4.311 |
| 5184.00 | 19970.000 | 0.000 | 46022. | 0.000 | 4.311 |
| 5192.00 | 19970.000 | 0.000 | 46022. | 0.000 | 4.311 |
| 5200.00 | 19970.000 | 0.000 | 46022. | 0.000 | 4.311 |
| 5208.00 | 19970.000 | 0.000 | 46022. | 0.000 | 4.311 |

| | | | | | |
|---|---|---|---|---|---|
| 5216.00 | 19970.000 | 0.000 | 46022. | 0.000 | 4.311 |
| 5224.00 | 19970.000 | 0.000 | 46022. | 0.000 | 4.311 |
| 5232.00 | 19970.000 | 0.000 | 46022. | 0.000 | 4.311 |
| 5240.00 | 19970.000 | 0.000 | 46022. | 0.000 | 4.311 |
| 5248.00 | 19970.000 | 0.000 | 46022. | 0.000 | 4.311 |
| 5256.00 | 19970.000 | 0.000 | 46022. | 0.000 | 4.311 |
| 5264.00 | 19970.000 | 0.000 | 46022. | 0.000 | 4.311 |
| 5272.00 | 19970.000 | 0.000 | 46022. | 0.000 | 4.311 |
| 5280.00 | 19970.000 | 0.000 | 46022. | 0.000 | 4.311 |
| 5288.00 | 19970.000 | 0.000 | 46022. | 0.000 | 4.311 |
| 5296.00 | 19970.000 | 0.000 | 46022. | 0.000 | 4.311 |
| 5304.00 | 19970.000 | 0.000 | 46022. | 0.000 | 4.311 |
| 5312.00 | 19970.000 | 0.000 | 46022. | 0.000 | 4.311 |
| 5320.00 | 19970.000 | 0.000 | 46022. | 0.000 | 4.311 |
| 5328.00 | 19970.000 | 0.000 | 46022. | 0.000 | 4.311 |
| 5336.00 | 19970.000 | 0.000 | 46022. | 0.000 | 4.311 |
| 5344.00 | 19970.000 | 0.000 | 46022. | 0.000 | 4.311 |
| 5352.00 | 19970.000 | 0.000 | 46022. | 0.000 | 4.311 |
| 5360.00 | 19970.000 | 0.000 | 46022. | 0.000 | 4.311 |
| 5368.00 | 19970.000 | 0.000 | 46022. | 0.000 | 4.311 |
| 5376.00 | 19970.000 | 0.000 | 46022. | 0.000 | 4.311 |
| 5384.00 | 19970.000 | 0.000 | 46022. | 0.000 | 4.311 |
| 5392.00 | 19970.000 | 0.000 | 46022. | 0.000 | 4.311 |
| 5400.00 | 19970.000 | 0.000 | 46022. | 0.000 | 4.311 |
| 5408.00 | 19970.000 | 0.000 | 46022. | 0.000 | 4.311 |
| 5416.00 | 19970.000 | 0.000 | 46022. | 0.000 | 4.311 |
| 5424.00 | 19970.000 | 0.000 | 46022. | 0.000 | 4.311 |
| 5432.00 | 19970.000 | 0.000 | 46022. | 0.000 | 4.311 |
| 5440.00 | 19970.000 | 0.000 | 46022. | 0.000 | 4.311 |
| 5448.00 | 19970.000 | 0.000 | 46022. | 0.000 | 4.311 |
| 5456.00 | 19970.000 | 0.000 | 46022. | 0.000 | 4.311 |
| 5464.00 | 19970.000 | 0.000 | 46022. | 0.000 | 4.311 |
| 5472.00 | 19970.000 | 0.000 | 46022. | 0.000 | 4.311 |
| 5480.00 | 19970.000 | 0.000 | 46022. | 0.000 | 4.311 |
| 5488.00 | 19970.000 | 0.000 | 46022. | 0.000 | 4.311 |
| 5496.00 | 19970.000 | 0.000 | 46022. | 0.000 | 4.311 |
| 5504.00 | 19970.000 | 0.000 | 46022. | 0.000 | 4.311 |
| 5512.00 | 19970.000 | 0.000 | 46022. | 0.000 | 4.311 |
| 5520.00 | 19970.000 | 0.000 | 46022. | 0.000 | 4.311 |
| 5528.00 | 19970.000 | 0.000 | 46022. | 0.000 | 4.311 |
| 5536.00 | 19970.000 | 0.000 | 46022. | 0.000 | 4.311 |
| 5544.00 | 19970.000 | 0.000 | 46022. | 0.000 | 4.311 |
| 5552.00 | 19970.000 | 0.000 | 46022. | 0.000 | 4.311 |
| 5560.00 | 19970.000 | 0.000 | 46022. | 0.000 | 4.311 |
| 5568.00 | 19970.000 | 0.000 | 46022. | 0.000 | 4.311 |
| 5576.00 | 19970.000 | 0.000 | 46022. | 0.000 | 4.311 |
| 5584.00 | 19970.000 | 0.000 | 46022. | 0.000 | 4.311 |
| 5592.00 | 19970.000 | 0.000 | 46022. | 0.000 | 4.311 |
| 5600.00 | 19970.000 | 0.000 | 46022. | 0.000 | 4.311 |
| 5608.00 | 19970.000 | 0.000 | 46022. | 0.000 | 4.311 |
| 5616.00 | 19970.000 | 0.000 | 46022. | 0.000 | 4.311 |
| 5624.00 | 19970.000 | 0.000 | 46022. | 0.000 | 4.311 |
| 5632.00 | 19970.000 | 0.000 | 46022. | 0.000 | 4.311 |
| 5640.00 | 19970.000 | 0.000 | 46022. | 0.000 | 4.311 |
| 5648.00 | 19970.000 | 0.000 | 46022. | 0.000 | 4.311 |
| 5656.00 | 19970.000 | 0.000 | 46022. | 0.000 | 4.311 |
| 5664.00 | 19970.000 | 0.000 | 46022. | 0.000 | 4.311 |
| 5672.00 | 19970.000 | 0.000 | 46022. | 0.000 | 4.311 |
| 5680.00 | 19970.000 | 0.000 | 46022. | 0.000 | 4.311 |
| 5688.00 | 19970.000 | 0.000 | 46022. | 0.000 | 4.311 |
| 5696.00 | 19970.000 | 0.000 | 46022. | 0.000 | 4.311 |
| 5704.00 | 19970.000 | 0.000 | 46022. | 0.000 | 4.311 |
| 5712.00 | 19970.000 | 0.000 | 46022. | 0.000 | 4.311 |
| 5720.00 | 19970.000 | 0.000 | 46022. | 0.000 | 4.311 |
| 5728.00 | 19970.000 | 0.000 | 46022. | 0.000 | 4.311 |
| 5736.00 | 19970.000 | 0.000 | 46022. | 0.000 | 4.311 |

| | | | | | |
|---|---|---|---|---|---|
| 5744.00 | 19970.000 | 0.000 | 46022. | 0.000 | 4.311 |
| 5752.00 | 19970.000 | 0.000 | 46022. | 0.000 | 4.311 |
| 5760.00 | 19970.000 | 0.000 | 46022. | 0.000 | 4.311 |
| 5768.00 | 19970.000 | 0.000 | 46022. | 0.000 | 4.311 |
| 5776.00 | 19970.000 | 0.000 | 46022. | 0.000 | 4.311 |
| 5784.00 | 19970.000 | 0.000 | 46022. | 0.000 | 4.311 |
| 5792.00 | 19970.000 | 0.000 | 46022. | 0.000 | 4.311 |
| 5800.00 | 19970.000 | 0.000 | 46022. | 0.000 | 4.311 |
| 5808.00 | 19970.000 | 0.000 | 46022. | 0.000 | 4.311 |
| 5816.00 | 19970.000 | 0.000 | 46022. | 0.000 | 4.311 |
| 5824.00 | 19970.000 | 0.000 | 46022. | 0.000 | 4.311 |
| 5832.00 | 19970.000 | 0.000 | 46022. | 0.000 | 4.311 |
| 5840.00 | 19970.000 | 0.000 | 46022. | 0.000 | 4.311 |
| 5848.00 | 19970.000 | 0.000 | 46022. | 0.000 | 4.311 |
| 5856.00 | 19970.000 | 0.000 | 46022. | 0.000 | 4.311 |
| 5864.00 | 19970.000 | 0.000 | 46022. | 0.000 | 4.311 |
| 5872.00 | 19970.000 | 0.000 | 46022. | 0.000 | 4.311 |
| 5880.00 | 19970.000 | 0.000 | 46022. | 0.000 | 4.311 |
| 5888.00 | 19970.000 | 0.000 | 46022. | 0.000 | 4.311 |
| 5896.00 | 19970.000 | 0.000 | 46022. | 0.000 | 4.311 |
| 5904.00 | 19970.000 | 0.000 | 46022. | 0.000 | 4.311 |
| 5912.00 | 19970.000 | 0.000 | 46022. | 0.000 | 4.311 |
| 5920.00 | 19970.000 | 0.000 | 46022. | 0.000 | 4.311 |
| 5928.00 | 19970.000 | 0.000 | 46022. | 0.000 | 4.311 |
| 5936.00 | 19970.000 | 0.000 | 46022. | 0.000 | 4.311 |
| 5944.00 | 19970.000 | 0.000 | 46022. | 0.000 | 4.311 |
| 5952.00 | 19970.000 | 0.000 | 46022. | 0.000 | 4.311 |
| 5960.00 | 19970.000 | 0.000 | 46022. | 0.000 | 4.311 |
| 5968.00 | 19970.000 | 0.000 | 46022. | 0.000 | 4.311 |
| 5976.00 | 19970.000 | 0.000 | 46022. | 0.000 | 4.311 |
| 5984.00 | 19970.000 | 0.000 | 46022. | 0.000 | 4.311 |
| 5992.00 | 19970.000 | 0.000 | 46022. | 0.000 | 4.311 |
| 6000.00 | 19970.000 | 0.000 | 46022. | 0.000 | 4.311 |
| 6008.00 | 19970.000 | 0.000 | 46022. | 0.000 | 4.311 |
| 6016.00 | 19970.000 | 0.000 | 46022. | 0.000 | 4.311 |
| 6024.00 | 19970.000 | 0.000 | 46022. | 0.000 | 4.311 |
| 6032.00 | 19970.000 | 0.000 | 46022. | 0.000 | 4.311 |
| 6040.00 | 19970.000 | 0.000 | 46022. | 0.000 | 4.311 |
| 6048.00 | 19970.000 | 0.000 | 46022. | 0.000 | 4.311 |
| 6056.00 | 19970.000 | 0.000 | 46022. | 0.000 | 4.311 |
| 6064.00 | 19970.000 | 0.000 | 46022. | 0.000 | 4.311 |
| 6072.00 | 19970.000 | 0.000 | 46022. | 0.000 | 4.311 |
| 6080.00 | 19970.000 | 0.000 | 46022. | 0.000 | 4.311 |
| 6088.00 | 19970.000 | 0.000 | 46022. | 0.000 | 4.311 |
| 6096.00 | 19970.000 | 0.000 | 46022. | 0.000 | 4.311 |
| 6104.00 | 19970.000 | 0.000 | 46022. | 0.000 | 4.311 |
| 6112.00 | 19970.000 | 0.000 | 46022. | 0.000 | 4.311 |
| 6120.00 | 19970.000 | 0.000 | 46022. | 0.000 | 4.311 |
| 6128.00 | 19970.000 | 0.000 | 46022. | 0.000 | 4.311 |
| 6136.00 | 19970.000 | 0.000 | 46022. | 0.000 | 4.311 |
| 6144.00 | 19970.000 | 0.000 | 46022. | 0.000 | 4.311 |
| 6152.00 | 19970.000 | 0.000 | 46022. | 0.000 | 4.311 |
| 6160.00 | 19970.000 | 0.000 | 46022. | 0.000 | 4.311 |
| 6168.00 | 19970.000 | 0.000 | 46022. | 0.000 | 4.311 |
| 6176.00 | 19970.000 | 0.000 | 46022. | 0.000 | 4.311 |
| 6184.00 | 19970.000 | 0.000 | 46022. | 0.000 | 4.311 |
| 6192.00 | 19970.000 | 0.000 | 46022. | 0.000 | 4.311 |
| 6200.00 | 19970.000 | 0.000 | 46022. | 0.000 | 4.311 |
| 6208.00 | 19970.000 | 0.000 | 46022. | 0.000 | 4.311 |
| 6216.00 | 19970.000 | 0.000 | 46022. | 0.000 | 4.311 |
| 6224.00 | 19970.000 | 0.000 | 46022. | 0.000 | 4.311 |
| 6232.00 | 19970.000 | 0.000 | 46022. | 0.000 | 4.311 |
| 6240.00 | 19970.000 | 0.000 | 46022. | 0.000 | 4.311 |
| 6248.00 | 19970.000 | 0.000 | 46022. | 0.000 | 4.311 |
| 6256.00 | 19970.000 | 0.000 | 46022. | 0.000 | 4.311 |
| 6264.00 | 19970.000 | 0.000 | 46022. | 0.000 | 4.311 |

| | | | | | |
|---|---|---|---|---|---|
| 6272.00 | 19970.000 | 0.000 | 46022. | 0.000 | 4.311 |
| 6280.00 | 19970.000 | 0.000 | 46022. | 0.000 | 4.311 |
| 6288.00 | 19970.000 | 0.000 | 46022. | 0.000 | 4.311 |
| 6296.00 | 19970.000 | 0.000 | 46022. | 0.000 | 4.311 |
| 6304.00 | 19970.000 | 0.000 | 46022. | 0.000 | 4.311 |
| 6312.00 | 19970.000 | 0.000 | 46022. | 0.000 | 4.311 |
| 6320.00 | 19970.000 | 0.000 | 46022. | 0.000 | 4.311 |
| 6328.00 | 19970.000 | 0.000 | 46022. | 0.000 | 4.311 |
| 6336.00 | 19970.000 | 0.000 | 46022. | 0.000 | 4.311 |
| 6344.00 | 19970.000 | 0.000 | 46022. | 0.000 | 4.311 |
| 6352.00 | 19970.000 | 0.000 | 46022. | 0.000 | 4.311 |
| 6360.00 | 19970.000 | 0.000 | 46022. | 0.000 | 4.311 |
| 6368.00 | 19970.000 | 0.000 | 46022. | 0.000 | 4.311 |
| 6376.00 | 19970.000 | 0.000 | 46022. | 0.000 | 4.311 |
| 6384.00 | 19970.000 | 0.000 | 46022. | 0.000 | 4.311 |
| 6392.00 | 19970.000 | 0.000 | 46022. | 0.000 | 4.311 |
| 6400.00 | 19970.000 | 0.000 | 46022. | 0.000 | 4.311 |
| 6408.00 | 19970.000 | 0.000 | 46022. | 0.000 | 4.311 |
| 6416.00 | 19970.000 | 0.000 | 46022. | 0.000 | 4.311 |
| 6424.00 | 19970.000 | 0.000 | 46022. | 0.000 | 4.311 |
| 6432.00 | 19970.000 | 0.000 | 46022. | 0.000 | 4.311 |
| 6440.00 | 19970.000 | 0.000 | 46022. | 0.000 | 4.311 |
| 6448.00 | 19970.000 | 0.000 | 46022. | 0.000 | 4.311 |
| 6456.00 | 19970.000 | 0.000 | 46022. | 0.000 | 4.311 |
| 6464.00 | 19970.000 | 0.000 | 46022. | 0.000 | 4.311 |
| 6472.00 | 19970.000 | 0.000 | 46022. | 0.000 | 4.311 |
| 6480.00 | 19970.000 | 0.000 | 46022. | 0.000 | 4.311 |
| 6488.00 | 19970.000 | 0.000 | 46022. | 0.000 | 4.311 |
| 6496.00 | 19970.000 | 0.000 | 46022. | 0.000 | 4.311 |
| 6504.00 | 19970.000 | 0.000 | 46022. | 0.000 | 4.311 |
| 6512.00 | 19970.000 | 0.000 | 46022. | 0.000 | 4.311 |
| 6520.00 | 19970.000 | 0.000 | 46022. | 0.000 | 4.311 |
| 6528.00 | 19970.000 | 0.000 | 46022. | 0.000 | 4.311 |
| 6536.00 | 19970.000 | 0.000 | 46022. | 0.000 | 4.311 |
| 6544.00 | 19970.000 | 0.000 | 46022. | 0.000 | 4.311 |
| 6552.00 | 19970.000 | 0.000 | 46022. | 0.000 | 4.311 |
| 6560.00 | 19970.000 | 0.000 | 46022. | 0.000 | 4.311 |
| 6568.00 | 19970.000 | 0.000 | 46022. | 0.000 | 4.311 |
| 6576.00 | 19970.000 | 0.000 | 46022. | 0.000 | 4.311 |
| 6584.00 | 19970.000 | 0.000 | 46022. | 0.000 | 4.311 |
| 6592.00 | 19970.000 | 0.000 | 46022. | 0.000 | 4.311 |
| 6600.00 | 19970.000 | 0.000 | 46022. | 0.000 | 4.311 |
| 6608.00 | 19970.000 | 0.000 | 46022. | 0.000 | 4.311 |
| 6616.00 | 19970.000 | 0.000 | 46022. | 0.000 | 4.311 |
| 6624.00 | 19970.000 | 0.000 | 46022. | 0.000 | 4.311 |
| 6632.00 | 19970.000 | 0.000 | 46022. | 0.000 | 4.311 |
| 6640.00 | 19970.000 | 0.000 | 46022. | 0.000 | 4.311 |
| 6648.00 | 19970.000 | 0.000 | 46022. | 0.000 | 4.311 |
| 6656.00 | 19970.000 | 0.000 | 46022. | 0.000 | 4.311 |
| 6664.00 | 19970.000 | 0.000 | 46022. | 0.000 | 4.311 |
| 6672.00 | 19970.000 | 0.000 | 46022. | 0.000 | 4.311 |
| 6680.00 | 19970.000 | 0.000 | 46022. | 0.000 | 4.311 |
| 6688.00 | 19970.000 | 0.000 | 46022. | 0.000 | 4.311 |
| 6696.00 | 19970.000 | 0.000 | 46022. | 0.000 | 4.311 |
| 6704.00 | 19970.000 | 0.000 | 46022. | 0.000 | 4.311 |
| 6712.00 | 19970.000 | 0.000 | 46022. | 0.000 | 4.311 |
| 6720.00 | 19970.000 | 0.000 | 46022. | 0.000 | 4.311 |
| 6728.00 | 19970.000 | 0.000 | 46022. | 0.000 | 4.311 |
| 6736.00 | 19970.000 | 0.000 | 46022. | 0.000 | 4.311 |
| 6744.00 | 19970.000 | 0.000 | 46022. | 0.000 | 4.311 |
| 6752.00 | 19970.000 | 0.000 | 46022. | 0.000 | 4.311 |
| 6760.00 | 19970.000 | 0.000 | 46022. | 0.000 | 4.311 |
| 6768.00 | 19970.000 | 0.000 | 46022. | 0.000 | 4.311 |
| 6776.00 | 19970.000 | 0.000 | 46022. | 0.000 | 4.311 |
| 6784.00 | 19970.000 | 0.000 | 46022. | 0.000 | 4.311 |
| 6792.00 | 19970.000 | 0.000 | 46022. | 0.000 | 4.311 |

| | | | | | |
|---|---|---|---|---|---|
| 6800.00 | 19970.000 | 0.000 | 46022. | 0.000 | 4.311 |
| 6808.00 | 19970.000 | 0.000 | 46022. | 0.000 | 4.311 |
| 6816.00 | 19970.000 | 0.000 | 46022. | 0.000 | 4.311 |
| 6824.00 | 19970.000 | 0.000 | 46022. | 0.000 | 4.311 |
| 6832.00 | 19970.000 | 0.000 | 46022. | 0.000 | 4.311 |
| 6840.00 | 19970.000 | 0.000 | 46022. | 0.000 | 4.311 |
| 6848.00 | 19970.000 | 0.000 | 46022. | 0.000 | 4.311 |
| 6856.00 | 19970.000 | 0.000 | 46022. | 0.000 | 4.311 |
| 6864.00 | 19970.000 | 0.000 | 46022. | 0.000 | 4.311 |
| 6872.00 | 19970.000 | 0.000 | 46022. | 0.000 | 4.311 |
| 6880.00 | 19970.000 | 0.000 | 46022. | 0.000 | 4.311 |
| 6888.00 | 19970.000 | 0.000 | 46022. | 0.000 | 4.311 |
| 6896.00 | 19970.000 | 0.000 | 46022. | 0.000 | 4.311 |
| 6904.00 | 19970.000 | 0.000 | 46022. | 0.000 | 4.311 |
| 6912.00 | 19970.000 | 0.000 | 46022. | 0.000 | 4.311 |
| 6920.00 | 19970.000 | 0.000 | 46022. | 0.000 | 4.311 |
| 6928.00 | 19970.000 | 0.000 | 46022. | 0.000 | 4.311 |
| 6936.00 | 19970.000 | 0.000 | 46022. | 0.000 | 4.311 |
| 6944.00 | 19970.000 | 0.000 | 46022. | 0.000 | 4.311 |
| 6952.00 | 19970.000 | 0.000 | 46022. | 0.000 | 4.311 |
| 6960.00 | 19970.000 | 0.000 | 46022. | 0.000 | 4.311 |
| 6968.00 | 19970.000 | 0.000 | 46022. | 0.000 | 4.311 |
| 6976.00 | 19970.000 | 0.000 | 46022. | 0.000 | 4.311 |
| 6984.00 | 19970.000 | 0.000 | 46022. | 0.000 | 4.311 |
| 6992.00 | 19970.000 | 0.000 | 46022. | 0.000 | 4.311 |
| 7000.00 | 19970.000 | 0.000 | 46022. | 0.000 | 4.311 |
| 7008.00 | 19970.000 | 0.000 | 46022. | 0.000 | 4.311 |
| 7016.00 | 19970.000 | 0.000 | 46022. | 0.000 | 4.311 |
| 7024.00 | 19970.000 | 0.000 | 46022. | 0.000 | 4.311 |
| 7032.00 | 19970.000 | 0.000 | 46022. | 0.000 | 4.311 |
| 7040.00 | 19970.000 | 0.000 | 46022. | 0.000 | 4.311 |
| 7048.00 | 19970.000 | 0.000 | 46022. | 0.000 | 4.311 |
| 7056.00 | 19970.000 | 0.000 | 46022. | 0.000 | 4.311 |
| 7064.00 | 19970.000 | 0.000 | 46022. | 0.000 | 4.311 |
| 7072.00 | 19970.000 | 0.000 | 46022. | 0.000 | 4.311 |
| 7080.00 | 19970.000 | 0.000 | 46022. | 0.000 | 4.311 |
| 7088.00 | 19970.000 | 0.000 | 46022. | 0.000 | 4.311 |
| 7096.00 | 19970.000 | 0.000 | 46022. | 0.000 | 4.311 |
| 7104.00 | 19970.000 | 0.000 | 46022. | 0.000 | 4.311 |
| 7112.00 | 19970.000 | 0.000 | 46022. | 0.000 | 4.311 |
| 7120.00 | 19970.000 | 0.000 | 46022. | 0.000 | 4.311 |
| 7128.00 | 19970.000 | 0.000 | 46022. | 0.000 | 4.311 |
| 7136.00 | 19970.000 | 0.000 | 46022. | 0.000 | 4.311 |
| 7144.00 | 19970.000 | 0.000 | 46022. | 0.000 | 4.311 |
| 7152.00 | 19970.000 | 0.000 | 46022. | 0.000 | 4.311 |
| 7160.00 | 19970.000 | 0.000 | 46022. | 0.000 | 4.311 |
| 7168.00 | 19970.000 | 0.000 | 46022. | 0.000 | 4.311 |
| 7176.00 | 19970.000 | 0.000 | 46022. | 0.000 | 4.311 |
| 7184.00 | 19970.000 | 0.000 | 46022. | 0.000 | 4.311 |
| 7192.00 | 19970.000 | 0.000 | 46022. | 0.000 | 4.311 |
| 7200.00 | 19970.000 | 0.000 | 46022. | 0.000 | 4.311 |

LIST OF CONTROL PARAMETERS FOR SEDSAT_REF39 (Last update May 15, 1995)

Here below is the complete list of the control parameters for SEDSAT control law SEDSAT_Ref39 as they stand before the characteristics of the new tether are measured and the deployment tests are carried out.

The values of the parameters for SEDS2 Ref1_14jun93 (the flight control law for SEDS2) are also shown to point out the differences wherever applicable.

-------- CONTROL PARAMETERS ----------

| No. | PARAMETER | TYPE | Units | SEDSAT | SEDS-II |
|---|---|---|---|---|---|
| 1. | c | Filter Coefficient | | 0.125 | 0.125 |
| 2. | GTC | TurnCount Gain | (1/Turn) | 0.002 | 0.002 |
| 3. | DZTC | TurnCount Deadzone | (Turn) | 5 | 5 |
| 4. | TCELIM | Maximum Turn Count Error | (Turn) | 5000 | 3000 |
| 5. | GTCR | TurnCount Rate Gain | (s/Turn) | 0.2 | 0.2 |
| 6. | DZTCR | TurnCountRate Deadzone | (Turn/s) | 0.5 | 0.5 |
| 7. | TCRELIM | Maximum Turn CountRate Error | (Turn/s) | 10 | 5 |
| 8. | WAILP | Wrap Increment Upper Limit | | 2 | 1 |
| 9. | TBD s | Time after which Bias is applied | (s) | 65535 | 65535 |
| 10. | BIAS | BrakePost Bias | (Turn) | 0 | 0 |
| 11. | WACLP | WrapAdjustment Upper Limit | (Turn) | 7 | 6 |
| 12.* | TCBS | Turn Count Brake Stop | (Turn) | 46000** | 45500 |
| 13.* | A1 | Coeff_1 in Variable Gains | | 0.6980403 | 0.6980403 |
| 14.* | A2 | Coeff_2 in Variable Gain | | 5.7380313E-6 | 5.7380313E-6 |
| 15. | STOPDEPLOY | Time from Ejection for Brake Ramping up | (s) | 5000 | 6560 |

* These parameters are very likely to change for the new tether.
** Value updated on May 15, 1995.
++++++++++++++++++++++++++++++++++++++++++++++++++++++++++++++++++++++++++END